UNIVERSITY OF TECHNOLOGY SYDNEY
Faculty of Engineering and Information Technology

Stochastic Geometry Based Modeling and Performance Analysis of Ultra-dense Cellular Networks

by

Junnan Yang

A Thesis Submitted
in Partial Fulfillment of the
Requirements for the Degree

Doctor of Philosophy

Sydney, Australia

2019

Certificate of Authorship/Originality

I, Junnan Yang, certify that the work in this thesis has not been previously submitted for a degree nor has it been submitted as a part of the requirements for other degree except as fully acknowledged within the text.

I also certify that this thesis has been written by me. Any help that I have received in my research and in the preparation of the thesis itself has been fully acknowledged. In addition, I certify that all information sources and literature used are quoted in the thesis.

This research is supported by the Australian Government Research Trainning Program.

© Copyright 2019 Junnan Yang

Production Note:
Signature removed
prior to publication.

1/10/2019

ABSTRACT

Stochastic Geometry Based Modeling and Performance Analysis of Ultra-dense Cellular Networks

by

Junnan Yang

In the last decade, there has been an explosive increase in the demand for wireless network data traffic. To deal with such monumental consumer requirement for information communications, several notable technologies have been proposed, such as small cell networks (SCNs), device-to-device (D2D) communications.

In the first half of the thesis, we address the critical issue of interference management in the D2D enhanced cellular network. To reduce the severe interference caused by active D2D links, we consider a mode selection scheme based on the maximum received signal strength (MRSS) for each user equipment (UE) to control the D2D-to-cellular interference. This will mitigate the overlarge interference from the D2D links to the cellular links. Moreover, to improve the capacity of D2D-enhanced networks, we consider that the typical user is no longer a random user which is selected by a round-robin (RR) scheduler, as assumed in most studies in the literature. Instead, a cellular user with the maximum proportional fair (PF) metric is chosen by its serving BS as the typical user, which is referred to as the PF scheduler in the cellular tier. Furthermore, we quantify the performance gains brought by D2D communications in cellular networks and we find an optimum mode selection threshold to maximize the total area spectrum efficiency (ASE) in the network.

In the second half of the thesis, we adjust the antenna pattern to boost the area spectral efficiency (ASE) of cellular networks when considering the height of the base stations. Very recent studies have shown that the area spectral efficiency of downlink (DL) cellular networks will continuously decrease and finally crash to zero

as the base station (BS) density increases towards infinity if the absolute height difference between BS antenna and user equipment (UE) antenna is larger than zero. Such a phenomenon is referred to as the ASE Crash. We revisit this issue by considering optimizing the BS antenna downtilt in cellular networks. We investigated the relationship between the BS antenna downtilt and the downlink network performance in terms of the coverage probability and the ASE. Our results reveal a notable conclusion that there exists an optimal antenna downtilt to achieve the maximum coverage probability for each BS density. After applying the optimal antenna downtilt, the network performance can be significantly improved, and hence the ASE crash can be delayed by nearly one order of magnitude in terms of the BS density.

Dissertation directed by Professor Guoqiang Mao
School of Electrical and Data Engineering

Acknowledgements

The completion of this dissertation has been possible with the inspiration and encouragement from many people, to whom I am greatly indebted.

First of all, I should pay my immesurable appreciation and deepest gratitude to my PhD supervisor Professor Guoqiang Mao and Dr. Ming Ding, for their never-ending guidance, strict requirements and clear training methods. These have helped me find a right way to do research and make great progress.

I feel extremely fortunate to be mentored by these two excellent scholars during my Ph.D. candidature. I will always remember their guidance and be grateful.

I am also grateful to other members in our research team, especially Dr. Jieqiong Chen, Dr. Tian Ding and Dr. Bin Yang, for making a friendly working environment, and for their support, great assistance and valuable advice to my research.

I also wish to express my gratitude to my friends who accompanied me during my studies. Dr. Shijin Li, Dr. Yifan Zuo, Dr. Lina Li, Dr. Rongrong Hu and Mr. Aaron Han, I will remember the times we spent together and hope that our friendship will last forever.

Finally, but mostly, I wish to express my deepst gratitude to My father Wanneng Yang, my mother Aisu Shen and my beloved wife Shuyun Sun. Although our family has experienced a very difficult period, you have given me tremendous support and encouragement so that I can successfully complete my work.

Junnan Yang

Sydney, Australia, 2019.

List of Publications

Journal Papers

J-1. **Junnan Yang**, Ming Ding, Guoqiang Mao, Zihuai Lin and Xiaohu Ge, Analysis of Underlaid D2D-Enhanced Cellular Networks: Interference Management and Proportional Fair Scheduler, IEEE Access, Vol. 16, No. 3, pp. 1779-1791, 2019.

J-2. **Junnan Yang**, Ming Ding, Guoqiang Mao, Zihuai Lin, De-gan Zhang, Tom Hao Luan, Optimal Base Station Antenna Downtilt in Downlink Cellular Networks, IEEE Transactions on Wireless Communications, Vol. 18, No. 3, pp. 1779-1791, March 2019.

J-3. **Junnan Yang**, Ming Ding, Guoqiang Mao and Zihuai Lin, Interference Management in In-band D2D Underlaid Cellular Networks, accepted to IEEE Transactions on Cognitive Communications and Networking, May 2019.

Conference Papers

C-1. **Junnan Yang**, Ming Ding, Guoqiang Mao and Tom H. Luan, Interference Management in Underlay In-band D2D-Enhanced Cellular Networks, in the 24th Asia-Pacific Conference on Communications, 2018. Invited Paper

Contents

List of Figures

List of Tables

Chapter 1

Introduction

1.1 Research Background

1.1.1 Ultra Dense Cellular Network

Wireless networking technology development has brought huge changes to everyday life. There has been a tremendous rise in the number of mobile devices and also a sharp rise in the demand for mobile data communication at the same time. In the last decade, the mobile industry grows very fast, where the penetration rate has grown from 3.6 billion in 2014 to 4.6 billion in 2020, and the data traffic will grow 1000 times to the year 2020 [1]. Facing such massive consumer demand for mobile data, especially from the skyrocketing number of mobile user equipment (UEs) and smartphones, a lot of techniques have been proposed in the last decade such as ultra dense cellular network, Femtocells, white space, device-to-device (D2D) communications. We can conclude complementary solutions to boost the network capacity into three aspects: more spectrum in low and higher bands (millimeter wave); heterogenous networks with small cells; the higher efficiency including the intelligent access, evolved 4G, D2D technology and LTE broadcast.

One wireless networking trend is network desification. According to the [2] , in third generation (3G) cellular networks, the aim of densification of macro base stations (BSs) is to improve the transmission rate in partial areas, such as macrocell BSs deployed in urban areas. To avoid interference caused by frequency reuse, sectorized BS technologies and adjacent macrocell BSs have been developed for macrocell densification, where macrocell BSs' density is about 4-5 BS/km^2. In fourth gen-

eration (4G) cellular networks, such as Long Term Evolution-Advanced (LTE-A) mobile communication systems, the microcell BSs, picocell BSs and femtocell BSs, have been deployed to satisfy the high speed transmission in specified regions, where density of microcell BSs is approximate 8-10 BS/km^2. In 4G and 3G cellular networks, BSs densification aims to improve the wireless transmission rate in partial regions and the greatest challenge of BSs densification is the interference coordination for cellular networks.

In 5G cellular networks, the massive MIMO antennas have been integrated into wireless networks, where hundreds of antennas are utilized for transmitting huge wireless traffic [3, 4]. When the 5G BS transmission power is constrained at the same level of 4G BS transmission power, every antenna transmission power at 5G BS has to be decreased 10-20 times compared with every antenna transmission power at 4G BS. Another potential key technology for 5G cellular networks is millimeter wave communication technology, which is expected to provide wireless transmissions with a bandwidth of over hundreds of MHz. Transmission distance of millimeter wave communications, however, has to be restricted to 100 meters considering the propagation degradation of millimeter wave in the atmosphere. Motived by the above two technologies, small cell networks have been presented for 5G cellular networks. To satisfy seamless coverage, the density of 5G BS is highly anticipated to be up to 40-50 BS/km^2. The future of 5G cellular networking therefore is an ultra-dense cellular network.

Since the beginning of cell splitting, densification and the mobile industry has been one of the most effective means to deliver improving user experience and ever-increasing capacity. In recent years, ultra-dense networks (UDNs) have emerged as a prominent solution to meet the challenges of fulfilling 5G extremely high capacity density requirements of up to 10 Mbps/m^2. Qualitatively, UDN is a network whose radio resources have a much higher density than that in current networks, which is

much denser small cell network in terms of either relative density or absolute density of the BSs.

1.1.2 Device-to-Device Communications

D2D communications in cellular networks provide a direct communication between two mobile users without going through a BS and can provide four types of performance gain. The first one is proximity gain as short range communication using a D2D link enables high bit rates, low delays, and lower power consumption. The second one is hop gain as D2D communications uses one hop rather than two hops consisting of one uplink and one downlink communication. The third one is reuse gain as D2D communications can reuse cellular spectrum in an underlay mode. The last one is paring gain, which facilitates new types of wireless services. System spectral efficiency and energy efficiency can be significantly boosted from this new communication paradigm.

However, existing works considered only the operator controlled D2D communication, in which the BS was assumed of all network information and was able to make the optimal decision to share band resource with D2D UEs. Obviously, it is of high computational complexity when applied to the practical cellular networks where each BS is required to simultaneously support various applications for a large number of mobile UEs. Another common limitation is that available works considered a very limited number of BSs and mobile UEs, which necessary failed to take into account the spatial distribution of other BSs and mobile UEs and thus the impact of accumulated interference from other surrounding cells. Towards this end, we consider a D2D communication enabled multi-channel cellular network with a careful consideration of the spatial distribution properties of both BSs and mobile UEs.

1.2 Research Motivation

1.2.1 Network Modeling and D2D-Enhanced Network

Although the reuse of the cellular spectrum via D2D can improve the area spectral efficiency of the network, such D2D operations also pose great challenges. The major challenge in the D2D-enabled cellular network is the existence of inter-tier and intra-tier interference due to aggressive frequency reuse, where cellular UEs and D2D UEs share the same spectrum. It is essential to design an effective interference management scheme to control the interference generated by the D2D links to the cellular links, and vice versa. Consequently, there has been a surge of academic studies in this area. Transmission power control [5–8], distance-based mode selection [9–11] and guard-zone interference control schemes [12–14] have been proposed to solve this problem.

On the other hand, as pointed out in [15], one major weakness of recent research on D2D communications is a lack of realistic scenarios for future mobile networks such as heterogeneous networks with densely deployed small cells. As a straightforward way to increase network capacity, the SCN densification also opens up new research questions, especially in the context of D2D communications. First, scheduling has been conceived as an effective use selection technique used at base stations (BSs) to efficiently use the available spectrum and improve the overall system throughput. Second, the path loss models of D2D links and cellular links in D2D-enabled cellular networks are different due to the difference in the heights and locations of transmitters [16]. Third, it is well known that line-of-sight (LoS) transmission may occur when the distance between a transmitter and a receiver is small, and non-line-of-sight (NLoS) transmission is common in office environments and central business districts. When the distance between a transmitter and a receiver decreases, the probability that a LoS path exists between them increases, thereby causing a tran-

sition from NLoS transmission to LoS transmission with a higher probability. Due to the proximity between D2D users, the physical channels which constitute D2D communications are expected to be complex, experiencing both LoS and NLoS conditions across these pairs, which are distinctly different from conventional cellular environments [17].

1.2.2 Antenna Downtilt in UDN

It has been widely acknowledged that wireless networks continue to face significant challenges and opportunities [18]. In the first decade of 2000, network densification continued to underpin the capacity increases in the 3rd Generation Partnership Project (3GPP) 4th-generation (4G) Long Term Evolution (LTE) networks, and is expected to remain as one of the main forces to drive the 5th-generation (5G) networks onward [19]. Various emerging technologies have been developed in this context, such as small cell networks (SCNs), cognitive radio, massive MIMO, etc [2]. In particular, in the past few years, a few noteworthy studies have been carried out to revisit the performance analyses for cellular networks under more practical propagation models. In [20], the authors considered a multi-slope piecewise path loss function, while in [21], the authors investigated line-of-sight (LoS) and non-line-of-sight (NLoS) transmission as a probabilistic event for a millimeter wave communication scenario. The most important finding in these two works is that the per-BS coverage probability performance starts to decrease when the base station (BS) density is sufficiently large. Fortunately, such a decrease of the coverage probability will not change the monotonic increase of the area spectral efficiency (ASE) as the BS density increases [20, 21]. However, in very recent works, the authors in [16, 22, 23] found that the ASE performance will continuously decrease toward zero with the network densification for SCNs when the absolute antenna height difference between a base station and a user equipment (UE) is larger than zero, which

is referred to as the ASE Crash [16, 22, 23].

Having a closer look at the problem, we realize that in a three-dimensional (3D) channel model, the antenna patterns may increase the received signal and at the same time reduce inter-cell interference [24]. In particular, horizontal beamforming is a signal processing method that generates directional antenna beam patterns using multiple antennas at the transmitter. It is possible to steer the transmitted signal toward the desired direction and, at the same time, avoid receiving the unwanted signals from undesired directions [25]. The benefits of horizontal beamforming in cellular networks are well-understood and such technology has already been adopted in the LTE networks, e.g., the macro BSs. However, vertical beamforming (based on an antenna downtilt) receives much less attention. Recent studies have made some initial efforts that shed new light on adjusting antenna downtilt to improve the performance of cellular networks [26–28], but most of these studies were solely based on computer simulations.

1.3 Research Objectives and Contributions

From the aforementioned research background and motivation, this thesis focuses on the following research problems;(1) design D2D-enhanced cellular networks for communication systems to achieve fast and reliable data dissemination; and (2) investigating the optimal antenna downtilt when considering a 3-D antenna pattern to achieve the maximum performance of cellular network. In the following section, the detailed research problems and the corresponding contributions will be elaborated upon.

For the first research problem, to the best of our knowledge, there has been no research on investigating the interference management in D2D-Enhanced cellular networks based on the strongest received signal strength. A distinction is shown by our analysis on the network performance while in the light of Lognormal

shadow fading and dissimilar path loss models for the D2D connections and the cellular connections respectively, which captures the dissimilar environmental circumstances D2D connections and cellular connections operate in. The novelty and major contributions of this research work are summarized as follows:

- We investigate a general D2D-enhanced network performance in which UEs can adaptively switch between conventional cellular UEs and D2D UEs. In most previous studies, the authors have considered D2D receiver UEs as an additional tier of nodes, independent of the cellular UEs and the D2D transmitter UEs. In our study, cellular UEs, D2D transmit UEs and D2D receiver UEs constitute the entire UE set, which is a more practical assumption than dropping more UEs for D2D reception only.

- A tractable interference management scheme is proposed based on the mode selection method for each user equipment (UE) to control the co-channel interference. A UE will specifically operate in a cellular mode if its received signal strength from the strongest base station (BS) is larger than a threshold; conversely, it will perform an operation in a D2D mode. Potential large interference is mitigated by such an interference management scheme from D2D transmitter to cellular network.

- We present a general analytic framework using an intensity matching approach. Based on the proposed model incorporating interference management, LOS/NLOS transmission and shadow fading, we derive analytical results of coverage probability and ASE for both the cellular mode and D2D mode. Our analysis adopts two different path loss models for cellular links and D2D links, respectively. The results show the interference management scheme mitigates the potential overlarge interference from D2D transmitter to cellular network, and there is an optimum mode selection threshold to achieve the maximum

ASE when cellular tier's performance is ensured.

The second research problem considered in this thesis is an extension of the first. In this part, we consider interference management and the PF scheduler [19] in D2D-enhanced ultra dense networks. A cellular user with the maximum proportional fair (PF) metric is chosen by its serving BS as the typical user, which is referred to as the PF scheduler. The novelty and major contributions of this research work are summarized as follows:

- We propose a tractable interference management scheme for each user equipment (UE) to control the co-channel interference. Specifically, a UE will operate in a cellular mode if its received signal strength from the strongest base station (BS) is larger than a threshold; otherwise, it will operate in a D2D mode. Such an interference management scheme mitigates large interference from a D2D transmitter to cellular network. Through our theoretical and numerical analyses, we quantify the performance gains brought by D2D communications in cellular networks and we find an optimum mode selection threshold β to maximize the total ASE in the network.

- We investigate the general D2D-enhanced dense network performance with the consideration of PF schedulers. For the first time, we use stochastic geometry [29] to derive the analytical results of the coverage probability and the area spectral efficiency (ASE) performance of the D2D-enhanced UDNs with PF schedulers used at BSs. The key point of our analysis is that the typical user is no longer a random user as assumed in most exiting studies of stochastic geometry.

- Different from the existing work that does not differentiate the path loss models between cellular links and D2D links, our analysis adopts two different path loss models for cellular links and D2D links, respectively. Our results

demonstrate that the D2D links can provide a considerable ASE gain when the threshold parameter β is appropriately chosen. More specifically, our analysis shows the interference from the D2D tier can be controlled by using our mode selection scheme, and there is an optimal antenna downtilt to achieve the maximum ASE while the performance of cellular tier is guaranteed.

The third research problem considered in this thesis is investigating the impact of the antenna pattern and downtilt on the performance of downlink (DL) cellular networks, in terms of the coverage probability and the area spectral efficiency. We also derive the analytical expressions for the optimal antenna downtilt that can achieve the best coverage probability of the network given a certain BS density.

The novelty and major contributions of this research work are summarized as follows:

- We analytically investigate the relationship between the antenna downtilt and cellular network performance in terms of the coverage probability and the ASE based on the 3D antenna pattern model which includes horizontal and vertical antenna patterns, possibly with sectorization.. Our results reveal an interesting finding that there exists a unique optimal antenna downtilt that strikes a balance between increasing the received signal power and reducing the interference power to achieve the maximum coverage probability for a certain BS density.

- We study and analyze the optimal antenna downtilt for a certain BS density considering the 3D antenna pattern model which includes horizontal and vertical antenna patterns. As a consequence, we derive numerically solvable expressions for the optimal antenna downtilt for a certain BS density, which includes three components, namely the LoS links, the NLoS links and the noise, contributing to the optimal antenna downtilt.

- Our theoretical and numerical results demonstrate that the performance of cellular network can be improved significantly using the optimal antenna downtilt. In particular, applying the optimal antenna downtilt can delay the ASE crash by nearly one order of magnitude in terms of the base station density. Using the derived expressions and the simulation results, network operators optimally select determine the antenna downtilt of BSs to maximize the system throughput for a given the base station density.

1.4 Thesis Organization

This thesis is organised as follows; Chapter 2 presents a survey of related works, including cellular network modeling using stochastic geometry, Device-to-Device communications networks and interference management in cellular networks. Chapter 3 proposes a novel mode selection method to control the interference in D2D enhanced cellular netwotks, and investigates the coverage probablity and the ASE of the neworks. Chapter 4 deals with the scenario that there is only Rayleigh fading in the D2D enhanced cellular network, a novel proportional fair scheduler has been taken into account. Chapter 5 investigates the optimal antenna downtilt in UDN and the results reveal an intersting finding that there exists an optimal antenna downtilt to achieve the maximum coverage probablity for each BS density. Chapter 6 presents a brief summary of the thesis contents, and gives recommendation for future works.

Chapter 2

Literature Review

This chapter is dedicated to reviewing related works to this thesis, including works on cellular network modeling using stochastic geometry, Device-to-Device communications networks and interference management in cellular networks.

2.1 Cellular Network Modeling using Stochastic Geometry

To analyze the performance of cellular network, stochastic geometry has been used in this thesis. In stochastic geometry theory, a wireless communication network can be viewed as a collection of nodes, located in some domain, which can in turn be transmitters or receivers. This theory provides a natural way of defining and computing macroscopic properties of such networks, by averaging over all potential geometrical patterns for the nodes. Stochastic geometry has been widely used to analyze network performance [30,31]. Andrews, et al. conducted network performance analyses for the downlink (DL) [30] and the uplink (UL) [31] of SCNs, in which user equipment (UEs) and/or base stations (BSs) were assumed to be randomly deployed according to a homogeneous Poisson point process (HPPP). Furthermore, a stochastic model of the 3D environment was used to evaluate the network performance [22, 32–34]. In [22], Ming, et al. presented a new finding that if the absolute height difference between a BS antenna and a UE antenna is larger than zero, then the ASE performance will continuously decrease toward zero with the network densification for SCNs. In [34], the authors investigated the performance of the small cell networks by considering the anisotropic path loss fading in wireless channels.

In [30] and [31], the author proposed a tractable approach to calculate the aggregation interference using the probability generating functional (PGFL) of PPP in DL and UL. In [35], the author investigated the optimal SNR, the optimal SINR with constrainting on P_B and λ_{BS} in single tier downlink, $P_B * \lambda_{BS} \leq \rho$. In [36], the authors derive the meta distribution of the SIR in Poisson Bipolar distribution which can provide information on the success probabilities of the individual links. The authors use the Poisson Bipolar model where BS is HPPP and each BS has a connected UE in a certain distace with random direction, chose a typical UE in the origin, then the success probability can be calculated. In [37] and [38], the authors calculate the meta distribution of the SINR in D2D network in millimeter wave (mm Wave). In [39], the authors calculate the meta distribution of the SINR in the Hetnet network. In [40], the author derived the meta distribution using interference cancellation where C-IC is studied. In [41], the author presents a tractable model for PB-assisted millimeter wave (mm Wave) wireless ad hoc networks where the model accounts for realistic aspects of WPT and mmWave transmissions, such as power circuit activation threshold, allowed maximum harvested power, maximum transmit power, beamforming, and blockage. In [42], the author derived exact expressions for the ergodic rate of clustered mmWave ad hoc network for uncoordinated channel access and TDMA with sectored antenna pattern. In [43], the author provides a useful upper-bound on the possible gains from different operator BS coordination inmillimeter wave (mm Wave). In [44], the author derive and optimize the exclusion radii to maximize the probability that a given D2D node can find a desired file at another node's cache within its communication range with a hardcore model. In [45], the author considers a novel approach to reduce the power consumption and improve the energy efficiency of IoT devices over cellular networks. In [46], for Poisson bipolar networks with ALOHA and Rayleigh fading, the author provides an exact analytical expression and a simple approximation for

the density of reliable links. In [47], the author proposed a mathematical framework to model BS locations of a multi-operator cellular millimeter wave (mm Wave) system, and provided analytical expressions for the SINR coverage probability as a performance metric. In [48], the author develops a framework for determining the LOS probability as a function of the number of BSs, when taking into account the correlation between blockages. In [49], the authors propose a new cellular network model in which the BS locations are modeled as the superposition of two independent stationary point processes. In [50], the authors propose a stretched exponential path loss model for downlink cellular networks. In [51], the authors investigate the coverage probability and the rate in Hetnet using a PPP based cluster model. In [52], the authors concentrate on the secure communication in millimeter wave (mm Wave) ad hoc networks by using physical layer security and derive the average achievable secrecy rate. In [53], the authors present a general framework for the coverage analysis in mm-wave networks, with arbitrary interference power distributions and antenna patterns, under the assumption that the information signal power is gamma distributed. In [54], the author examines the combined impacts of the distance-dependent Rician fading channel model and the absolute difference between the heights of base station and user equipment antennas on the coverage probability and the area spectral efficiency in an interference-limited ultra-dense small cell network. In [55], the author compares the coverage and rate performance of hybrid beamforming enabled multiuser (MU) MIMO and single-user spatial multiplexing (SM) with single-user analog beamforming (SU-BF). In [56], the authors study the performance of device-to-device (D2D) communication underlaying cellular wireless networks in terms of the meta distribution of the signal-to-interference ratio. In [57], the authors derive the downlink coverage probability of a reference receiver located at an arbitrary position on the ground assuming Nakagami-m fading for all wireless links in a finite network of unmanned aerial vehicles serving a given

region. In [58], the authors analyze UL and DL SINR distribution and mean rates in dynamic TDD enabled mmWave cellular networks. In [59], the author focuses on an analytical performance assessment of scalable video coding transmission over two-tier HCNs utilizing tools from stochastic geometry. In [60], the author derived the meta distribution using power control. In [61], using energy harvesting for user uplink, the authors derive the expressions of the energy coverage probability in order to provide comparisons between sub-6 GHz and mmWave. In [9], the author provides a unified framework to analyze the downlink outage probability in a multi-channel environment with Rayleigh fading, where D2D UEs were selected based on the average received signal strength from the nearest BS, which is equivalent to a distance-based selection. In [62], the author derives the optimal UL/DL configuration to minimize the service time of a typical small cell, and show that the UL/DL configuration that minimizes the service time also results in an optimal network EE when given the queue length distribution of small cell access points and mobile users. In [63], the author presents analytical characterizations of the ergodic spectral efficiency of cellular networks with singleuser multiple-input multiple-output and sectorization. In [17], the author derives the coverage probability and rate in a $k-\mu$ and $\eta-\mu$ fading in D2D-enhanced cellular networks. In [64], the author analyses the performance of the Hetnet using a two tier Poisson hardcore process while there is a guard zone for the first tier, so the second tier is Poisson hard-core hole process. In [65], the author analyses the initial access in mm Wave in a system level. In particular, several new system design insights have been obtained by deriving the expected initial access delay, as well as a new metric called average user-perceived downlink throughput for four sample initial access protocols. In [66], the author derived the outage probability in a two tier Hetnet with considering the dependentce of BSs. Modeling the MBS as a PPP and PBSs as the Matren cluster process, the results provide a tradeoff between accuracy and tractability. In [67],

the author derived the outage probability in a micro BS network by modeling the BS located in a Ginibre point process. In [68], the author proposed the CEA-ZF precoder, which exploits the excess spatial degrees of freedom available at massive MIMO BSs to suppress inter-cell interference at the most vulnerable UEs in the network when BS and UEs are HPPP. In [69], the author describes the two most important physical challenges, blocking and the need for strong directionality, and provided a baseline mathematical model and analysis for these systems accounting for these factors. In [70], the author models a mm Wave cellular system, where an operator that primarily owns an exclusive-use license of a certain band can sell a restricted secondary license of the same band to another operator. Using stochastic geometry, we derive expressions for the coverage and the rate of both networks, and establish the feasibility of secondary licensing in licensed mmWave bands when the secondary network has a restriction on the maximum interference it can cause to the original network. In [71], the author derived the probability of successful content delivery using the results from stochastic geometry under Rayleigh, Ricean, and Nakagami small-scale fading distributions in a D2D cellular network. In [72], the author modeled a two-level architecture of a mm Wave multi-operator system and derived the SINR and per-user rate distribution. In [73], the author models the WiFi as Micro BS and LTE as eNBs which are both HPPP. The author derives the performance metrics including the medium access probability, SINR coverage probability, density of successful transmission and rate coverage probability. In [8], the author proposes a power control algorithm to maximize the sum rate of the D2D links in one cellular network cell in which the D2D UEs are distributed as HPPP. Then the coverage probability and the sum rate are derived. In [5], the author derived the coverage probability for D2D users and the cellular user both for D2D tier overlay and underlay of the cellular tier. In [20], the author proposed a multi slope path loss model which is more practical than the single slope path loss model and derived

the coverage probability appling this path loss model. They find the coverage probability will decrease as the BS density increases after using this path loss model. In [74], the author develops a general analytical model to characterize and derive the uplink and downlink cell association in the view of the SINR and rate coverage probabilities in such a mixed deployment. In [75], the author derived a tight lower bound on the optimum number of feedback MRT for single-user when deployed in a cellular network. In [76], the author derives a general and closed-form result for the success probability in downlink MIMO HetNets by utilizing a novel Toeplitz matrix representation. The multi-user transmission in massive MIMO may lead to increased cellular-to-D2D interference. In [77], the author studied the spectral efficiency of a D2D underlaid massive MIMO system under perfect and imperfect CSI. In [78], the author developes a K tier D2D Poisson bipolar network. The analytical performance of the typical receiver is derived. The author further provides an approximation for the interference distribution by a mixture of the inverse gamma and the log-normal distributions. In [79], the author studied the performance of rateless codes in the cellular downlink and compares it with the performance of fixed-rate codes using a stochastic geometry model. In [80], the author studies a general multi-hop-based uplink communication scheme for M2M communication, and develops a new data aggregation model for M2M devices. In [81], the author proposes the use of the determinantal point process (DPP) to take into account the repulsiveness among macro BS locations in cellular network. In [82], the author developes a novel analytical framework for asynchronous wireless networks deploying multicarrier transmission over flat-fading channels. In [83], the author proposes a novel model to analyze uplink SINR and rate coverage in K-tier HCNs with load balancing and derived the uplink rate distribution in HCNs incorporating offloading and fractional power control. In [84], the author integrates self-backhauling among BSs and co-existence with a conventional macrocellular network into the analysis

of mm Wave networks and analyse the performance of the typical user in both DL and UL. In [85], the author presented a decentralized spectrum management for a shared network consisting of D2D and cellular links. In [86], the author investigated downlink multi-antenna HetNets with flexible cell selection. In [87], the author characterized the SINR CDF for a typical user for the case of user-centric BS clustering with NCJT base station cooperation. In [88], the author combines queueing theory and stochastic geometry to analyze the stability region of a static Poisson network. In [89], the author investigates the Gauss poisson process model for the wireless network. In [90] and [91], the author established the asymptotics of the SIR ccdf for arbitrary stationary cellular models and proposed a theorem that allows the calculation of a class of functionals on PPP that have the form of expected values of sum products of functions. In [92], the author investigates the throughput for wireless networks with full duplex radios using the marked PPP model. In [93], the author investigates the problem of joint beamforming design and tilt angle adaptation of the BS antenna array for maximizing energy efficiency in downlink of multi-cell multi-user coordinated cellular networks. In [94], the author investigates the impact of the elevation angle of the BS antenna pattern on the performance of the considered network and used the results of this investigation to propose a novel hybrid multicell cooperation technique. In [95], the author proposed a novel transmission technique in which intercell interference management is performed via coordinating the beamforming jointly in the horizontal and vertical planes of the wireless channel. In [96], the author considered the problem of spatiotemporal cooperation in interference limited Hetnet wireless networks. In [97], the author proposed a novel interference nulling strategy for downlink small cell networks, which means each user can identify and mitigate the dominant interference effectively.

Table 2.1 : A research map of Stochastic Geometry.

Assumptions	**downlink**	**uplink**	**dynTDD/FD**	**D2D**	**HetNet**	**UAV**
inFinite BS and UE densities	[30, 40, 41, 43, 46, 70, 73, 87, 98]	[30, 35, 36, 61, 74, 83, 99]	[58, 65, 92]	[9, 38, 45, 56, 71, 100]	[37, 59, 66, 96, 102]	[57]
Deterministic BS densities	[88]			[103]		[103]
Non-uniform BS deployment	[49, 63, 64, 81, 89]		[62]		[51]	
LoS/NLoS transmissions	[41–43, 47, 48, 52, 53, 55, 69, 72]	[61]	[58, 65]	[38, 100]		
BS/UE antenna heights	[54]					
Generalized multi-path fading	[54]			[71, 100]		[57]
Correlated shadow fading	[48, 63, 69, 84]					
variable BS transmission power		[61]				
BS vertical antenna pattern	[42, 43, 93, 95, 104]					
PF scheduler	[88]					
MIMO	[55, 63, 68, 75]		[62]	[77]	[76, 86]	

2.2 Device-to-Device Communications

The implementation of Device-to-device (D2D) communications underlying cellular networks is a promising approach to offload cellular traffic and avoid congestion in the core network [105]. Stochastic geometry, which is accurate in modeling irregular deployment of base stations and mobile user equipment, has been widely used to analyze network performance [30, 31, 56, 106–108]. Andrews, et al. conducted network performance analyses for the downlink (DL) [30] and uplink (UL) [31] of SCNs, in which UEs and/or BSs were assumed to be randomly deployed according to a homogeneous Poisson point process (HPPP). In [56], the authors developed an analytical framework for the D2D communications underlying cellular networks in the DL in terms of the meta distribution of the SIR. Moreover, [108] introduced a self-organized D2D clustering scheme to relieve the congestion on the resources using the stochastic geometry.

On the other hand, as one of the fundamental issues in the D2D communication system, the interference's management has been analyzed in the literature [5, 6, 12–14, 109]. Transmission power control [5–7], distance-based mode selection [10, 109] and a guard zone interference control scheme [12–14] have been proposed to sort this issue out. Specifically, in [5], the authors proposed a power control algorithm to manage the co-channel interference in which worldwide channel state information is needed at BSs. In [109], the authors provided a unified framework to manage the interference in a multi-channel surroundings with Rayleigh fading, where D2D UEs were chosen based on the average received signal strength from the closest BS, which correspond to a distance-based selection. These two references [5, 109] only consider the signal power and a single slope path loss model which do not distinguish LoS and NLoS, the 'guard zone' only depended on the distance from the transmitter to receiver. According to the reference [12–14], they do not only consider the power

strength of the signal or single slope pathloss model. In [12], the authors proposed a δD-interference limited area interference control scheme which is defined as the area in which the ISR (interference signal ratio) is higher than the threshold δD. The shape of the guard zone is based on the threshold δD. In [13], the authors considered both the path loss and the short-term distributions of the signal and interference, and they model the independent short-term distributions of interference as zero-mean complex Gaussian with matched conditional covariances. In [14], the authors proposed a guard zone based D2D-activation scheme by enabling the capabilities of BS interference cancellation where the guard zone is defined as a given BS-centric circular ring area.

Meanwhile, limited studies have been conducted to consider D2D networks with general fading channels, for example, in [17] and [110], the authors considered generalized fading conditions and analyzed the network performance, while they did not differentiate the path loss models between D2D links and cellular links.

There are several remaining issues, though the existent works have provided precious insights into capacity enhancement and interference management for D2D communications:

- In most research, the authors viewed D2D receiver UEs to be an extra tier of nodes, independent of the D2D transmitter UEs and the cellular UEs. Such tier of D2D receiver UEs without cellular capabilities appears from nowhere and is hard to justify in practice.

- The mode selection schemes in the literature were not very accurate. It is notable that in a number of existing works [10, 109], it was assumed that each UE ought to connect to the closest BS and choose an operation mode that is based on the distance. However, maximum received signal strength based mode selection scheme is more practical than the distance-based mode selec-

tion since in practice it is possible that the strongest received signal strength is not associated with the closest BS but the one with the minimum path loss with a LoS link.

2.3 Interference Management in Cellular Networks

As one of the fundamental problems in cellular networks, the management of the interference has been analyzed in the literature [5, 6, 12–14, 109]. In [5], Lee proposed a power control algorithm to control the co-channel interference in which global channel state information is required at BSs. In [109], Liu provided a unified framework to control the interference in a multi-channel environment with Rayleigh fading, where D2D UEs were selected based on the average received signal strength from the nearest BS, which is equivalent to a distance-based selection. A distributed power control scheme has been proposed in [11] to mitigate interference in a D2D underlaid cellular system. In [12], the author proposed an interference-limited area control scheme to mitigate the interference from cellular to D2D considering a single slope path loss model. The authors of [13] and [14] proposed novel approaches to model the interference in uplink or downlink underlaid/overlaid with Rayleigh fading and single path loss model.

Although the existing works have provided precious insights into interference management, there are remaining problems: the mode selection schemes in the literature were not very practical. Note that in some existing works [10, 109], it was assumed that each UE should connect to the nearest BS and select operation mode based on the distance. However, a maximum received signal strength based mode selection scheme is more practical than the distance-based mode selection since in practice it is possible that the strongest received signal strength is not associated with the closest BS but the one with the minimum path loss with a LoS link.

On the other hand, as the de facto standard in cellular networks, proportional

fair (PF) scheduling has been extensively studied [111–113]. In [111], the authors develops the predictive finite-horizon PF scheduling framework that exploits mobility. In [113], the authors proposed a low-complexity waterfilling-based power allocation (PA) technique, incorporated within the proportional fairness scheduler. Nevertheless, there has been no prior work on the theoretical study of the PF scheduler in the context of D2D-enhanced cellular network or UDNs. Generally speaking, the existing work on PF schedulers does not scale well with the network densification. In [114], the authors analyzed the PF scheduler to obtain cell throughput in a scenario with merely one BS. In [115], the authors studied the PF scheduler in a scenario with a limited number of BSs, which quickly becomes computationally infeasible for UDNs. In [116], only system-level simulations are studied for large-scale networks, which lacks analytical rigor. The benefits of horizontal beamforming in cellular networks are well understood. The authors in [117] considered the sectorized antennas in the analysis and investigated the performance of the network. The authors in [21] also incorporated directional beamforming by modeling the beamforming gains as marks of the base station PPPs. On the other hand, many researchers have realized that a practical antenna can target its antenna beam towards a given direction via downtilt in the vertical domain, which may be exploited to improve the network performance [24, 118–121]. For example, the authors in [24] found via an empirical study that the antenna downtilt could bring a significant improvement to cellular network capacity. In [118], the authors showed that vertical beamforming could increase the SIR by about 5-10 dB for a set of UE locations. N. Seifi and M. Coldrey investigated the performance impact of using antenna downtilt in traditional hexagonal 3D cellular networks in [119]. In [120], the author investigated, for the first time, the impact of the antenna downtilt on the coverage probability and shows the optimal antenna downtilt for two specific BS densities by simulations. In [121], the author first investigated the joint beamforming and tilt angle optimization which

maximizes the total energy efficiency in downlink transmission multi-cell cellular networks. However, most of the works investigated the impact of the antenna downtilt using field trials or simulations. To the best of our knowledge, none of the existing works have analytically studied the impact of the antenna downtilt of BSs on cellular network performance and the empirical approach in these studies limits extension of their finding to more general scenarios.

In chapter 5, we will investigate the impact of the antenna pattern and downtilt on the performance of the downlink (DL) cellular networks with a focus on analytically studying for the optimal antenna downtilt to achieve the best coverage probability of the network for a given and fixed BS density. It is important to note that our study can also be applied to drone networks flying at a certain altitude [122].

Chapter 3

Interference Management in D2D Underlaid Cellular Network

In this chapter, we address the critical issue of interference management in the network considering a practical path loss model incorporating both line-of-sight (LoS) and non-line-of-sight (NLoS) transmissions. To reduce the severe interference caused by active D2D links, we consider a mode selection scheme based on the maximum received signal strength (MRSS) for each user equipment (UE) to control the D2D-to-cellular interference. Furthermore, we analyze the performance in terms of the coverage probability and the area spectral efficiency (ASE) for both cellular network and the D2D one. Analytical results are obtained and the accuracy of the proposed analytical framework is validated through Monte Carlo simulations. Through our theoretical and numerical analyses, we quantify the performance gains brought by D2D communications in cellular networks and we find an optimum mode selection threshold β to maximize the total ASE in the network. This insight is expected to provide a design guideline for D2D mode selections.

The rest of this chapter is structured as follows: Section 3.1 provides a brief introduction of this problem. Section 3.2 describes the system model. Section 3.3 presents our theoretical analysis on the coverage probability and the area spectral efficiency (ASE) with applications in a 3GPP special case. The numerical and simulations results are discussed in Section 3.5. Our conclusions are drawn in Section 3.6.

3.1 Introduction

Driven by the 5-th generation (5G) of wireless user equipment (UE), mobile data traffic and network load are increasing in an exponential manner, and are straining current cellular networks to a breaking point [1].To deal with such monumental consumer requirement for information communications, several notable technologies have been proposed [19], such as dynamic TDD [123], small cell networks (SCNs), cognitive radio, device-to-device (D2D) communications, etc. D2D communications allow direct information transfer between a pair of neighboring mobile UEs. Because of the inadequate communication distance between such pairs of D2D UEs, D2D communications hold in great promise enhancing network performance like the coverage, spectral efficiency, energy efficiency and so on [105]. The orthogonal frequency division multiple access (OFDMA) based D2D communications adopt two types of spectrum that shares approaches in the 5G networks' standardization, (i) in-band (e.g., using cellular spectrum) or (ii) out-band (e.g., unlicensed spectrum). In particular, in the in-band D2D communications, D2D users can set their communications up in an underlay or overlay manner. More specifically, in an underlying setting, D2D users get to the same spectrum of cellular users (CUs) while in overlay, D2D users get to a dedicated proportion of cellular spectrum [124]. The major challenge in the in-band D2D-underlaid cellular network is the existence of inter-tier and intra-tier interference due to the aggressive frequency reuse, where cellular UEs and D2D UEs share the same spectrum. It is essential to design an effective interference management scheme to control the interference generated by the D2D links to the cellular links, and vice versa.

In this chapter, we show a novel mode selection scheme that is based on the maximum received signal strength for each user equipment (UE) to manage the interference. Such maximum that is received signal strength based mode selection

scheme is more realistic than the distance-based mode selection in most existent researches as in practice it is imaginable that the strongest received signal strength is not connected with the nearest BS but the one with the minimum path loss with a line-of-sight (LoS) connection. In more detail, a UE will operate in a cellular mode if its received signal strength from the strongest base station (BS) is larger than a threshold β; otherwise, it will operate in a D2D mode. This will mitigate the potential overlarge interference from the D2D links to the cellular links. To analyze the proposed interference control scheme, we develop a theoretical framework that takes power control, practical path loss model and lognormal fading into account.

Furthermore, the path loss models of cellular connections and D2D connections in a D2D-enabled cellular network are dissimilar owning to the distinction in the positions and the heights of transmitters [16]. Everyone knows that LoS transmission may happen while the distance between a receiver and a transmitter is small, and non-line-of-sight (NLoS) transmission is usual in office surroundings and in key commerce areas. Moreover, when the distance between a receiver and a transmitter declines, the probability that a LoS route occurs between them grows, thereby leading to a transition from NLoS transmission to LoS transmission with a higher probability. Because of the proximity between D2D users, it is expected that the forcible channels which make D2D communications up will be complex, undergoing both LoS and NLoS circumstances throughout these pairs, which are clearly dissimilar from traditional cellular environments [17].

3.2 System Model

In this section, the D2D communication enhanced cellular network scenario is first explained. We then present the mode selection scheme and the path loss model.

3.2.1 D2D Netwotk Model

We consider a D2D underlaid UL cellular network, where BSs and UEs, including cellular uplink UEs and D2D UEs, are assumed to be distributed on an infinite two-dimensional plane $\mathbb{R}^2$. We assume that the cellular BSs are spatially distributed according to a homogeneous PPP of intensity λ_b , i.e., $\Phi_b = \{X_i\}$, where X_i denotes the spatial locations of the ith BS. Moreover, the UEs are also distributed in the network region according to another independent homogeneous PPP Φ_u of intensity λ_u. We incorporate both NLoS and LoS transmissions into the path loss model. As a special case to show our analytical results, we consider the two-piece path loss and the liner LoS probability functions defined by the 3GPP [124], in which the path loss $\zeta(r)$, as a function of the distance r, is segmented into 2 pieces written as

$$\zeta(r) = \begin{cases} \zeta_1(r), & \text{when } 0 \leq r \leq d_1 \\ \zeta_2(r), & \text{when } r > d_1 \end{cases}, \tag{3.1}$$

where each piece $\zeta_n(r), n \in \{1, 2\}$ is modeled as

$$\zeta_n(r) = \begin{cases} \zeta_n^{\mathrm{L}}(r) = A_L r^{-\alpha_n^{\mathrm{L}}}, & \text{LoS} \\ \zeta_n^{\mathrm{NL}}(r) = A_{NL} r^{-\alpha_n^{\mathrm{NL}}}, & \text{NLoS} \end{cases}, \tag{3.2}$$

where

- $\zeta_n^{\mathrm{L}}(r)$ and $\zeta_n^{\mathrm{NL}}(r), n \in \{1, 2\}$ are the n-th piece path loss functions for the LoS transmission and the NLoS transmission, respectively,
- A_L and A_{NL} are the path losses at a reference distance $r = 1$ for the LoS and the NLoS cases, respectively,
- α_n^{L} and α_n^{NL} are the path loss exponents for the LoS and the NLoS cases, respectively.

In practice, A_L, A_{NL}, α_n^{L} and α_n^{NL} are constants obtainable from field tests and continuity constraints [125]. The adopted linear LoS probability function is very useful because it can include other LoS probability functions as its special cases [16].

Moreover, we adopt two different path loss models for cellular links as

$$\zeta_B(r)=\begin{cases} A_{BL}r^{-\alpha_{BL}}, & \text{LoS Probability: } \Pr_B^{\mathrm{L}}(r) \\ A_{BN}r^{-\alpha_{BN}}, & \text{NLoS Probability: } 1-\Pr_B^{\mathrm{L}}(r) \end{cases}, \tag{3.3}$$

together with a linear LoS probability function as follows [124],

$$\Pr_B^{\mathrm{L}}(r) = \begin{cases} 1-\frac{r}{d_B} & 0<r\leq d_B \\ 0 & r>d_B \end{cases}, \tag{3.4}$$

where 'BL' and 'BN' represent the cellular links between BS and cellular UE with LoS and NLoS links. Parameters $A_{BL} = 10^{-3.08}$, $A_{BN} = 10^{-0.27}$, $\alpha_{BL} = 2.42$, $\alpha_{BN} = 4.28$.

For D2D links,

$$\zeta_D(r)=\begin{cases} A_{DL}r^{-\alpha_{DL}}, & \text{LoS Probability: } \Pr_D^{\mathrm{L}}(r) \\ A_{DN}r^{-\alpha_{DN}}, & \text{NLoS Probability: } 1-\Pr_D^{\mathrm{L}}(r) \end{cases}, \tag{3.5}$$

and

$$\Pr_D^{\mathrm{L}}(r) = \begin{cases} 1-\frac{r}{d_D} & 0<r\leq d_D \\ 0 & r>d_D \end{cases}, \tag{3.6}$$

where 'DL' and 'DN' represent the D2D links between D2D transmitter and D2D receiver with LoS and NLoS links. Parameters $A_{DL} = 10^{-3.845}$, $A_{DN} = 10^{-5.578}$, $\alpha_{DL} = 2$, $\alpha_{DN} = 4$.Where d_B and d_D is the cut-off distance of the LoS link for UE-to-BS links and UE-to-UE links.

3.2.2 User Mode Selection Scheme

We assume two modes for UEs in the considered D2D-enabled UL cellular network namely the cellular mode and the D2D mode. Each UE is assigned with an operation mode pursuant to the maximum received DL power's comparison from its serving BS with a threshold. It is worth noting that using the downlink power for mode selection is an approximate method. Using the uplink signal as a test signal will be more accurate. However, the performance analysis of the uplink link which is UE to BS communication is particularly challenging because the UL power control mechanism operates according to the random UE positions in the network, which is quite different from the constant power setting in the DL. Moreover, implementing power control requires knowledge of the channel quality of the link. If all users sending test signals at the same time, it will cause the user of the cell edge to be easily ignored.

So, we formulate the regarded user mode selection criterion as

$$Mode = \begin{cases} \text{Cellular}, & \text{if } P^* = \max\limits_{\Phi_b} \left\{ P^{\text{rx}}_{\Phi_b} \right\} > \beta \\ \text{D2D}, & \text{otherwise} \end{cases}, \tag{3.7}$$

where the string variable $Mode$ takes the value of 'Cellular' or 'D2D' to denote the cellular mode and the D2D mode, respectively. P^{rx} is the received signal strength from a BS. In particular, for a tagged UE, if P^* is larger than a specific threshold $\beta > 0$. This UE is not appropriate to work in the D2D mode due to its potentially large interference to cellular UEs. Hence, it should operate in the cellular mode and directly connect with the strongest BS; otherwise, it should operate in the D2D mode. For a D2D UE, we adopt the same assumption in [109] that it randomly takes the role of a D2D transmitter (TU) or a D2D receiver (RU) with equal probability at the beginning of each time slot, and each D2D receiver UE selects the strongest D2D transmitter UE for its signal reception, with one D2D receiver only allowed

to connect with one D2D transmitter. The UEs which are associated with cellular BSs are referred to as cellular UEs (CUs). The distance from a CU to its associated BS is denoted by R_B. From [6], we assume CUs are distributed following a non-homogeneous PPP Φ_c. Such maximum received signal strength based mode selection scheme is more practical than the distance-based mode selection in most existing studies because in practice it is possible that the strongest received signal strength is not associated with the closest BS but the one with the minimum path loss with a LoS link.

The received power for a typical UE from a BS b can be written as

$$P_b^{\mathrm{rx}} = \begin{cases} A_{BL} P_B \mathcal{H}_{\mathrm{B}}(b) R_B^{-\alpha_{BL}} & \text{LoS} \\ A_{BN} P_B \mathcal{H}_{\mathrm{B}}(b) R_B^{-\alpha_{BN}} & \text{otherwise} \end{cases}, \tag{3.8}$$

where $A_{BL} = 10^{\frac{1}{10}A_{BL}^{\mathrm{dB}}}$ and $A_{BN} = 10^{\frac{1}{10}A_{BN}^{\mathrm{dB}}}$ denote a constant determined by the transmission frequency for BS-to-UE links in LoS and NLoS conditions, respectively. P_B is the transmission power of a BS, $\mathcal{H}_{\mathrm{B}}(b)$ is the lognormal shadowing from a BS b to the typical UE. Base on the above system model, we can obtain the intensity of CU as $\lambda_c = q\lambda_u$, where q denotes the probability of $P^* > \beta$ and will be derived in closed-form expressions in Section 3.3.1. It is apparent that the D2D UEs are distributed as a point process Φ_d, the intensity of which is $\lambda_d = (1-q)\lambda_u$. Considering that a required content file might not exist in a D2D transmitter, in reality, we assume that $\rho\%$ D2D transmitters possess the required content files and deliver them to D2D receivers. In other words, $\rho\%$ of the D2D links will eventually work in one time slot. The value of is related to the social network interest and the type of dissemination content. Base on [126], we adopt $\rho = 10\%$ in this chapter. There is no intra-cell interference between cellular UEs since we assume an orthogonal multiple access technique in a BS. Here, we consider a fully loaded network with $\lambda_u \gg \lambda_b$, so that on each time-frequency resource block, each BS has at least one active UE to serve

in its coverage area. Note that the case of $\lambda_u < \lambda_b$ is not trivial, which even changes the capacity scaling law [127]. In this chapter, we focus on the former case, and leave the study of $\lambda_u < \lambda_b$ as our future work. Generally speaking, the active CUs can be treated as a thinning PPP Φ_c with the same intensity λ_b as the cellular BSs.

Moreover, we assume a channel inversion strategy for the power control which has been standardized in 4G [124] for cellular UEs. As a result, the received signal at the BS will be a constant, we will use the results when we calculate the coverage probability of the network rather than the mode selection.

$$P_{c_i} = \begin{cases} P_0 \left(\frac{\mathrm{R_i^{\alpha_{BL}}}}{\mathcal{H}_{\mathrm{B}}(\mathrm{c_i})\mathrm{A_{BL}}} \right)^{\varepsilon} & \text{LoS} \\ P_0 \left(\frac{\mathrm{R_i^{\alpha_{BN}}}}{\mathcal{H}_{\mathrm{B}}(\mathrm{c_i})\mathrm{A_{BN}}} \right)^{\varepsilon} & \text{otherwise} \end{cases}, \tag{3.9}$$

where P_{c_i} is the transmission power of the i-th UE in cellular link, R_i is the distance of the i-th link from a CU to the target BS, $\mathcal{H}_{\mathrm{B}}(c_i)$ is the lognormal shadowing between target BS and the i-th cellular UE, $\varepsilon \in (0, 1]$ is the fractional path loss compensation, P_0 is the receiver sensitivity. For downlink BS and D2D transmitters, they use constant transmit powers P_B and P_d, respectively. This is too difficult for the UE to evaluate the position and the channel information. So, on the D2D side, we did not use power control. Using the constant power for D2D transmission has also been standardized in the industry [128]. Besides, we denote the additive white Gaussian noise (AWGN) power by σ^2. We define the coverage probability as a probability that a receiver's signal-to-interference-plus-noise ratio (SINR) is above a pre-designated threshold γ [30]:

$$p_{\mathrm{Mode}}^{\mathrm{cov}}(\lambda_{\mathrm{Mode}}, \alpha_{\mathrm{Mode}}) = \Pr[\mathrm{SINR} > \gamma], \tag{3.10}$$

where γ is the SINR threshold, the subscript string variable $Mode$ takes the value of 'Cellular' or 'D2D'. The interference in this chapter consists of the interference from both cellular UEs and D2D transmitters.

Furthermore, the area spectral efficiency in bps/Hz/km^2 can be formulated as

$$A_{Mode}^{\mathrm{ASE}}\left(\lambda_{Mode},\gamma_0\right) = \lambda_{Mode}\int_{\gamma_0}^{\infty}\log_2\left(1+x\right)f_X\left(\lambda_{Mode},\gamma_0\right)dx, \tag{3.11}$$

where γ_0 is the minimum working SINR for the considered network, and $f_X\left(\lambda_{Mode},\gamma_0\right)$ is the probability density function (PDF) of the SINR observed at the typical receiver for a particular value of λ_{Mode}. Based on the definition of $P_{Mode}\left(\lambda_{\mathrm{Mode}},\alpha_{\mathrm{Mode}}\right)$, which is the complementary cumulative distribution function (CCDF) of SINR, $f_X\left(\lambda_{Mode},x\right)$ can be computed as

$$f_X\left(\lambda_{Mode},x\right) = \frac{\partial\left(1-p_{\mathrm{Mode}}^{\mathrm{cov}}\left(x,\lambda_{Mode},\alpha_{\mathrm{Mode}}\right)\right)}{\partial x} \tag{3.12}$$

For the whole network consisting of both cellular UEs and D2D UEs, the sum ASE can be written as

$$A^{\mathrm{ASE}} = A_{\mathrm{Cellular}}^{\mathrm{ASE}} + A_{\mathrm{D2D}}^{\mathrm{ASE}}. \tag{3.13}$$

In order to make the chapter more clearly, the notations are summarized in Table 3.2.

3.3 Performance of the D2D Underlaid Cellular Network

In this section, UEs' performance is characterized in terms of their coverage probability and ASE both for the D2D tier and the cellular tier. The percentage of UE that operates in the cellular mode is derived in Section 3.3.1, the coverage probabilities of cellular UE and D2D UE are derived in Section 3.4.2.

3.3.1 User Mode Selection

We define the coverage probability as a probability that a receiver's signal-to-interference-plus-noise ratio (SINR) is above a pre-designated threshold γ [30]:

$$p_{\mathrm{Mode}}^{\mathrm{cov}}\left(\lambda_{\mathrm{Mode}},\alpha_{\mathrm{Mode}}\right) = \Pr\left[\mathrm{SINR}>\gamma\right], \tag{3.14}$$

Table 3.1 : Notations

Notations	Meaning
$p_{\mathrm{c}}^{\mathrm{cov}}$	The coverage probability of the cellular tier
λ_B	The density of the BSs
P_B	The transmit powers of BSs
P_{Mode}	P_{c_i} for the cellular UE and P_D for the D2D UE
$p_{\mathrm{D2D}}^{\mathrm{cov}}$	The coverage probability of the D2D tier
λ_u	The density of the UEs
P_d	The transmit powers of UEs

where γ is the SINR threshold, the subscript string variable $Mode$ takes the value of 'Cellular' or 'D2D'. The interference in this chapter consists of the interference from both cellular UEs and D2D transmitters. Furthermore, the area spectral efficiency in bps/Hz/km^2 can be formulated as

$$\begin{aligned} &A_{Mode}^{\mathrm{ASE}}\left(\lambda_{Mode}, \gamma_0\right) \\ &= \lambda_{Mode} \int_{\gamma_0}^{\infty} \log_2\left(1+x\right) f_X\left(\lambda_{Mode}, \gamma_0\right) dx, \end{aligned} \tag{3.15}$$

where γ_0 is the minimum working SINR for the considered network, and $f_X\left(\lambda_{Mode}, \gamma_0\right)$ is the probability density function (PDF) of the SINR observed at the typical receiver for a particular value of λ_{Mode}. Based on the definition of $P_{Mode}\left(\lambda_{\mathrm{Mode}}, \alpha_{\mathrm{Mode}}\right)$, which is the complementary cumulative distribution function (CCDF) of SINR, $f_X\left(\lambda_{Mode}, x\right)$ can be computed as

$$f_X\left(\lambda_{Mode}, x\right) = \frac{\partial\left(1 - p_{\mathrm{Mode}}^{\mathrm{cov}}\left(x, \lambda_{Mode}, \alpha_{\mathrm{Mode}}\right)\right)}{\partial x} \tag{3.16}$$

For the whole network consisting of both cellular UEs and D2D UEs, the sum ASE can be written as

$$A^{\mathrm{ASE}} = A_{\mathrm{Cellular}}^{\mathrm{ASE}} + A_{\mathrm{D2D}}^{\mathrm{ASE}}. \tag{3.17}$$

Table 3.2 : Notations

Notations	Meaning
$p_{\mathrm{c}}^{\mathrm{cov}}$	The coverage probability of the cellular tier
λ_B	The density of the BSs
P_B	The transmit powers of BSs
P_{Mode}	P_{c_i} for the cellular UE and P_D for the D2D UE
$p_{\mathrm{D2D}}^{\mathrm{cov}}$	The coverage probability of the D2D tier
λ_u	The density of the UEs
P_d	The transmit powers of UEs

In order to make the chapter more clearly, the notations are summarized in Table 3.2.

3.4 Main Results

In this section, UEs' performance is characterized in terms of their coverage probability and ASE both for the D2D tier and the cellular tier. The percentage of UE that operates in the cellular mode is derived in Section 3.4.1, the coverage probabilities of cellular UE and D2D UE are derived in Section 3.4.2.

3.4.1 Percentage of UE operating in the cellular mode

In this subsection, we present our results on the percentage of UE operating in the cellular mode and the equivalence distance distributions in the cellular mode and D2D mode, respectively. To obtain the probability of UE operate in the cellular mode, we first choose a UE as the typical UE, using the method of stochastic geometry, we can get the probability that a generic mobile UE registers to the strongest BS and operates in cellular mode.

Due to the consideration of lognormal shadowing in this mode we use the in-

tensity equivalence method in [129] to first obtain an equivalent network for further analysis. In particular, we transform the original PPP with lognormal shadowing to an equivalent PPP which has the matched intensity measure and intensity. More specifically, define $\overline{R}_i^{BL} = \mathcal{H}_{\mathrm{B}}^{-1/\alpha_{\mathrm{BL}}} R_i^{BL}$ and $\overline{R}_i^{BN} = \mathcal{H}_{\mathrm{B}}^{-1/\alpha_{\mathrm{BN}}} R_i^{BN}$, where R_i^{BL} and R_i^{BN} are the distance separating a typical user from its tagged strongest base station with LoS and NLoS. $\overline{R}_i^{BL}$ and $\overline{R}_i^{BN}$ is the equivalent distance separating a typical user from its tagged nearest base station in the new PPP with a LoS or NLoS link. $\mathcal{H}_B$ is the lognormal shadowing between target BS and the UE.

The network consists of two non-homogeneous PPPs with intensities $\lambda p^{NL}(R_i)$ and $\lambda p^{L}(R_i)$, which representing the sets of NLoS and LoS links respectively. Each UE is associated with the strongest transmitter. Moreover, intensities $\lambda^{NL}(\cdot)$ and $\lambda^{L}(\cdot)$ are given by

$$\lambda^{NL}(t) = \frac{d}{dt} \Lambda^{NL}\left([0,t]\right) \tag{3.18}$$

and

$$\lambda^{L}(t) = \frac{d}{dt} \Lambda^{L}\left([0,t]\right) \tag{3.19}$$

respectively, where

$$\Lambda^{NL}\left([0,t]\right) = \mathbb{E}_{\mathcal{H}_{\mathcal{B}}}\left[2\pi\lambda_b \int_0^{t(\mathcal{H}_{\mathcal{B}})^{1/\alpha_{BN}}} p^{NL}(r) r dr\right] \tag{3.20}$$

and

$$\Lambda^{L}\left([0,t]\right) = \mathbb{E}_{\mathcal{H}_{\mathcal{B}}}\left[2\pi\lambda_b \int_0^{t(\mathcal{H}_{\mathcal{B}})^{1/\alpha_{BL}}} p^{L}(r) r dr\right]. \tag{3.21}$$

Similar definitions are adopted to D2D tier as well. The transformed network has the exact same performance for the typical receiver (BS or D2D RU) on the coverage probability with the original network. In the following, we present our first result in Lemma 2, which will be used in the later analysis of the coverage probability.

Lemma 1. *The percentage of typical UE operates in the cellular mode q is given by*

$$q = 1 - \exp\left[-\mathbb{E}_{\mathcal{H}_\mathcal{B}}\left[2\pi\lambda_b \int_0^{\left(\frac{P_B A_{BL}\mathcal{H}_\mathcal{B}}{\beta}\right)^{1/\alpha_{BL}}} p^L(r) r dr\right]\right.$$
$$\left. - \mathbb{E}_{\mathcal{H}_\mathcal{B}}\left[2\pi\lambda_b \int_0^{\left(\frac{P_B A_{BN}\mathcal{H}_\mathcal{B}}{\beta}\right)^{1/\alpha_{BN}}} p^{NL}(r) r dr\right]\right], \tag{3.22}$$

and the percentage that the UE operating in the D2D mode is $(1-q)$.

Proof. The probability that the RSS is larger than the threshold is given by

$$P = \Pr\left[\max_b \{P_b^{\mathrm{rx}}\} > \beta\right], \tag{3.23}$$

where we use the standard power loss propagation model with a path loss exponent α_{BL} (for LoS UE-BS links) and α_{BN} (for NLoS UE-BS links).The probability that a generic mobile UE operates in the cellular mode i

$$\begin{aligned} q &= 1 - \Pr\left[\max_b \{P_b^{\mathrm{rx}}\} \leq \beta\right] \\ &= 1 - \Pr\left[\max\{P_{LoS}^{rx}\} \leq \beta \cap \max\{P_{NLoS}^{rx}\} \leq \beta\right] \\ &= 1 - \Pr\left[\min \overline{R}_i^{BL} \geq \left(\frac{P_B \mathrm{A}_{BL}}{\beta}\right)^{1/\alpha_{BL}}\right. \\ &\cap \quad \left.\min \overline{R}_i^{BN} \geq \left(\frac{P_B \mathrm{A}_{BN}}{\beta}\right)^{1/\alpha_{BN}}\right] \end{aligned} \tag{3.24}$$

which means there is no nodes in the disk around the typical UE with a radius $\left(\frac{P_B \mathrm{A}_{BL}}{\beta}\right)^{1/\alpha_{BL}}$ when the link is LoS, and there is no nodes in the disk around the typical UE with a radius $\left(\frac{P_B \mathrm{A}_{BN}}{\beta}\right)^{1/\alpha_{BN}}$ when the link is NLoS. Therefore,

$$\begin{aligned} q =& 1 - \exp\left[-\wedge^{\mathrm{NL}}\left(\left[0, \left(\frac{P_B \mathrm{A}_{BL}}{\beta}\right)^{1/\alpha_{BL}}\right]\right)\right] \\ &\times \exp\left[-\wedge^{\mathrm{L}}\left[0, \left(\frac{P_B \mathrm{A}_{BN}}{\beta}\right)^{1/\alpha_{BN}}\right]\right] \end{aligned}$$

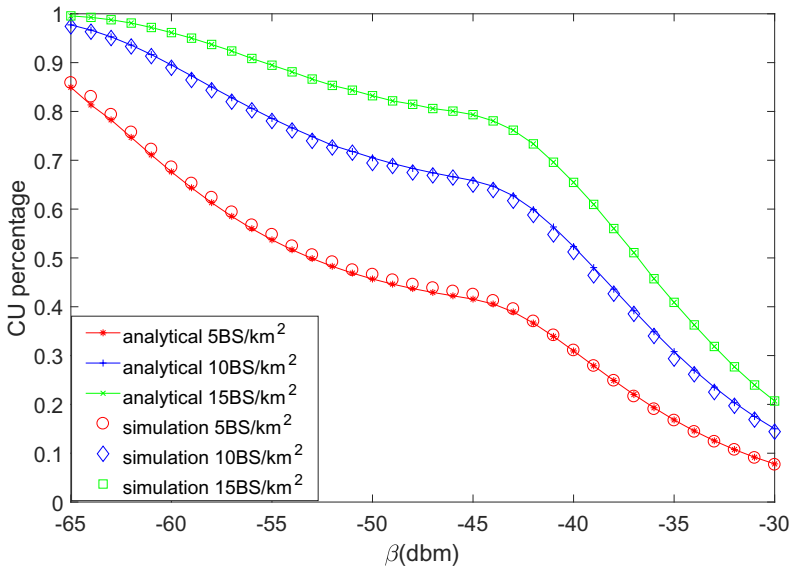

Figure 3.1 : The probability for a UE to operate in the cellular mode vary the RSS threshold β , $\mathrm{P}_B = 46\mathrm{dBm}$

$$
\begin{aligned}
=&1-\exp\left[-\mathbb{E}_{\mathcal{H}_\mathcal{B}}\left[2\pi\lambda_b\int_0^{\left(\frac{P_B \mathrm{A}_{BL}\mathcal{H}_\mathcal{B}}{\beta}\right)^{\frac{1}{\alpha_{BL}}}} p^L(r)rdr\right]\right]\\
&\times\exp\left[-\mathbb{E}_{\mathcal{H}_\mathcal{B}}\left[2\pi\lambda_b\int_0^{\left(\frac{P_B \mathrm{A}_{BN}\mathcal{H}_\mathcal{B}}{\beta}\right)^{\frac{1}{\alpha_{BN}}}} p^{NL}(r)rdr\right]\right], \qquad (3.25)
\end{aligned}
$$

which concludes our proof. □

Note that Eq.(4.17) explicitly account for the effects of shadow fading, pathloss, transmit power, spatial distribution of BSs and mode selection threshold β . From the result, one can see that the HPPP ϕ_u can be divided into two point processes: the PP with intensity $q\lambda_u$ and the PP with intensity $(1-q)\lambda_u$. Same as in [6,109], We assume the two PPs which representing cellular UEs and D2D UEs are independent.

This figure illustrates the probability for a UE to operate in the cellular mode based on Eq.(4.17). It can be seen that the simulation results perfectly match the analytical results. From the figure, we can find that the value increases by

approximately to -37 dBm and -35 dBm when the BS intensity is 10BS/km^2 and 15BS/km^2, respectively. It indicates that the percentage of CUs will increase as the BS intensity grows.

3.4.2 Coverage Probabality of D2D-Enhanced Cellular Network

In this subsection, we investigate the coverage probability that a receiver's signal-to-interference-plus-noise ratio (SINR) is above a pre-designated threshold γ:

$$p_{\text{Mode}}^{\text{cov}}(\lambda_{\text{Mode}}, \gamma) = \Pr[\text{SINR} > \gamma] \tag{3.26}$$

where γ is the SINR threshold, the subscript string variable $Mode$ takes the value of 'Cellular' or 'D2D'. The SINR can be calculated as

$$\text{SINR} = \frac{P_{Mode}\zeta_{Mode}(r)\mathcal{H}_{Mode}}{I_{cellular} + I_{d2d} + N_0}, \tag{3.27}$$

where $\mathcal{H}_{\text{Mode}}$ is the lognormal shadowing between transmitter and receiver in cellular mode or D2D mode. P_B, P_d and N_0 are the transmission power of each cellular and D2D UE transmitter and the additive white Gaussian noise (AWGN) power at each receiver, respectively. Based on the path loss model in Eq.(5.40) and the equivalence method in subsection 3.4.1, we present our main result on $p_c^{\text{cov}}(\lambda, \gamma)$ in Theorem 1.

Theorem 1. *For the typical BS which is located at the origin, considering the path loss model in Eq.(5.40) and the equivalence method, the coverage probability* $p_c^{\text{cov}}(\lambda, \gamma)$ *can be derived as*

$$p_c^{\text{cov}}(\lambda, \gamma) = T_c^{\text{L}} + T_c^{\text{NL}}, \tag{3.28}$$

where

$$T_c^{\text{L}} = \int_0^{t_{LoS}} \left(\int_{-\infty}^{\infty} \left[\frac{1 - \mathrm{e}^{-\mathrm{i}\omega/\gamma}}{2\pi\mathrm{i}\omega} \right] \mathcal{F}_{\frac{1}{\text{SINR}^{\text{L}}}}(\omega) d\omega \right) \times f_{\overline{R_{LCU}}}(r) dr \tag{3.29}$$

and

$$T_c^{\mathrm{NL}} = \int_0^{t_{NLoS}} \left(\int_{-\infty}^{\infty} \left[\frac{1 - \mathrm{e}^{-\mathrm{i}\omega/\gamma}}{2\pi \mathrm{i}\omega} \right] \mathcal{F}_{\frac{1}{\mathrm{SINR}^{\mathrm{NL}}}}(\omega) d\omega \right), \times f_{\overline{R_{NLCU}}}(r) dr \tag{3.30}$$

$$t_{LoS} = \left(\frac{\beta}{P_B A_{BL}} \right)^{-1/\alpha_{BL}} \tag{3.31}$$

and

$$t_{NLoS} = \left(\frac{\beta}{P_B A_{BN}} \right)^{-1/\alpha_{BN}}, \tag{3.32}$$

$f_{\overline{R_{LCU}}}(r)$ *and* $f_{\overline{R_{NLCU}}}(r)$ *, are represented by*

$$\begin{aligned} f^{\mathrm{L}}_{\overline{R_{LCU}}}(r) = \exp & \left(- \int_0^{\overline{r_1}} \left(\Pr^{\mathrm{NL}}(u) \right) \lambda_B^{NL}(u) du \right) \\ & \times \exp \left(- \int_0^{r} \Pr^{\mathrm{L}}(u) \lambda_B^{L}(u) du \right) \\ & \times \Pr^{\mathrm{L}}(r) \lambda_B^{L}(r)/q \end{aligned} \tag{3.33}$$

and

$$\begin{aligned} f^{\mathrm{NL}}_{\overline{R_{NLCU}}}(r) = \exp & \left(- \int_0^{\overline{r_2}} \Pr^{\mathrm{L}}(u) \lambda(u) du \right) \\ & \times \exp \left(- \int_0^{r} \left(\Pr^{\mathrm{NL}}(u) \right) \lambda_B^{NL}(u) du \right) \\ & \times \Pr^{\mathrm{NL}}(r) \lambda_B^{NL}(r)/q \end{aligned} \tag{3.34}$$

where $\overline{r_1}$ and $\overline{r_2}$ are given implicitly by the following equations as

$$\overline{r_1} = \underset{\overline{r_1}}{\arg} \left\{ \zeta^{\mathrm{NL}}(\overline{r_1}) = \zeta_n^{\mathrm{L}}(\overline{r}) \right\} \tag{3.35}$$

and

$$\overline{r_2} = \underset{\overline{r_2}}{\arg} \left\{ \zeta^{\mathrm{L}}(\overline{r_2}) = \zeta_n^{\mathrm{NL}}(\overline{r}) \right\}. \tag{3.36}$$

In addition, $\mathcal{F}_{\frac{1}{SINR^{L}}}(\omega)$ and $\mathcal{F}_{\frac{1}{SINR^{NL}}}(\omega)$ are respectively computed by follows.

$\mathcal{F}_{\frac{1}{SINR^L}}(\omega)$ can be written as three parts, namely $\mathcal{L}_{\mathrm{I_c}}(\omega)$, $\mathcal{L}_{\mathrm{I_d}}(\omega)$ and $\mathcal{L}_{\mathrm{n}}(\omega)$,

$$\begin{aligned}\mathcal{L}_{\mathrm{I_c}}(\omega) &= \exp\left(\mathrm{i}\omega\frac{\mathrm{I_{CL}}+\mathrm{I_{CN}}}{\mathrm{S^L}}\right)\\ &= \exp\left\{-\int_r^{\infty}\left(1-\int_0^{t_{LoS}}\exp\left(\mathrm{i}\omega\frac{\left(\mathrm{z}^{\alpha_{\mathrm{BL}}}\right)^{\varepsilon}\mathrm{v}^{-\alpha_{\mathrm{BL}}}}{\mathrm{A_{BL}^{2\varepsilon}}\left(\mathrm{r}^{-\alpha^{\mathrm{BL}}}\right)^{1-\varepsilon}}\right)\right.\right.\\ &\quad \left.f_{\overline{R_{LCU}}}(z)dz\right)\lambda_B^L(v)dv\\ &\quad -\int_r^{\infty}\left(1-\int_0^{t_{LoS}}\exp\left(\mathrm{i}\omega\frac{\left(\mathrm{z}^{\alpha_{\mathrm{BL}}}\right)^{\varepsilon}\mathrm{v}^{-\alpha_{\mathrm{BN}}}}{\mathrm{A_{BL}^{2\varepsilon}}\left(\mathrm{r}^{-\alpha^{\mathrm{BL}}}\right)^{1-\varepsilon}}\right)\right.\\ &\quad \left.\left.f_{\overline{R_{LCU}}}(z)dz\right)\lambda_B^{NL}(v)dv\right\}\end{aligned} \tag{3.37}$$

and

$$\begin{aligned}\mathcal{L}_{\mathrm{I_d}}(\omega) &= \exp\left(\mathrm{i}\omega\frac{\mathrm{I_{DL}}+\mathrm{I_{DN}}}{\mathrm{S^L}}\right)\\ &= \exp\left\{-\int_{t_{LoS}}^{\infty}\left(1-\exp\left(\mathrm{i}\omega\frac{\mathrm{P_dA_{BL}v}^{-\alpha_{\mathrm{BL}}}}{\mathrm{P_0}\left(\mathrm{A_{BL}r}^{-\alpha^{\mathrm{BL}}}\right)^{1-\varepsilon}}\right)\right.\right.\\ &\quad \left.\lambda_{tu}^L(v)dv\right.\\ &\quad \left.-\int_{t_{LoS}}^{\infty}\left(1-\exp\left(\mathrm{i}\omega\frac{\mathrm{P_dA_{BN}v}^{-\alpha_{\mathrm{BN}}}}{\mathrm{P_0}\left(\mathrm{A_{BL}r}^{-\alpha^{\mathrm{BL}}}\right)^{1-\varepsilon}}\right)\right)\lambda_{tu}^{NL}(v)dv\right\}\end{aligned} \tag{3.38}$$

and $\mathcal{L}_{\mathrm{n}}(\omega) = \exp\left(\mathrm{iw}\frac{\sigma^2}{\mathrm{P_0}\left(\mathrm{A_{BL}r}^{-\alpha^{\mathrm{BL}}}\right)^{1-\varepsilon}}\right)$ which are the cellular interference , D2D interference and noise part in characteristic function.

$$\mathcal{F}_{\frac{1}{SINR^{NL}}}(\omega) =$$

$$\begin{aligned}
&\exp\left\{-\int_r^{\infty}\left(1-\int_0^{t_{NLoS}}\exp\left(\frac{\mathrm{i}\omega \mathrm{z}^{\varepsilon\alpha_{\mathrm{BL}}}\mathrm{A}_{\mathrm{BL}}\mathrm{v}^{-\alpha_{\mathrm{BL}}}}{\mathrm{A}_{\mathrm{BL}}^{\varepsilon}\left(\mathrm{A}_{\mathrm{BN}}\mathrm{r}^{-\alpha^{\mathrm{BN}}}\right)^{1-\varepsilon}}\right)\right.\right.\\
&\left.\times f_{\overline{R_{NLCU}}}(z)dz\right)\lambda_B^L(v)dv\\
&-\int_r^{\infty}\left(1-\int_0^{t_{NLoS}}\exp\left(\frac{\mathrm{i}\omega \mathrm{z}^{\varepsilon\alpha_{\mathrm{BL}}}\mathrm{A}_{\mathrm{BN}}\mathrm{v}^{-\alpha_{\mathrm{BN}}}}{\mathrm{A}_{\mathrm{BL}}^{\varepsilon}\left(\mathrm{A}_{\mathrm{BN}}\mathrm{r}^{-\alpha^{\mathrm{BN}}}\right)^{1-\varepsilon}}\right)\right.\\
&\left.\times f_{\overline{R_{NLCU}}}(z)dz\right)\lambda_B^{NL}(v)dv\\
&-\int_{t_{NLoS}}^{\infty}\left(1-\exp\left(\frac{\mathrm{i}\omega \mathrm{P}_{\mathrm{d}}\mathrm{A}_{\mathrm{BL}}\mathrm{v}^{-\alpha_{\mathrm{BL}}}}{\mathrm{P}_0\left(\mathrm{A}_{\mathrm{BN}}\mathrm{r}^{-\alpha^{\mathrm{BN}}}\right)^{1-\varepsilon}}\right)\right)\lambda_{tu}^L(v)dv\\
&-\int_{t_{NLoS}}^{\infty}\left(1-\exp\left(\frac{\mathrm{i}\omega \mathrm{P}_{\mathrm{d}}\mathrm{A}_{\mathrm{BN}}\mathrm{v}^{-\alpha_{\mathrm{BN}}}}{\mathrm{P}_0\left(\mathrm{A}_{\mathrm{BN}}\mathrm{r}^{-\alpha^{\mathrm{BN}}}\right)^{1-\varepsilon}}\right)\right)\lambda_{tu}^{NL}(v)dv\\
&+\frac{\mathrm{i}\omega\sigma_{\mathrm{c}}^2}{\mathrm{P}_0\left(\mathrm{A}_{\mathrm{BN}}\mathrm{r}^{-\alpha^{\mathrm{BN}}}\right)^{1-\varepsilon}}\Bigg\}
\end{aligned}\tag{3.39}$$

It gives general results that can be applied to various multi-path fading or shadowing model, e.g., Rayleigh fading, Nakagami-m fading, etc, and various NLoS/LoS transmission models as well. When the mode selection threshold β increases, we can find the intensity of D2D transmitter also increases. This will reduce the coverage probability performance of cellular tier, so we make $p_c^{\mathrm{cov}} > \delta$ as a condition to guarantee the performance for the cellular mode when choosing β for the optimal system ASE. Alike to the analysis in cellular mode, we concentrate on a typical D2D UE located at the origin o and scheduled to pick up information from another D2D UE. Following Slivnyak's theorem, the coverage probability result derived for the typical D2D UE also holds for any generic D2D UE located at any location.

Theorem 2. *For a typical D2D receiver, the probability of coverage $p_{D2D}^{\mathrm{cov}}(\lambda,\gamma)$ can be derived as*

$$p_{D2D}^{\mathrm{cov}}(\lambda,\gamma) = T_{D2D}^{\mathrm{L}} + T_{D2D}^{\mathrm{NL}},\tag{3.40}$$

where

$$T_{D2D}^{\mathrm{L}} = \int_0^{\infty} \left(\int_{-\infty}^{\infty} \left[\frac{1 - \mathrm{e}^{-\mathrm{i}\omega/\gamma}}{2\pi \mathrm{i}\omega} \right] \mathcal{F}_{\frac{1}{\mathrm{SINR}_{\mathrm{D2D}}^{\mathrm{L}}}}(\omega) d\omega \right) \times f_{\overline{R_{LD2D}}}(\overline{R_{d,0}}) d\overline{R_{d,0}} \tag{3.41}$$

and

$$T_{D2D}^{\mathrm{NL}} = \int_0^{\infty} \left(\int_{-\infty}^{\infty} \left[\frac{1 - \mathrm{e}^{-\mathrm{i}\omega/\gamma}}{2\pi \mathrm{i}\omega} \right] \mathcal{F}_{\frac{1}{\mathrm{SINR}_{\mathrm{D2D}}^{\mathrm{NL}}}}(\omega) d\omega \right) \times f_{\overline{R_{NLD2D}}}(\overline{R_{d,0}}) d\overline{R_{d,0}}, \tag{3.42}$$

$f_{\overline{R_{LD2D}}}(r)$ and $f_{\overline{R_{NLD2D}}}(r)$ can be calculated from cumulative distribution function (CDF) of $\overline{R}_d^{LOS}$ and $\overline{R}_d^{NLOS}$ in appendix C.

In addition, $\mathcal{F}_{\frac{1}{SINR_{D2D}^{L}}}(\omega)$ and $\mathcal{F}_{\frac{1}{SINR_{D2D}^{NL}}}(\omega)$ are respectively computed by

$$\begin{aligned}
\mathcal{F}_{\frac{1}{SINR_{D2D}^{L}}}(\omega) = \\
&\exp\left\{ - \int_0^{\infty} \left(1 - \int_0^{t_{LoS}} \exp\left(\frac{\mathrm{i}\omega \mathrm{P}_0 \overline{\mathrm{R}}_{\mathrm{i}}^{\varepsilon\alpha_{\mathrm{BL}}} \mathrm{v}^{-\alpha_{\mathrm{DL}}}}{\mathrm{A}_{\mathrm{BL}}^{\varepsilon} \mathrm{P}_{\mathrm{d}} (\overline{\mathrm{R}_{\mathrm{d},0}})^{-\alpha_{\mathrm{DL}}}} \right) \right. \right. \\
&\left. \times f_{\overline{R_{LCU}}}(\overline{R}_i) d\overline{R}_i \right) \lambda_B^L(v) dv \\
&- \int_0^{\infty} \left(1 - \int_0^{t_{LoS}} \exp\left(\frac{\mathrm{i}\omega \mathrm{P}_0 \overline{\mathrm{R}}_{\mathrm{i}}^{\varepsilon\alpha_{\mathrm{BL}}} \mathrm{A}_{\mathrm{DN}} \mathrm{v}^{-\alpha_{\mathrm{DN}}}}{\mathrm{A}_{\mathrm{BL}}^{\varepsilon} \mathrm{P}_{\mathrm{d}} \mathrm{A}_{\mathrm{DL}} (\overline{\mathrm{R}_{\mathrm{d},0}})^{-\alpha_{\mathrm{DL}}}} \right) \right. \\
&\left. \times f_{\overline{R_{LCU}}}(\overline{R}_i) d\overline{R}_i \right) \lambda_B^{NL}(v) dv \\
&- \int_r^{\infty} \left(1 - \exp\left(\frac{\mathrm{i}\omega \mathrm{v}^{-\alpha_{\mathrm{DL}}}}{(\overline{\mathrm{R}_{\mathrm{d},0}})^{-\alpha_{\mathrm{DL}}}} \right) \right) \lambda_{tu}^L(v) dv \\
&- \int_r^{\infty} \left(1 - \exp\left(\frac{\mathrm{i}\omega \mathrm{A}_{\mathrm{DN}} \mathrm{v}^{-\alpha_{\mathrm{DN}}}}{\mathrm{A}_{\mathrm{DL}} (\overline{\mathrm{R}_{\mathrm{d},0}})^{-\alpha_{\mathrm{DL}}}} \right) \right) \lambda_{tu}^{NL}(v) dv \\
&+ \frac{\mathrm{i}\omega \sigma_{\mathrm{d}}^2}{\mathrm{P}_{\mathrm{d}} \mathrm{A}_{\mathrm{DL}} (\overline{\mathrm{R}_{\mathrm{d},0}})^{-\alpha_{\mathrm{DL}}}} \Bigg\}
\end{aligned} \tag{3.43}$$

and

$$\mathcal{F}_{\frac{1}{SINR_{D2D}^{NL}}}(\omega) =$$

$$\begin{aligned}
&\exp\left\{-\int_0^{\infty}\left(1-\int_0^{t_{NLoS}}\exp\left(\frac{\mathrm{i}\omega \mathrm{P}_0\overline{\mathrm{R}_\mathrm{i}}^{\varepsilon\alpha_{\mathrm{BL}}}\mathrm{A}_{\mathrm{DL}}\mathrm{v}^{-\alpha_{\mathrm{DL}}}}{\mathrm{A}_{\mathrm{BL}}^{\varepsilon}\mathrm{P}_\mathrm{d}\mathrm{A}_{\mathrm{DN}}(\overline{\mathrm{R}_{\mathrm{d},0}})^{-\alpha_{\mathrm{DN}}}}\right)\right.\right.\\
&\left.\times f_{\overline{R_{NLCU}}}(\overline{R}_i)d\overline{R}_i\right)\lambda_B^L(v)dv\\
&-\int_0^{\infty}\left(1-\int_0^{t_{NLoS}}\exp\left(\frac{\mathrm{i}\omega \mathrm{P}_0\overline{\mathrm{R}_\mathrm{i}}^{\varepsilon\alpha_{\mathrm{BL}}}\mathrm{v}^{-\alpha_{\mathrm{DN}}}}{\mathrm{A}_{\mathrm{BL}}^{\varepsilon}\mathrm{P}_\mathrm{d}(\overline{\mathrm{R}_{\mathrm{d},0}})^{-\alpha_{\mathrm{DN}}}}\right)\right.\right.\\
&\left.\times f_{\overline{R_{NLCU}}}(\overline{R}_i)d\overline{R}_i\right)\lambda_B^{NL}(v)dv\\
&-\int_r^{\infty}\left(1-\exp\left(\frac{\mathrm{i}\omega \mathrm{A}_{\mathrm{DL}}\mathrm{v}^{-\alpha_{\mathrm{DL}}}}{\mathrm{A}_{\mathrm{DN}}(\overline{\mathrm{R}_{\mathrm{d},0}})^{-\alpha_{\mathrm{DN}}}}\right)\right)\lambda_{tu}^L(v)dv\\
&-\int_r^{\infty}\left(1-\exp\left(\frac{\mathrm{i}\omega \mathrm{v}^{-\alpha_{\mathrm{DN}}}}{(\overline{\mathrm{R}_{\mathrm{d},0}})^{-\alpha_{\mathrm{DN}}}}\right)\right)\lambda_{tu}^{NL}(v)dv\\
&+\left.\frac{\mathrm{i}\omega\sigma_\mathrm{d}^2}{\mathrm{P}_\mathrm{d}\mathrm{A}_{\mathrm{DN}}(\overline{\mathrm{R}_{\mathrm{d},0}})^{-\alpha_{\mathrm{DN}}}}\right\},
\end{aligned} \tag{3.44}$$

where $A_{DL} = 10^{\frac{1}{10}A_{DL}^{dB}}$ *and* $A_{DN} = 10^{\frac{1}{10}A_{DN}^{dB}}$ *denote a constant determined by the transmission frequency for UE-to-UE links in LoS and NLoS, respectively.*

Proof. The typical D2D receiver selects the equivalent nearest UE as a potential transmitter. If the potential D2D transmitter is operating in a cellular mode, D2D RU must search for another transmitter. We approximately consider that the second neighbor can be found as the transmitter under this situation both for LoS/NLoS links. In order to evaluate the accuracy of this approximation, we use the results which did not distinguish LoS/NLoS, but added mode selection, compared with simulation results.

As can be seen from the results, the error of this estimation is small, especially when the link distance is 0 to 40 meters. The approximate cumulative distribution

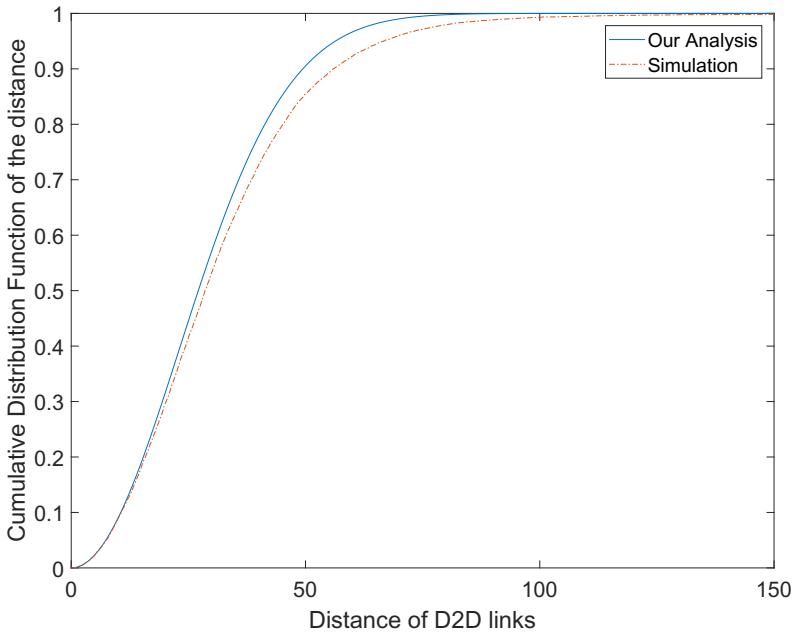

Figure 3.2 : The D2D links distance (m) with simulation and using the second neighbor approximation.

function (CDF) of $\overline{R}_d^{LoS}$ can be written as

$$\begin{aligned}
\Pr\left[\overline{R}_d^{LoS} < R\right] \approx & \int_{R+t_L}^{\infty} \left(\int_0^R f_{R_d^L}(\overline{R}_d) d\overline{R}_d \right) f_{r_1^L}(r_1) dr_1 \\
& + \int_{t_L}^{R+t_L} \left(\int_0^{r_1 - t_L} f_{R_d}(\overline{R}_d) d\overline{R}_d \right. \\
& + \int_{r_1 - t_L}^{R} (1 - P_c^L) \cdot f_{R_d^L}(\overline{R}_d) d\overline{R}_d \\
& \left. + \int_{r_1 - t_L}^{R} P_c^L \cdot f_{R_{d_2}^L}\left(\overline{R}_d\right) d\overline{R}_d \right) f_{r_1^L}(r_1) dr_1 \\
& + \int_{R+t_{NL}}^{\infty} \left(\int_0^R f_{R_d^L}(\overline{R}_d) d\overline{R}_d \right) f_{r_1^{NLoS}}(r_1) dr_1 \\
& + \int_{t_{NL}}^{R+t_{NL}} \left(\int_0^{r_1 - t} f_{R_d^L}(\overline{R}_d) d\overline{R}_d \right. \\
& + \int_{r_1 - t_{NL}}^{R} (1 - P_c^L) \cdot f_{R_d^L}(\overline{R}_d) d\overline{R}_d \\
& \left. + \int_{r_1 - t_{NL}}^{R} P_c^L \cdot f_{R_{d_2}^L}\left(\overline{R}_d\right) d\overline{R}_d \right) f_{r_1^{NL}}(r_1) dr_1, \qquad (3.45)
\end{aligned}$$

where r_1 is the equivalent distance from TU to the strongest LoS/NLoS BS, P_c^L and

$P_c^{NL}$is the probability of a D2D receiver be a CU with LoS and NLoS.

$$\begin{aligned} f_{r_1^L}(r) = &\exp\left[-\Lambda^L\left([0,r]\right)\right] \\ &\times \exp\left[-\Lambda^{NL}\left([0,\overline{r_1}]\right)\right] \\ &\times \Pr_{\mathrm{B}}^{\mathrm{L}}(r)\,\lambda_B^L(r)/\left(1-q\right) \end{aligned} \tag{3.46}$$

and

$$\begin{aligned} f_{r_1^{NL}}(r) = &\exp\left[-\Lambda^{NL}\left([0,r]\right)\right] \\ &\times \exp\left[-\Lambda^{L}\left([0,\overline{r_1}]\right)\right] \\ &\times \Pr_{\mathrm{B}}^{\mathrm{NL}}(r)\,\lambda_B^{NL}(r)/\left(1-q\right) \end{aligned} \tag{3.47}$$

According to [16], if there is no difference between CUs and D2D UEs, the pdf of the distance for a tier of PPP LoS UEs is

$$\begin{aligned} f_{R_d^L}(r) = &\exp\left(-\int_0^{\overline{r_1}} \Pr_{\mathrm{D}}^{\mathrm{NL}}(u)\,\lambda_u^{NL}(u)du\right) \\ &\times \exp\left(-\int_0^{r} \Pr_{\mathrm{D}}^{\mathrm{L}}(u)\,\lambda_u^{L}(u)du\right) \\ &\times \Pr_{\mathrm{D}}^{\mathrm{L}}(r)\,\lambda_u^L(r) \end{aligned} \tag{3.48}$$

and if there is no difference between CUs and D2D UEs, the pdf of the distance for a tier of PPP NLoS UEs is

$$\begin{aligned} f_{R_d^{NL}}(r) = &\exp\left(-\int_0^{\overline{r_2}} \Pr_{\mathrm{D}}^{\mathrm{L}}(u)\,\lambda_u^{L}(u)du\right) \\ &\times \exp\left(-\int_0^{r} \Pr_{\mathrm{D}}^{\mathrm{NL}}(u)\,\lambda_u^{NL}(u)du\right) \\ &\times \Pr_{\mathrm{D}}^{\mathrm{NL}}(r)\,\lambda_u^{NL}(r), \end{aligned} \tag{3.49}$$

where

$$\begin{aligned} &\lambda_u^L(r) \\ &= \frac{d}{dt}\left(\mathbb{E}_{\mathcal{H}_\mathcal{D}}\left[2\pi\left(1-q\right)\lambda_u \int_0^{t(\mathcal{H}_\mathcal{D})^{\frac{1}{\alpha_{DL}}}} \Pr_{\mathrm{D}}^{\mathrm{L}}(r) r dr\right]\right) \end{aligned} \tag{3.50}$$

and

$$\lambda_u^{NL}(r) = \frac{d}{dt}\left(\mathbb{E}_{\mathcal{H}_\mathcal{D}}\left[2\pi\left(1-q\right)\lambda_u\int_0^{t(\mathcal{H}_\mathcal{D})^{\frac{1}{\alpha_{DN}}}}\Pr_{\mathrm{D}}^{\mathrm{NL}}(r)rdr\right]\right). \tag{3.51}$$

According to [130] , the second neighbor point is distributed as

$$f_{R_{d_2}^L}(r) = 2\pi^2 r^3 \lambda_u^L(t)^2 \times \exp\left[-\mathbb{E}_{\mathcal{H}_\mathcal{D}}\left[2\pi\lambda_u\int_0^{r(\mathcal{H}_\mathcal{D})^{\frac{1}{\alpha_{DL}}}}\Pr_{\mathrm{D}}^{\mathrm{L}}rdr\right]\right] \tag{3.52}$$

and

$$f_{R_{d_2}^{NL}}(r) = 2\pi^2 r^3 \lambda_u^{NL}(t)^2 \times \exp\left[-\mathbb{E}_{\mathcal{H}_\mathcal{D}}\left[2\pi\lambda_u\int_0^{r(\mathcal{H}_\mathcal{D})^{\frac{1}{\alpha_{DN}}}}\Pr_{\mathrm{D}}^{\mathrm{NL}}rdr\right]\right]. \tag{3.53}$$

similarity, the cdf of the distance of NLoS D2D signal can be written as

$$\begin{aligned}\Pr\left[\overline{R}_d^{NL} < R\right] \approx & \int_{R+t_L}^{\infty}\left(\int_0^R f_{R_d^{NL}}(\overline{R}_d)d\overline{R}_d\right)f_{r_1^L}(r_1)dr_1 \\ & + \int_{t_L}^{R+t_L}\left(\int_0^{r_1-t_L} f_{R_d^{NL}}(\overline{R}_d)d\overline{R}_d\right. \\ & + \int_{r_1-t_L}^{R}(1-P_c^{NL})\cdot f_{R_d^{NL}}(\overline{R}_d)d\overline{R}_d \\ & \left. + \int_{r_1-t_L}^{R} P_c^{NL}\cdot f_{R_{d_2}^{NL}}\left(\overline{R}_d\right)d\overline{R}_d\right)f_{r_1^L}(r_1)dr_1 \\ & + \int_{R+t_{NL}}^{\infty}\left(\int_0^R f_{R_d^{NL}}(\overline{R}_d)d\overline{R}_d\right)f_{r_1^{NL}}(r_1)dr_1 \\ & + \int_{t_{NL}}^{R+t_{NL}}\left(\int_0^{r_1-t} f_{R_d^{NL}}(\overline{R}_d)d\overline{R}_d\right. \\ & + \int_{r_1-t_{NL}}^{R}(1-P_c^{NL})\cdot f_{R_d^{NL}}(\overline{R}_d)d\overline{R}_d \\ & \left. + \int_{r_1-t_{NL}}^{R} P_c^{NL}\cdot f_{R_{d_2}^{NL}}\left(\overline{R}_d\right)d\overline{R}_d\right)f_{r_1^{NL}}(r_1)dr_1, \end{aligned} \tag{3.54}$$

the pdf of $\overline{R_d}^{L(NL)}$ can be written as

$$f_{\overline{R_d}^{L(NL)}}(r) = \frac{\partial\Pr\left[R_d^{L(NL)} > r\right]}{\partial\overline{R_d}}, \tag{3.55}$$

where P_c is the probability of the potential D2D receiver operating in the cellular mode, and it can be calculated as

$$P_c^{L/NL} = \arccos\left(\frac{\overline{R}_d + r_1^2 - t_{L/NL}^2}{2\overline{R}_d r_1}\right)/\pi, \tag{3.56}$$

which concludes our proof. □

The coverage probability of D2D users is evaluated by Eq.(4.26). The typical D2D receiver selects the equivalent nearest UE as a potential transmitter. If the potential D2D transmitter is operating in a cellular mode, D2D RU must search for another transmitter. We approximately consider that the second neighbor can be found as the transmitter under this situation both for LoS/NLoS links, the accuracy of this estimate is compared to the simulation results in appendix C. Although the analytical results are complicated, it provides general results that can be applied to various multi-path fading or shadowing models in the D2D-enhanced cellular networks.

3.5 Simulation and Discussion

In this section, we use numerical results to validate our results and analyze the performance of the D2D-enabled UL cellular network. To this end, we present the simulation parameters, the results for the coverage probability, the results for the area spectral efficiency in Section 3.5.1,Section 3.5.2,Section 3.5.4, respectively.

3.5.1 Simulation setup

We set the system parameters according to the 3GPP Long Term Evolution (LTE) specifications [128], the BS intensity to $\lambda_b = 5\,\text{BSs/km}^2$, which results in an average inter-site distance of about 500 m. The UE intensity is chosen as $\lambda = 200\,\text{UEs/km}^2$, which is a typical value in 5G [16]. The transmit power of each BS and each D2D transmitter are set to $P_B = 46\,\text{dBm}$ and $P_D = 10\,\text{dBm}$, respectively.

Table 3.3 : Simulation Parameters

Parameters	Values	Parameters	Values
BW	10MHz	f_c	2GHz
λ_B	5 BSs/km^2	σ_c^2	-95 dBm
λ_u	200 UEs/km^2	σ_d^2	-114 dBm
ε	0.8	P_0	-70 dBm
α_{BL}	2.42	A_{BL}	$10^{-3.08}$
α_{BN}	4.28	A_{BN}	$10^{-0.27}$
α_{DL}	2	A_{DL}	$10^{-3.845}$
α_{DN}	4	A_{DN}	$10^{-5.578}$
P_B	46 dBm	P_d	10 dBm
d_B	0.3km	d_D	0.1km

Moreover, the threshold for selecting cellular mode communication is $\beta = -70 \sim -30$dBm. The standard deviation of lognormal shadowing is 8 dB between UEs to BSs and 7 dB between UEs to UEs. The noise powers are set to -95 dBm for a UE receiver and -114 dBm for a BS receiver, respectively. The simulation parameters are summarized in Table 4.1.

3.5.2 Validation of analytical results of $p^{\text{cov}}(\lambda, \gamma)$

In Fig. 4.2, we plot the results of the coverage probability of cellular tier and D2D tier, we can draw the following observations:

- The analytical results of the coverage probability from Eq.(3.28) and Eq.(4.26) match well with the simulation results, which validates our analysis and shows that the adopted model accurately captures the features of D2D communications.

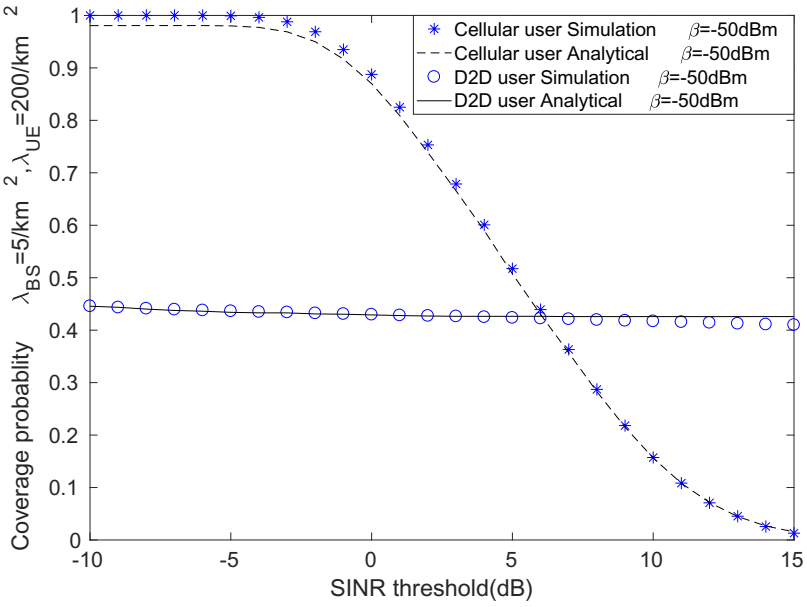

Figure 3.3 : The Coverage Probability $p^{\text{cov}}(\lambda, \gamma)$ vs. SINR threshold ($\lambda_{UE} = 200\,\text{UEs/km}^2$, $\lambda_{BS} = 5\,\text{UEs/km}^2$ and $\rho = 10\%$). The mode select threshold β is -50dBm.

- For the cellular tier, the coverage probability decreases with the increase of SINR threshold because a higher SINR requirement makes it more difficult to satisfy the coverage criterion in Eq.(4.20).
- The coverage probability reduces very slowly in D2D tier because the signals in most of the successful links are LoS while the interference is most likely NLoS, hence the SINR is relatively large, e.g., well above 15 dB.

To fully study the SINR coverage probability with respect to the values of β , the results of coverage probability with various β and γ_0=0 dB are plotted in Fig 4.4. From this figure, we can draw the following observations:

- The coverage probability of cellular users increases as β grows from -70 dBm to -57 dBm, which is because a larger β reduces the distance between the typical

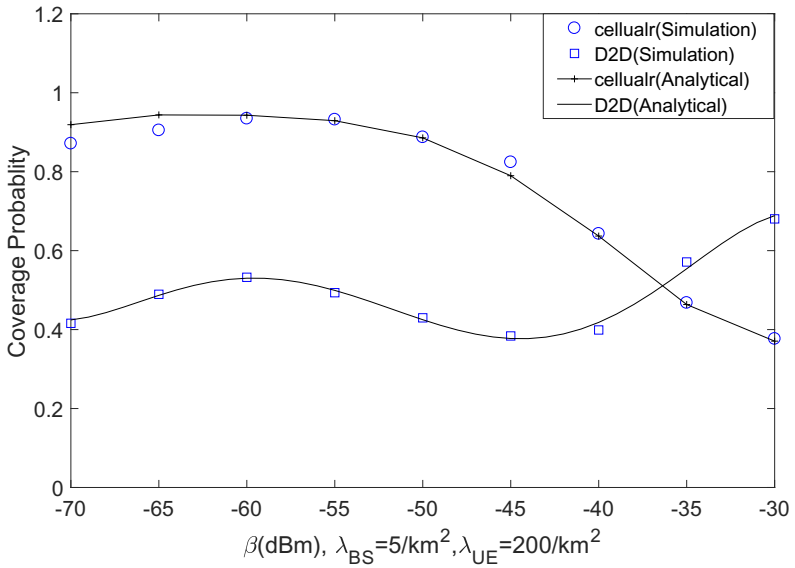

Figure 3.4 : The Coverage Probability $p^{\text{cov}}(\lambda, \gamma)$ vs. β for 3GPP Case 1 ($\gamma_0 = 0\,\text{dB}$, $\lambda_{UE} = 200\,\text{UEs/km}^2$, $\lambda_{BS} = 5\,\text{UEs/km}^2$ and $\rho = 10\%$).

CU to the typical BS so that the signal link's LoS probability increases. Then, the coverage probability performance decreases because the interference from D2D tier is growing. When we set $\delta = 0.9$, we should choose β no larger than -45 dBm to guarantee the cellular performance.

- In the D2D mode, the coverage probability also increases as β increases from -70 dBm to -60 dBm, this is because the distance between the typical D2D pair UEs decreases while the transmit power is constant. From $\beta = -60$ dBm to $\beta = -45$ dBm, the coverage probability decreases because of the interference from the D2D tier increases. Then, the coverage probability increases when β is larger than -45 dBm because the signal power experience the NLoS to LoS transition while the aggregate interference remains to be mostly NLoS interference.

3.5.3 Network Performance Without Interference Management

In this subsection, we will show the results in terms of the coverage probability of cellular tier and the D2D tier with and without the proposed interference management scheme. From Fig.3.5, we can draw the following observations:

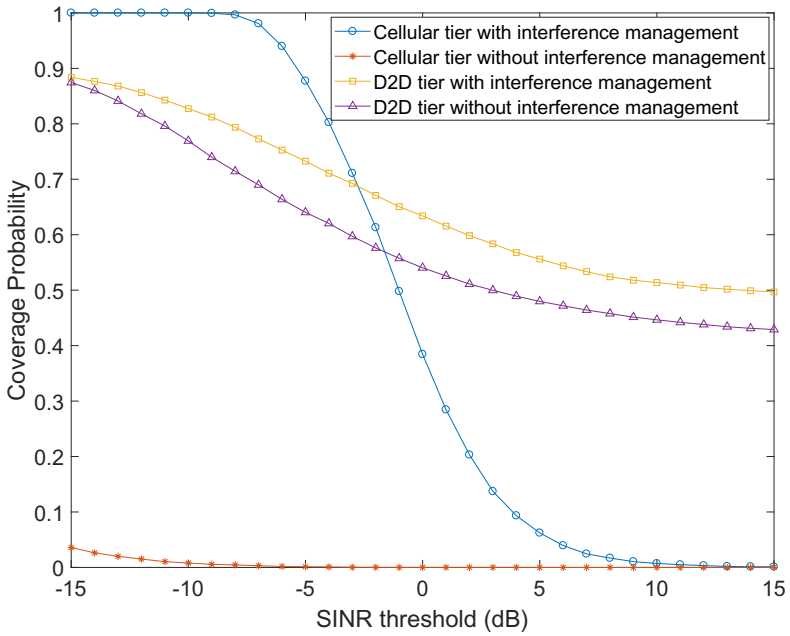

Figure 3.5 : The coverage probability with and without the proposed interference management scheme ($\gamma_0 = 0\,\text{dB}$, $\lambda_{UE} = 300\,\text{UEs/km}^2$, $\lambda_{BS} = 5\,\text{UEs/km}^2$).

- For the cellular tier, in the absence of the interference management scheme, the coverage probability is almost zero due to interference from the D2D tier.
- For the D2D tier, the interference management scheme also improves coverage probability because this scheme makes D2D UEs more concentrated in location.

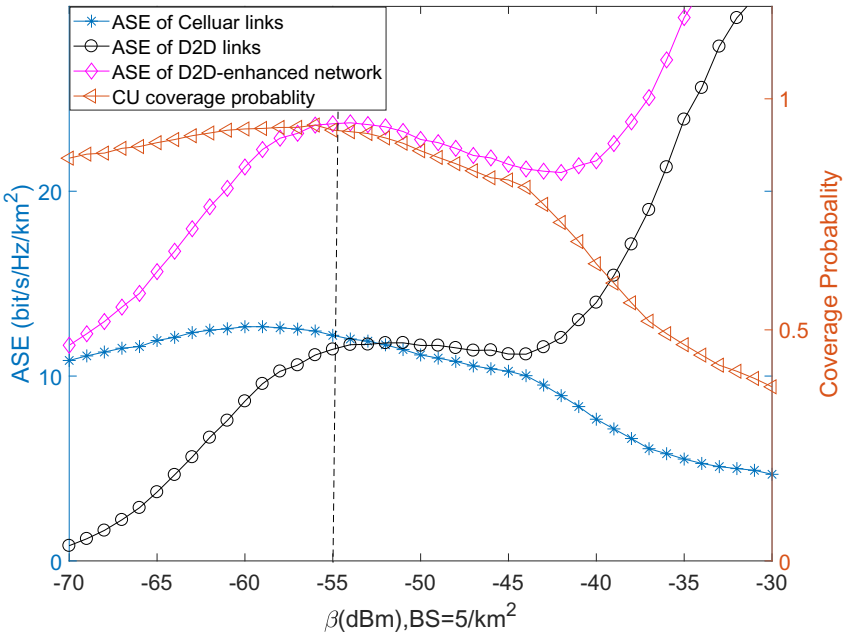

Figure 3.6 : The ASE $A^{\mathrm{ASE}}(\lambda, \gamma_0)$ vs. β for 3GPP Case 1 ($\gamma_0 = 0\,\mathrm{dB}$, $\lambda_{UE} = 200\,\mathrm{UEs/km}^2$, $\lambda_{BS} = 5\,\mathrm{UEs/km}^2$ and $\rho = 10\%$).

3.5.4 Discussion on the analytical results of ASE

In Fig.4.5, the triangle mark represents coverage probability, and the other three curves represent ASE. The analytical results of ASE with γ_0=0 db vs various β values are shown in Eq.(5.10). Fig.4.5 illustrates the ASEs of Cellular links, D2D links and of the whole network with respect to different mode selection thresholds β . From this figure we can draw the following observations:

- The total ASE increases as the D2D links increases when $\beta \in [-70dBm, -55dBm]$ this is because D2D links increase which cellular links keep stable.
- An optimal β around-55 dBm can achieve the maximum ASE while the coverage probability of the cellular tier is above 0.9.
- The total ASE decreases when $\beta \in [-55dBm, -42dBm]$, because the D2D

links generate more interference which makes the coverage probability of cellular decreases.

- When $\beta \in [-42dBm, -30dBm]$, the additional D2D links make a significant contribution to the ASE performance so that the total ASE grows again. Then, the total ASE approaches that of the D2D ASE because the percentage of D2D UE is approaching 100%, which has been analyzed in Eq.(4.17). Although the total ASE grows very quickly when $\beta \in [-42dBm, -30dBm]$, the interference from D2D links to the cellular tier remains to be large so that the performance of the cellular tier is poor. Hence, we do not recommend the network operate in this range of β.

From Fig.4.5 we can find D2D links will increase as β increase for all different densities of BS. In conclusion, there is an optimal beta which can get the optimal ASE of the D2D-enabled cellular while the coverage probability in cellular tier is maximum. The mode selection threshold can control the interference from both cellular tier and D2D tier. D2D tier can bring nearly double ASE for the network when set the optimal threshold for mode selection.

3.6 Summary

In this chapter, we designed a D2D enhanced cellular network to boost the network capacity. We proposed a mode selection method which can eliminate the potential overlarge interferene in a D2D-enhanced uplink cellular network, where the locations of all mobile UEs modeled as a PPP distribution. In particular, each UE selects its operation mode based on its downlink received power and a threshold β. This interference management scheme mitigates the potential overlarge interferene from D2D transmitter to cellular network. Moreover, The results in terms of the coverage probability and the ASE for various values of the mode selection threshold

β showed that the D2D links could provide high ASE when the threshold parameter is appropriately chosen.

Chapter 4

Interference Management and Proportional Fair Scheduler in D2D Underlaid Cellular Network

In this chapter, we extend the work introduced in Chapter 3 and consider the proportional fair scheduler in D2D underliad cellular network. The rest of this chapter is structured as follows: Section 4.1 provides a brief introduction of this problem. Section 4.2 describes the system model. Section 4.3 presents our theoretical analysis on the coverage probability and the area spectral efficiency (ASE) with applications in a 3GPP special case. The numerical and simulations results are discussed in Section 4.4. Our conclusions are drawn in Section 4.5.

4.1 Introduction

In the last decade, there has been an explosive increase in the demand for data traffic [1]. To address such massive consumer demand for data communications, several noteworthy technologies have been proposed [19], such as small cell networks (SCNs), cognitive radio, device-to-device (D2D) communications, etc [105].

In the standardization of the 5-th generation (5G) networks, the orthogonal frequency division multiple access (OFDMA) based D2D communications adopt two types of spectrum sharing methods, (i) in-band (e.g., using cellular spectrum) or (ii) out-band (e.g., unlicensed spectrum). In particular, in the in-band D2D communications, D2D users can set up their communications in an underlay or overlay manner. More specifically, in an underlying setting, D2D users use the same spectrum of cellular users (CUs) whereas in the overlay, D2D users access a dedicated portion of

cellular spectrum [124]. Recently, it has been standardized by the 3rd Generation Partnership Project (3GPP) [131] that Proximity Services (ProSe) should use uplink resources when coexisting with conventional cellular communications. This means that practical D2D communications will underlay with cellular networks in the uplink.

Although the reuse of the cellular spectrum via D2D can improve the area spectral efficiency of the network, such D2D operations also pose great challenges. The major challenge in the D2D-enabled cellular network is the existence of inter-tier and intra-tier interference due to the aggressive frequency reuse, where cellular UEs and D2D UEs share the same spectrum. It is essential to design an effective interference management scheme to control the interference generated by the D2D links to the cellular links, and vice versa. Consequently, there has been a surge of academic studies in this area. Transmission power control [5–7], distance-based mode selection [10, 11, 109] and guard-zone interference control schemes [12–14] have been proposed to solve this problem.

On the other hand, as pointed out in [132], one major weakness of recent research on D2D communications is a lack of realistic scenarios for future mobile networks such as heterogeneous networks with densely deployed small cells. As a straightforward way to increase network capacity, the SCN densification also opens up new research questions, especially in the context of D2D communications. First, scheduling has been conceived as an effective use selection technique used at base stations (BSs) to efficiently use the available spectrum and improve the overall system throughput. Second, the path loss models of D2D links and cellular links in a D2D-enabled cellular network are different due to the difference in the heights and the locations of transmitters [16]. Third, It is well known that LoS transmission may occur when the distance between a transmitter and a receiver is small, and non-line-of-sight (NLoS) transmission is common in office environments and in

central business districts. When the distance between a transmitter and a receiver decreases, the probability that a LoS path exists between them increases, thereby causing a transition from NLoS transmission to LoS transmission with a higher probability. Due to the proximity between D2D users, the physical channels which constitute D2D communications are expected to be complex, experiencing both LoS and NLoS conditions across these pairs, which are distinctly different from conventional cellular environments [17].

In this chapter, we will consider the above network models and will also present a novel mode selection scheme based on the maximum received signal strength for D2D transmitter (TU) to control the interference and focus on the analysis of the orthogonal deployment of uplink sharing D2D-enhanced UDNs. The maximum received signal strength based mode selection scheme is more practical than the distance-based mode selection in most existing studies because in practice it is possible that the strongest received signal strength is not associated with the closest BS but the one with the minimum path loss with a line-of-sight (LoS) link. In more detail, a UE will operate in a cellular mode if its received signal strength from the strongest base station (BS) is larger than a threshold β; otherwise, it will operate in a D2D mode. This will mitigate the overlarge interference from the D2D links to the cellular links.To analyze the proposed framework, we develop a theoretical framework that takes practical path loss model and Rayleigh fading into account. Based on our analytical results, we find a tradeoff between the maximization of the area spectral efficiency (ASE) performance and the fairness of the D2D links, and the optimum setting of the threshold β that maximizes the ASE.

4.2 System Model

In this section, we first explain the scenario of the D2D communication coexisting with cellular network. Then, we present the path loss model, interference

management scheme, the PF scheduler and the performance metrics.

4.2.1 Scenario Description

We consider a D2D underlaid UL cellular network, where BSs and UEs, including cellular uplink UEs and D2D UEs, are assumed to be distributed on an infinite two-dimensional (2D) plane $\mathbb{R}^{\mathbf{2}}$. We assume that the cellular BSs are spatially distributed according to a 2D homogeneous PPP of intensity λ_b , i.e., $\Phi_b = \{X_i\}$, where X_i denotes the spatial locations of the ith BS. For cellular network, we assume the uplink UEs which only operate in cellular mode are deployed following an arbitrary stationery and ergodic Poisson point process of intensity λ_u. Moreover, the D2D transmitters are also distributed in the network region according to another independent homogeneous PPP Φ_{TU} of intensity λ_{TU}. We assume that each D2D transmitter has a dedicated receiver located at distance l in a random direction as [56]. In this chapter, we take a PF scheduler into account in the cellular tier, which will be described in detail in Subsection 4.2.4.

Furthermore, we assume that each UE and each BS transmit with constant powers P_D and P_B, respectively. Finally, we adopt a unified channel model that only Rayleigh fading h is considered for both cellular and D2D links: where h is the fading factor following an exponential distribution with unit mean, i.e., $h \sim \exp(1)$.

In this chapter, we incorporate both NLoS and LoS transmissions into the path loss model. Following [16, 133], path loss functions adopted in the 3GPP [124] for cellular links and D2D links are considered, which can be written as

$$\zeta_B(r) = \begin{cases} A_{BL} r^{-\alpha_{BL}}, & \text{LoS Probability: } \Pr_B^{\mathrm{L}}(r) \\ A_{BN} r^{-\alpha_{BN}}, & \text{NLoS Probability: } 1 - \Pr_B^{\mathrm{L}}(r) \end{cases} \tag{4.1}$$

and

$$\zeta_D(r)=\begin{cases} A_{DL}r^{-\alpha_{DL}}, & \text{LoS Probability: } \Pr_D^{\mathrm{L}}(r) \\ A_{DN}r^{-\alpha_{DN}}, & \text{NLoS Probability: } 1-\Pr_D^{\mathrm{L}}(r) \end{cases}. \tag{4.2}$$

Specifically,

$$\Pr_B^{\mathrm{L}}(r) = \begin{cases} 1-5\exp(-R_1/r) & 0 < r \le d_B \\ 5\exp(-r/R_2) & r > d_B \end{cases} \tag{4.3}$$

and

$$\Pr_D^{\mathrm{L}}(r) = \begin{cases} 1 & 0 < r \le d_D \\ 0 & r > d_D \end{cases} \tag{4.4}$$

where $A_{BL} = 10^{\frac{1}{10}A_{BL}^{\mathrm{dB}}}$ and $A_{BN} = 10^{\frac{1}{10}A_{BN}^{\mathrm{dB}}}$, $A_{DL} = 10^{\frac{1}{10}A_{DL}^{\mathrm{dB}}}$ and $A_{DN} = 10^{\frac{1}{10}A_{DN}^{\mathrm{dB}}}$ are determined by the transmission frequency for BS-to-UE links and UE-to-UE links in LoS and NLoS conditions, respectively. Parameters α_{BL} and α_{BN} , α_{DL} and α_{DN} denote the path loss exponents for BS-to-UE links and UE-to-UE links with LoS and NLoS conditions, respectively. Parameters $R_1 = 156$ m, $R_2 = 30$ m, and $d_B = \frac{R_1}{\ln 10} = 67.75$ m [124]. Parameter $d_D = 50$ m is the cut-off distance of the LoS link for UE-to-UE links.

4.2.2 Interference Management Scheme

There are two modes for TUs in the considered D2D-enabled UL cellular network, i.e., cellular mode and D2D mode. Each TU is assigned with an operation mode according to the comparison of the maximum received DL power from its strongest BS with a threshold. In more detail, the considered mode selection criterion is formulated as

$$Mode = \begin{cases} \text{Cellular}, & \text{if } P^* = \max\limits_{\Phi_b} \left\{P_{\Phi_b}^{\mathrm{rx}}\right\} > \beta \\ \text{D2D}, & \text{otherwise} \end{cases}, \tag{4.5}$$

where the string variable $Mode$ takes the value of 'Cellular' or 'D2D' to denote the cellular mode and the D2D mode, respectively. P^{rx} is the received signal strength from a BS. In particular, for a tagged TU, if P^* is larger than a specific threshold $\beta > 0$. This TU is not appropriate to work in the D2D mode due to its potentially large interference to cellular UEs. Hence, it should operate in the cellular mode and directly connect with the strongest BS, i.e., the BS that offers the highest received signal strength; otherwise, it should operate in the D2D mode. The UEs which are associated with cellular BSs are referred to as cellular UEs (CUs). The distance from a CU to its associated BS is denoted by R_B. From [6], we assume CUs are distributed following a PPP Φ_c.

The received power for a typical TU from a BS b can be written as

$$P_b^{\text{rx}} = \begin{cases} P_B A_{BL} R_B^{-\alpha_{BL}} & \text{LoS} \\ P_B A_{BN} R_B^{-\alpha_{BN}} & \text{otherwise} \end{cases}, \tag{4.6}$$

where P_B is the transmission power of a BS. Based on the above system model, we can obtain the intensity of CU as $\lambda_c = \lambda_u + p\lambda_{TU}$, where p denotes the probability of $P^* > \beta$ and will be derived in closed-form expressions in Section 3.4. It is apparent that the TUs operating in D2D mode are distributed following another PPP Φ_d, the intensity of which is $\lambda_d = (1-p)\,\lambda_{TU}$. We assume an underlay D2D in the UL dense cellular network model. That is, each D2D transmitter reuses the same frequency with cellular UEs, which incurs inter-tier interference from the D2D tier to the cellular tier. However, there is no intra-cell interference between cellular UEs since we assume an orthogonal multiple access technique in a BS.

4.2.3 BS Activation and UE Distribution

In practice, a BS will enter an idle mode if there is no UE connected to it, which reduces the interference to neighboring UEs as well as the energy consumption of the network. The set of active BSs should be determined by a user association

strategy (UAS). In this paper, we assume a practical UAS as in [16], where each UE is connected to the BS having the maximum average received signal strength. Note that such BS idle mode operation is not trivial, which even changes the capacity scaling law [127]. Since UEs are randomly and uniformly distributed in the network, we assume that the active BSs also follow an HPPP distribution $\tilde{\Phi}$ [134], the density of which is denoted by $\tilde{\lambda}$ BSs/km^2. Note that $\tilde{\lambda} \leq \lambda_b$ and $\tilde{\lambda} \leq \lambda_c$, since one UE is served by at most one BS.

From [134, 135], $\tilde{\lambda}$ is given by

$$\tilde{\lambda} = \lambda_b \left[1 - \frac{1}{\left(1 + \frac{\lambda_c}{q\lambda_b}\right)^q} \right], \tag{4.7}$$

where according to [135], q depends on the path loss model, but a good approximation is suggested as q=3.5 [134].

According to [134],the per-BS coverage area size X can be approximately characterized by a Gamma distribution and the probability density function (PDF) of X can be expressed as

$$f_X(x) = (q\lambda_b)^q \, x^{q-1} \frac{\exp(q\lambda_b x)}{\Gamma(q)}, \tag{4.8}$$

where $\Gamma(\cdot)$ is the Gamma function [136]. The UE number per BS is denoted by a random variable (RV) K, and the probability mass function (PMF) of K can be calculated as

$$\begin{aligned} f_K(k) &= \Pr[K = k] \\ &\overset{(a)}{=} \int_0^{+\infty} \frac{(\lambda_c x)^k}{k!} \exp(-\lambda_c x) f_X(x) dx \\ &\overset{(b)}{=} \frac{\Gamma(k+q)}{\Gamma(k+1)\Gamma(q)} \left(\frac{\lambda_c}{\lambda_c + q\lambda_b}\right)^k \left(\frac{q\lambda_b}{\lambda_c + q\lambda_b}\right)^q, \end{aligned} \tag{4.9}$$

where (a) is due to the HPPP distribution of UEs and (b) is obtained from (4.8). Note that $f_K(k)$ satisfies the normalization condition: $\sum_{k=0}^{+\infty} f_K(k) = 1$. It can be

seen from (4.9) that K follows a Negative Binomial distribution [136], i.e., $K \sim \mathrm{NB}\left(q, \frac{\lambda_c}{\lambda_c+q\lambda}\right)$.

We assume that a BS with $K = 0$ is not active. Thus, we focus on the active BSs and denote *the UE number per active BS* by a positive RV $\tilde{K}$. Considering (4.9), we can conclude that $\tilde{K}$ follows a truncated Negative Binomial distribution, the PMF of which is denoted by $f_{\tilde{K}}\left(\tilde{k}\right), \tilde{k} \in \{1, 2, \ldots, +\infty\}$ and can be written as

$$f_{\tilde{K}}\left(\tilde{k}\right) = \Pr\left[\tilde{K} = \tilde{k}\right] = \frac{f_K\left(\tilde{k}\right)}{1 - f_K\left(0\right)}. \tag{4.10}$$

Furthermore, the cumulative mass function (CMF) of $\tilde{K}$ can be written as

$$F_{\tilde{K}}\left(\tilde{k}\right) = \sum_{t=1}^{\tilde{k}} f_{\tilde{K}}\left(t\right). \tag{4.11}$$

4.2.4 Proportional Fair Scheduler

The original operation of the PF scheduler is as follows [114],

- First, the average throughput of each CU is tracked by an exponential moving average at the BS.
- Second, each CU frequently feeds back its channel state information (CSI) to its serving BS, so that such BS can calculate the ratio of the instantaneous achievable rate to the average throughput for each user, which is defined as a PF metric for CU selection.
- Finally, the CU with the maximum PF metric will be selected for UL transmission, which is formulated as

$$u^* = \underset{u \in \left\{1,2,\ldots,\tilde{k}\right\}}{\arg\max} \left\{\frac{\tilde{R}_u}{\bar{R}_u}\right\}, \tag{4.12}$$

  where u, u^*, $\tilde{R}_u$ and $\bar{R}_u$ denote the CU index, the selected CU index, the instantaneous achievable rate of CU u and the average throughput of CU u, respectively. Note that the distribution of $\tilde{k}$ has been discussed in (4.10).

From a network performance analysis point of view, it is very difficult, if not impossible, to analyze the original PF scheduler given by (4.12). This is because the objective of a performance analysis is usually to derive the average user throughput $\bar{R}_u$ or aggregate inter-cell interference, but in this case it is part of the PF metric, i.e., $\frac{\tilde{R}_u}{\bar{R}_u}$, and it should be known and plugged into the CU selection criterion of (4.12) before the performance analysis of $\bar{R}_u$ is carried out. A widely adopted approach to tackle this dilemma is to use alternative measures of CSI in a PF metric, instead of $\tilde{R}_u$ and $\bar{R}_u$ [114, 137–139]. Here, we follow the framework developed in [114], where the authors proposed to use the ratio of the instantaneous signal-to-noise ratio (SNR) to the average SNR as a PF metric instead of the original one. More specifically, the CU selection criterion of the PF scheduler proposed in [114] is given by

$$u^* = \underset{u \in \{1,2,\ldots,\tilde{k}\}}{\arg\max} \left\{ \frac{\tilde{Z}_u}{\bar{Z}_u} \right\}, \tag{4.13}$$

where $\tilde{Z}_u$ and $\bar{Z}_u$ denote the instantaneous SNR of CU u and the average SNR of CU u, respectively. If we don't use PF, then we will use round Robin to randomly select a user to communicate, but we use PF schedular, we will choose the user with the strongest SNR in this time slot to communicate, which is obviously better than RR method. Although this criterion of (4.13) is not exactly the same as that of (4.12), it captures the essence of the PF scheduler:

- Allowing preference to CUs with relatively good instantaneous channels with respect to their average ones since $\tilde{R}_u$ *is a strictly monotonically increasing function of* $\tilde{Z}_u$.

- Allocating the same portion of resource to each CU in the long term to enforce fairness, because the chance of $\tilde{Z}_u \geq \bar{Z}_u$ is almost the same for all CUs. Since the accuracy and the practicality of (4.13) have been well established in [114], we will focus on studying the PF scheduler characterized by (4.13).

According to [30], we define the coverage probability as a probability that a receiver's signal-to-interference-plus-noise ratio (SINR) is above a pre-designated threshold γ:

$$P_{Mode}\left(\gamma, \lambda_b, \lambda_u, \lambda_{TU}\right) = \Pr\left[\text{SINR} > \gamma\right], \tag{4.14}$$

where γ is the SINR threshold, the subscript string variable $Mode$ takes the value of 'Cellular' or 'D2D'. The interference in this paper consists of the interference from both cellular UEs and D2D transmitters.

Furthermore, the area spectral efficiency in bps/Hz/km^2 can be formulated as

$$\begin{aligned} &A_{Mode}^{\text{ASE}}\left(\lambda_{Mode}, \gamma_0\right) \\ &= \lambda_{Mode} \int_{\gamma_0}^{\infty} \log_2\left(1+x\right) f_X\left(\lambda_{Mode}, \gamma_0\right) dx, \end{aligned} \tag{4.15}$$

where γ_0 is the minimum working SINR for the considered network, and $f_X\left(\lambda_{Mode}, \gamma_0\right)$ is the PDF of the SINR observed at the typical receiver for a particular value of λ_{Mode}.

For the whole network consisting of both cellular UEs and D2D UEs, the sum ASE can be written as

$$A^{\text{ASE}} = A_{\text{Cellular}}^{\text{ASE}} + A_{\text{D2D}}^{\text{ASE}}. \tag{4.16}$$

4.3 Performance of the D2D Underlaid Cellular Network Using PF

In this section, the performance of UEs is characterized in terms of their coverage probability and ASE both for the cellular tier and the D2D tier. The probability that a TU operating in the cellular mode is derived in Section 4.3.1, the coverage probabilities of cellular UE and D2D UE are derived in Section 4.3.2.

4.3.1 User Mode Selection

In this subsection, we present our results on the percentage that the TUs to operate in the cellular mode. In the following, we present our result in Lemma 2, which will be used in the later analysis of the coverage probability.

Lemma 2. *The percentage of a TU to operate in the cellular mode p is given by*

$$p = 1 - \exp\left[-2\pi\lambda_b \left(\int_0^{\left(\frac{P_B A_{BL}}{\beta}\right)^{1/\alpha_{BL}}} p^L(r) r dr + \int_0^{\left(\frac{P_B A_{BN}}{\beta}\right)^{1/\alpha_{BN}}} p^{NL}(r) r dr\right)\right], \tag{4.17}$$

the percentage that a TU to operate in the D2D mode is $(1-p)$.

Proof. The probability that the RSS is larger than the threshold is given by

$$P = \Pr\left[\max_b \{P_b^{\text{rx}}\} > \beta\right], \tag{4.18}$$

where we use the standard power loss propagation model with a path loss exponent α_{BL} (for LoS UE-BS links) and α_{BN} (for NLoS UE-BS links).The probability that a generic mobile UE operates in the cellular mode:

$$\begin{aligned}
q &= 1 - \Pr\left[\max_b \{P_b^{\text{rx}}\} \leq \beta\right] \\
&= 1 - \Pr\left[\max\{P_{LoS}^{rx}\} \leq \beta \cap \max\{P_{NLoS}^{rx}\} \leq \beta\right] \\
&= 1 - \Pr\left[\min R^{BL} \geq \left(\frac{P_B \mathrm{A}_{BL}}{\beta}\right)^{1/\alpha_{BL}}\right. \\
&\cap \quad \left.\min R^{BN} \geq \left(\frac{P_B \mathrm{A}_{BN}}{\beta}\right)^{1/\alpha_{BN}}\right] \\
&= 1 - \Pr\left[\text{no nodes within } \left(\frac{P_B \mathrm{A}_{BL}}{\beta}\right)^{1/\alpha_{BL}}\right. \\
&\cap \quad \left.\text{no nodes within } \left(\frac{P_B \mathrm{A}_{BN}}{\beta}\right)^{1/\alpha_{BN}}\right]
\end{aligned}$$

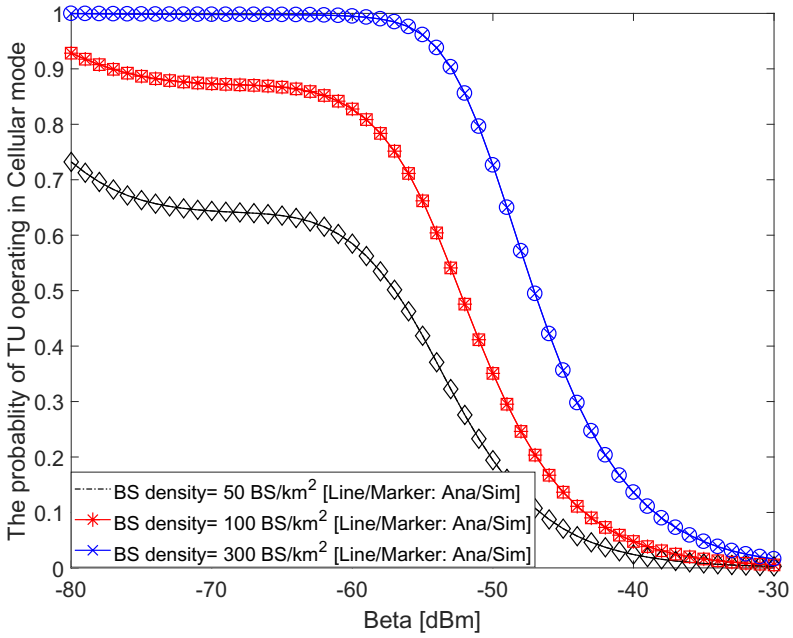

Figure 4.1 : The probability for a TU to operate in the cellular mode vary the RSS threshold β , $\mathrm{P}_B = 24\mathrm{dBm}$

$$
\begin{aligned}
=&1 - \exp\left[-\pi\lambda_b \int_0^{\left(\frac{P_B \mathrm{A}_{BL}}{\beta}\right)^{\frac{1}{\alpha_{BL}}}} \mathrm{Pr_B}^{\mathrm{L}} r dr\right] \\
&\times \exp\left[-\pi\lambda_b \int_0^{\left(\frac{P_B \mathrm{A}_{BN}}{\beta}\right)^{\frac{1}{\alpha_{BN}}}} \mathrm{Pr_B}^{\mathrm{NL}} r dr\right], \qquad (4.19)
\end{aligned}
$$

which concludes our proof. □

Note that Eq.(4.17) explicitly account for the effects of Rayleigh fading, path loss, transmit power, spatial distribution of BSs and mode selection threshold β . From the result, we can see that the HPPP ϕ_{TU} can be divided into two PPPs: the PPP with intensity $p\lambda_{TU}$ and the PPP with intensity $(1-p)\lambda_{TU}$, which representing cellular mode TUs and D2D mode TUs, respectively. Same as in [6], We assume these two PPs are independent.

Fig 4.1 illustrates the probability for a TU to operate in the cellular mode based on Eq.(4.17). It can be seen that the simulation results perfectly match the analytical results. From Fig.1, we can find that over 50% UEs can operate in the cellular mode when β is smaller than -57 dBm as the BS intensity is 50BS/km^2. This value increases by approximately to -52 dBm and -46 dBm when the BS intensity is 100BS/km^2 and 300BS/km^2, respectively. It indicates that the percentage of TU operating in cellular mode will increase as the BS intensity grows.

4.3.2 Coverage Probabality

In this subsection, we investigate the coverage probability that a receiver's signal-to-interference-plus-noise ratio (SINR) is above a pre-designated threshold γ:

$$P_{Mode}\left(T, \lambda_{b,u}, \alpha_{B,D}\right) = \Pr\left[\text{SINR} > \gamma\right] \tag{4.20}$$

where γ is the SINR threshold, the subscript string variable $Mode$ takes the value of 'Cellular' or 'D2D'. The SINR can be calculated as

$$\text{SINR} = \frac{P_D \zeta_{Mode}\left(r\right) y\left(\tilde{k}\right)}{I_{cellular} + I_{d2d} + N_0}, \tag{4.21}$$

where P_D and N_0 are the transmission power of each cellular and D2D UE transmitter and the additive white Gaussian noise (AWGN) power at each receiver, respectively. $I_{cellular}$ and I_{d2d} are the cumulative interference given by

$$I_{cellular} = \sum_{i:\, c_i \in \Phi_c \setminus signal} P_D \beta_i y\left(\tilde{k}\right)_i, \tag{4.22}$$

and

$$I_{d2d} = \sum_{j:\, d_i \in \Phi_{d2d} \setminus signal} P_D \beta_j y\left(\tilde{k}\right)_j, \tag{4.23}$$

where c_i and d_j are the i-th interfering CU and j-th interfering TU, β_i ,β_j are the path loss associated with c_i and d_j, respectively. $signal$ is the typical CU to BS link

in the cellular mode and the typical TU to the RU link in the D2D mode. $y\left(\tilde{k}\right)$ is the channel gain on condition of the UE number $\tilde{k}$.

It is very important to note that the distribution of $y\left(\tilde{k}\right)$ should be derived according to (4.13). More specifically, we can reformulate (4.13) as

$$u^{*}=\underset{u\in\left\{1,2,\ldots,\tilde{k}\right\}}{\arg\max}\left\{\frac{\frac{P_{D}\zeta_{B}(r)h_{u}}{N_{0}}}{\frac{P_{D}\zeta_{B}(r)\times1}{N_{0}}}\right\}=\underset{u\in\left\{1,2,\ldots,\tilde{k}\right\}}{\arg\max}\left\{h_{u}\right\}, \tag{4.24}$$

where h_u is an i.i.d. RV with a *unit-mean* exponential distribution due to our consideration of Rayleigh fading mentioned in Subsection **??**. Thus, $y\left(\tilde{k}\right)$ can be modeled as the maximum RV of $\tilde{k}$ i.i.d. exponential RVs. The complementary cumulative distribution function (CCDF) of $y\left(\tilde{k}\right)$ is [140]

$$\bar{F}_{Y\left(\tilde{k}\right)}\left(y\right)=\Pr\left[Y\left(\tilde{k}\right)>y\right]=1-\left(1-\exp\left(-y\right)\right)^{\tilde{k}}. \tag{4.25}$$

It is easy to see that $\Pr\left[Y\left(\tilde{k}\right)>y\right]$ increases as $\tilde{k}$ grows, which in turn improves the typical UE's channel gain. Note that for the round-robin (RR) scheduler, the typical UE is randomly selected in the BS. Consequently, we have that $\tilde{k}=1$ in (4.25) and the analytical results for RR have been derived in [133].

Based on the path loss model in Eq.(5.40) and the PF scheduler model in (4.13), we present our main result on $p_{c}^{\mathrm{cov}}\left(\lambda,\gamma\right)$ in Theorem 6 and Theorem 4.

Theorem 3. *Considering the path loss model in (5.40) and the PF scheduler model in (4.13), we can derive* $p_{c}^{\mathrm{cov}}\left(\lambda,\gamma\right)$ *as*

$$p_{c}^{\mathrm{cov}}\left(\lambda,\gamma\right)=T_{c}^{\mathrm{L}}+T_{c}^{\mathrm{NL}}, \tag{4.26}$$

where

$$T_{c}^{\mathrm{L}}=\int_{d_{n-1}}^{d_{n}}\mathbb{E}_{[\tilde{k}]}\left\{\Pr\left[\frac{P_{D}\zeta_{B}^{\mathrm{L}}\left(r\right)y\left(\tilde{k}\right)}{I_{cellular}+I_{d2d}+N_{0}}>\gamma\right]\right\}f_{R,n}^{\mathrm{L}}\left(r\right)dr \tag{4.27}$$

and

$$T_c^{\mathrm{NL}} = \int_{d_{n-1}}^{d_n} \mathbb{E}_{[\tilde{k}]} \left\{ \Pr \left[\frac{P_D \zeta_B^{\mathrm{NL}}(r)\, y\left(\tilde{k}\right)}{I_{cellular} + I_{d2d} + N_0} > \gamma \right] \right\} f_{R,n}^{\mathrm{NL}}(r)\, dr \tag{4.28}$$

where $n = \{1, 2\}$, d_0 *and* d_2 *are defined as* 0 *and* $+\infty$, *respectively. Moreover,* $f_{R,n}^{\mathrm{L}}(r)$ *and* $f_{R,n}^{\mathrm{NL}}(r)$ $(d_{n-1} < r \leq d_n)$, *are represented by*

$$f_{R,n}^{\mathrm{L}}(r) = \exp\Bigg(-\int_0^{r_1} \left(1 - \mathrm{Pr_B}^{\mathrm{L}}(u)\right) 2\pi u \lambda_b du - \int_0^{r} \mathrm{Pr_B}^{\mathrm{L}}(u)\, 2\pi u \lambda_b du \Bigg) \Pr_B^{\mathrm{L}}(r)\, 2\pi r \lambda_b, \tag{4.29}$$

and

$$f_{R,n}^{\mathrm{NL}}(r) = \exp\Bigg(-\int_0^{r_2} \Pr_B^{\mathrm{L}}(u)\, 2\pi u \lambda_b du - \int_0^{r} \left(1 - \Pr_B^{\mathrm{L}}(u)\right) 2\pi u \lambda_b du \Bigg) \left(1 - \Pr_B^{\mathrm{L}}(r)\right) 2\pi r \lambda_b, \tag{4.30}$$

where $r_1 = \underset{r_1}{\arg} \left\{ \zeta_B^{\mathrm{NL}}(r_1) = \zeta_B^{\mathrm{L}}(r) \right\}$ *and* $r_2 = \underset{r_2}{\arg} \left\{ \zeta_B^{\mathrm{L}}(r_2) = \zeta_B^{\mathrm{NL}}(r) \right\}$.

Proof. By invoking the law of total probability, the coverage probability of cellular links can be divided into two parts, i.e., $T_c^{\mathrm{L}} + T_c^{\mathrm{NL}}$, which denotes the conditional coverage probability given that the typical CU is associated with a BS in LoS and NLoS, respectively. First, we derive the coverage probability for LoS link cellular tier. Conditioned on the strongest BS being at a distance r from the typical CU,

probability of coverage is given by

$$
\begin{aligned}
&\mathbb{E}_{[\tilde{k}]}\left\{\Pr\left[\frac{P_D\zeta_B^{\mathrm{L}}(r)\,y\left(\tilde{k}\right)}{I_{cellular}+I_{d2d}+N_0}>\gamma\right]\right\}\\
=&\mathbb{E}_{[\tilde{k}]}\left\{\Pr\left[y\left(\tilde{k}\right)>\gamma\left(\frac{I_{cellular}+I_{d2d}+N_0}{P_D\zeta_B^{\mathrm{L}}(r)}\right)\right]\right\}\\
=&\mathbb{E}_{[\tilde{k}]}\left\{1-\left[1-\exp\left(-\gamma\left(\frac{I_{cellular}+I_{d2d}+N_0}{P_D\zeta_B^{\mathrm{L}}(r)}\right)\right)\right]^{\tilde{k}}\right\}\\
=&\sum_{\tilde{k}=1}^{\tilde{K}^{\max}}\left[1-\sum_{t=0}^{\tilde{k}}\binom{\tilde{k}}{t}(-1)^t\times\exp\left(-t\gamma\left(\frac{I_{cellular}+I_{d2d}+N_0}{P_D\zeta_B^{\mathrm{L}}(r)}\right)\right)\right]f_{\tilde{K}}\left(\tilde{k}\right)\\
=&\sum_{\tilde{k}=1}^{\tilde{K}^{\max}}\left[1-\sum_{t=0}^{\tilde{k}}\binom{\tilde{k}}{t}\left(-\delta^{\mathrm{L}}(r)\right)^t\times\mathrm{L}_{\mathrm{I_{cellular}}}^{\mathrm{L}}\left(\frac{\mathrm{t}\gamma}{\mathrm{P_D}\zeta_{\mathrm{B}}^{\mathrm{L}}(\mathrm{r})}\right)\mathrm{L}_{\mathrm{I_{d2d}}}^{\mathrm{L}}\left(\frac{\mathrm{t}\gamma}{\mathrm{P_D}\zeta_{\mathrm{B}}^{\mathrm{L}}(\mathrm{r})}\right)\right]f_{\tilde{K}}\left(\tilde{k}\right)
\end{aligned}
$$

where $\delta^{\mathrm{L}}(r)$ is expressed by

$$\delta^{\mathrm{L}}(r)=\exp\left(-\frac{\gamma N_0}{P_D\zeta_B^{\mathrm{L}}(r)}\right), \tag{4.31}$$

and $\mathrm{L}_{\mathrm{I_{cellular}}}^{\mathrm{L}}(\mathrm{s})$ is the Laplace transform of $I_{cellular}$ for LoS signal transmission evaluated at s, which can be further written as

$$
\begin{aligned}
\mathrm{L}_{\mathrm{I_{cellular}}}^{\mathrm{L}}(\mathrm{s})=&\exp\left(-2\pi\tilde{\lambda}\int_r^{d_B}\frac{\mathrm{Pr_B}^{\mathrm{L}}(u)\,u}{1+\left(sP_D\zeta_B^{\mathrm{L}}(u)\right)^{-1}}du\right)\\
&\times\exp\left(-2\pi\tilde{\lambda}\int_{r_1}^{d_B}\frac{\mathrm{Pr_B}^{\mathrm{L}}(u)\,u}{1+\left(sP_D\zeta_B^{\mathrm{L}}(u)\right)^{-1}}du\right)\\
&\times\exp\left(-2\pi\tilde{\lambda}\int_{d_B}^{+\infty}\frac{\left[1-\mathrm{Pr_B}^{\mathrm{L}}(u)\right]u}{1+\left(sP_D\zeta_B^{\mathrm{NL}}(u)\right)^{-1}}du\right)
\end{aligned}
\tag{4.32}
$$

and $\mathrm{L}_{\mathrm{I_{d2d}}}^{\mathrm{L}}(\mathrm{s})$ is the Laplace transform of I_{d2d} for LoS signal transmission evaluated at s, which can be further written as

$$
\begin{aligned}
\mathrm{L}_{\mathrm{I_{d2d}}}^{\mathrm{L}}(\mathrm{s})=&\exp\left(-2\pi\lambda_d\right.\\
&\left.\times\int_{\left(\frac{P_B\mathrm{A}_{BL}}{\beta}\right)^{1/\alpha_{BL}}}^{d_B}\frac{\mathrm{Pr}_B^{\mathrm{L}}(u)\,u}{1+\left(sP_D\zeta_B^{\mathrm{L}}(u)\right)^{-1}}du\right)\\
&\times\exp\left(-2\pi\lambda_d\int_{r_1}^{d_B}\frac{\mathrm{Pr}_B^{\mathrm{L}}(u)\,u}{1+\left(sP_D\zeta_B^{\mathrm{L}}(u)\right)^{-1}}du\right)
\end{aligned}
$$

$$\times \exp\left(-2\pi\lambda_d \int_{d_B}^{+\infty} \frac{\left[1-\mathrm{Pr_B}^{\mathrm{L}}(u)\right] u}{1+\left(sP_D\zeta_B^{\mathrm{NL}}(u)\right)^{-1}} du\right). \tag{4.33}$$

The logic of the calculation of T_c^{NL} is similar to that of T_c^{L}. Which concludes our proof. □

Then, we will present the results in Theorem 4 as follows.

Theorem 4. *Considering the truncated Negative Binomial distribution of the UE number per active BS, $\tilde{K}$, characterized in (4.10), we can derive $\mathbb{E}_{[\tilde{k}]}\left\{\Pr\left[\frac{P_D\zeta_n^{\mathrm{L}}(r)y(\tilde{k})}{I_{\mathrm{agg}}+P_{\mathrm{N}}}>\gamma\right]\right\}$, which will be used in Theorem 6 as*

$$\begin{aligned}
&\mathbb{E}_{[\tilde{k}]}\left\{\Pr\left[\frac{P_D\zeta_B^{\mathrm{L}}(r)\,y\left(\tilde{k}\right)}{I_{\mathrm{agg}}+P_{\mathrm{N}}}>\gamma\right]\right\} \\
&=\sum_{\tilde{k}=1}^{\tilde{K}^{\max}}\left[1-\sum_{t=0}^{\tilde{k}}\binom{\tilde{k}}{t}\left(-\delta^{\mathrm{L}}(r)\right)^t \mathrm{L}_{\mathrm{I_{cellular}}}^{\mathrm{L}}\left(\frac{\mathrm{t}\gamma}{\mathrm{P_D}\zeta_{\mathrm{B}}^{\mathrm{L}}(\mathrm{r})}\right)\right. \\
&\left.\mathrm{L}_{\mathrm{I_{d2d}}}^{\mathrm{L}}\left(\frac{\mathrm{t}\gamma}{\mathrm{P_D}\zeta_{\mathrm{B}}^{\mathrm{L}}(\mathrm{r})}\right)\right] f_{\tilde{K}}\left(\tilde{k}\right),
\end{aligned} \tag{4.34}$$

where $I_{\mathrm{agg}}=I_{cellular}+I_{d2d}$, $\tilde{K}^{\max}$ is a large enough integer that makes $F_{\tilde{K}}\left(\tilde{K}^{\max}\right)$ in (4.11) close to one with a gap of a small value ϵ so that the expectation value in (5.8) can be accurately evaluated over $\tilde{k}$, $f_{\tilde{K}}\left(\tilde{k}\right)$ is obtained from (4.10), $\delta^{\mathrm{L}}(r)$ is expressed by

$$\delta^{\mathrm{L}}(r)=\exp\left(-\frac{\gamma N_0}{P_D\zeta_B^{\mathrm{L}}(r)}\right), \tag{4.35}$$

and $\mathrm{L}_{\mathrm{I_{cellular}}}^{\mathrm{L}}(\mathrm{s})$ is the Laplace transform of $I_{cellular}$ for LoS signal transmission evaluated at s, , which can be further written as

$$\begin{aligned}
\mathrm{L}_{\mathrm{I_{cellular}}}^{\mathrm{L}}(\mathrm{s}) &= \exp\left(-2\pi\tilde{\lambda}\int_{r}^{d_B}\frac{\mathrm{Pr_B}^{\mathrm{L}}(u)\,u}{1+\left(sP_D\zeta_B^{\mathrm{L}}(u)\right)^{-1}}du\right) \\
&\times\exp\left(-2\pi\tilde{\lambda}\int_{r_1}^{d_B}\frac{\mathrm{Pr_B}^{\mathrm{L}}(u)\,u}{1+\left(sP_D\zeta_B^{\mathrm{L}}(u)\right)^{-1}}du\right) \\
&\times\exp\left(-2\pi\tilde{\lambda}\int_{d_B}^{+\infty}\frac{\left[1-\mathrm{Pr_B}^{\mathrm{L}}(u)\right]u}{1+\left(sP_D\zeta_B^{\mathrm{NL}}(u)\right)^{-1}}du\right)
\end{aligned} \tag{4.36}$$

where $s = \frac{t\gamma}{P_D \zeta_B^{\mathrm{L}}(r)}$ *and* $\mathrm{L}_{\mathrm{I_{d2d}}}^{\mathrm{L}}(\mathrm{s})$ *is the Laplace transform of* I_{d2d} *for LoS signal transmission evaluated at* s*, which can be further written as*

$$\begin{aligned}\mathrm{L}_{\mathrm{I_{d2d}}}^{\mathrm{L}}(\mathrm{s}) = \exp\left(-2\pi\lambda_d \int_{\left(\frac{P_B A_{BL}}{\beta}\right)^{1/\alpha_{BL}}}^{d_B} \frac{\mathrm{Pr}_B^{\mathrm{L}}(u)\, u}{1 + \left(sP_D\zeta_B^{\mathrm{L}}(u)\right)^{-1}} du\right) \\ \times \exp\left(-2\pi\lambda_d \int_{r_1}^{d_B} \frac{\mathrm{Pr}_B^{\mathrm{L}}(u)\, u}{1 + \left(sP_D\zeta_B^{\mathrm{L}}(u)\right)^{-1}} du\right) \\ \times \exp\left(-2\pi\lambda_d \int_{d_B}^{+\infty} \frac{\left[1 - \mathrm{Pr_B}^{\mathrm{L}}(u)\right] u}{1 + \left(sP_D\zeta_B^{\mathrm{NL}}(u)\right)^{-1}} du\right). \end{aligned} \tag{4.37}$$

where $s = \frac{t\gamma}{P_D \zeta_B^{\mathrm{L}}(r)}$

In a similar way, $\mathbb{E}_{[\tilde{k}]}\left\{\Pr\left[\frac{P_D\zeta_B^{\mathrm{NL}}(r)y(\tilde{k})}{I_{\mathrm{agg}}+P_{\mathrm{N}}} > \gamma\right]\right\}$ *is computed by*

$$\begin{aligned}&\mathbb{E}_{[\tilde{k}]}\left\{\Pr\left[\frac{P_D\zeta_B^{\mathrm{NL}}(r)\, y\left(\tilde{k}\right)}{I_{\mathrm{agg}} + P_{\mathrm{N}}} > \gamma\right]\right\} \\ &= \sum_{\tilde{k}=1}^{\tilde{K}^{\max}} \left[1 - \sum_{t=0}^{\tilde{k}} \binom{\tilde{k}}{t} \left(-\delta^{\mathrm{NL}}(r)\right)^t \right. \\ &\left. \times\, \mathrm{L}_{\mathrm{I_{agg}}}^{\mathrm{NL}}\left(\frac{\mathrm{t}\gamma}{\mathrm{P_D}\zeta_{\mathrm{B}}^{\mathrm{NL}}(\mathrm{r})}\right)\right] f_{\tilde{K}}\left(\tilde{k}\right), \end{aligned} \tag{4.38}$$

where $\delta^{\mathrm{NL}}(r)$ *is expressed by*

$$\delta_n^{\mathrm{NL}}(r) = \exp\left(-\frac{\gamma N_0}{P\zeta_B^{\mathrm{NL}}(r)}\right), \tag{4.39}$$

and $\mathrm{L}_{\mathrm{I_{cellular}}}^{\mathrm{NL}}(\mathrm{s})$ *is the Laplace transform of* $I_{I_{cellular}}$ *for NLoS signal transmission evaluated at* s*, which can be further written as*

$$\begin{aligned}\mathrm{L}_{\mathrm{I_{cellular}}}^{\mathrm{NL}}(\mathrm{s}) = \exp\left(-2\pi\tilde{\lambda} \int_{r_2}^{d_B} \frac{\mathrm{Pr_B}^{\mathrm{L}}(u)\, u}{1 + \left(sP_D\zeta_B^{\mathrm{L}}(u)\right)^{-1}} du\right) \\ \times \exp\left(-2\pi\tilde{\lambda} \int_{r}^{d_B} \frac{\left[1 - \mathrm{Pr_B}^{\mathrm{L}}(u)\right] u}{1 + \left(sP_D\zeta_B^{\mathrm{NL}}(u)\right)^{-1}} du\right) \\ \times \exp\left(-2\pi\tilde{\lambda} \int_{d_B}^{+\infty} \frac{\left[1 - \mathrm{Pr_B}^{\mathrm{L}}(u)\right] u}{1 + \left(sP_D\zeta_B^{\mathrm{NL}}(u)\right)^{-1}} du\right) \end{aligned} \tag{4.40}$$

where $s = \frac{t\gamma}{P_D \zeta_B^{\mathrm{NL}}(r)}$ *and* $\mathrm{L}_{\mathrm{I_{d2d}}}^{\mathrm{NL}}(\mathrm{s})$ *is the Laplace transform of* I_{d2d} *for NLoS signal*

transmission evaluated at s, which can be further written as

$$\begin{aligned}\mathrm{L}_{\mathrm{I_{d2d}}}^{\mathrm{L}}(\mathrm{s}) = \exp\left(-2\pi\lambda_d \int_{r_2}^{d_B} \frac{\mathrm{Pr}_B^{\mathrm{L}}(u)\, u}{1+\left(sP_D\zeta_B^{\mathrm{L}}(u)\right)^{-1}} du\right) \\ \times \exp\left(-2\pi\lambda_d \int_{\left(\frac{P_B A_{BN}}{\beta}\right)^{1/\alpha_{BN}}}^{d_B} \frac{\left[1-\mathrm{Pr_B}^{\mathrm{L}}(u)\right] u}{1+\left(sP_D\zeta_B^{\mathrm{NL}}(u)\right)^{-1}} du\right) \\ \times \exp\left(-2\pi\lambda_d \int_{d_B}^{+\infty} \frac{\left[1-\mathrm{Pr_B}^{\mathrm{L}}(u)\right] u}{1+\left(sP_D\zeta_B^{\mathrm{NL}}(u)\right)^{-1}} du\right) \end{aligned} \tag{4.41}$$

where $s = \frac{t\gamma}{P_D\zeta_B^{\mathrm{NL}}(r)}$.

From [16], T_c^{L} and T_c^{NL} are independent of each other. When the mode selection threshold β increases, we can find the intensity of D2D transmitter also increases. This will reduce the coverage probability performance of cellular tier, so we make $p_c^{\mathrm{cov}} > \delta$ as a condition to guarantee the performance for the cellular mode when choosing β for the optimal system ASE. Although we have obtained the closed-form expressions of $p_c^{\mathrm{cov}}(\lambda,\gamma)$ for the PF scheduler in Theorems 6 and 4, it is important to note that Theorem 4 is computationally intensive for the case of sparse networks, where the maximum UE number per active BS $\tilde{K}^{\max}$ could be very large, leading to complex computations for $\mathrm{L}_{\mathrm{I_{agg}}}^{\mathrm{L}}\left(\frac{\mathrm{t}\gamma}{\mathrm{P}\zeta_{\mathrm{B}}^{\mathrm{L}}(\mathrm{r})}\right)$ and $\mathrm{L}_{\mathrm{I_{agg}}}^{\mathrm{NL}}\left(\frac{\mathrm{t}\gamma}{\mathrm{P}\zeta_{\mathrm{B}}^{\mathrm{NL}}(\mathrm{r})}\right), \mathrm{t} \in \left\{0,1,\ldots,\tilde{\mathrm{K}}^{\max}\right\}$ in (4.34) and (4.38), respectively. From [109], one can see that to derive the coverage probability of a generic D2D UE, we only need to derive the coverage probability for a typical D2D receiver UE. We focus on a typical D2D UE which is located at the origin o and scheduled to receive data from another D2D UE. Following Slivnyak's theorem for PPP, the coverage probability result derived for the typical D2D UE also holds for any generic D2D UE located at any location. In the following, we present the coverage probability for a typical D2D UE in Theorem 5.

Theorem 5. *We focus on a typical D2D RU which is located at the origin o and scheduled to receive data from another D2D TU, the probability of coverage* $p_{D2D}^{\mathrm{cov}}(\lambda,\gamma)$ *can be derived as*

$$p_{D2D}^{\mathrm{cov}}(\lambda,\gamma)=\begin{cases}T_D^{\mathrm{L}} & when\ 0<l\leq d_D\\ T_D^{\mathrm{NL}} & l>d_D\end{cases}, \tag{4.42}$$

where

$$\begin{aligned}T_D^{\mathrm{L,NL}}=&\exp\left(-2\pi\tilde{\lambda}\int_0^{d_D}\frac{\mathrm{Pr}_D^{\mathrm{L}}(u)\,u}{1+\left(sP_D\zeta_D^{\mathrm{L}}(u)\right)^{-1}}du\right)\\ &\times\exp\left(-2\pi\tilde{\lambda}\int_{d_D}^{+\infty}\frac{\left[1-\mathrm{Pr}_D^{\mathrm{L}}(u)\right]u}{1+\left(sP_D\zeta_D^{\mathrm{NL}}(u)\right)^{-1}}du\right)\\ &\times\exp\left(-2\pi\lambda_d\int_0^{d_D}\frac{\mathrm{Pr}_{\mathrm{D}}{}^{\mathrm{L}}(u)\,u}{1+\left(sP_D\zeta_D^{\mathrm{L}}(u)\right)^{-1}}du\right)\\ &\times\exp\left(-2\pi\lambda_d\int_{d_D}^{+\infty}\frac{\left[1-\mathrm{Pr}_D^{\mathrm{L}}(u)\right]u}{1+\left(sP_D\zeta_D^{\mathrm{NL}}(u)\right)^{-1}}du\right)\\ &\times\exp\left(-\frac{\gamma N_0}{P_D\zeta_D^{\mathrm{L}}(l)}\right)\end{aligned} \tag{4.43}$$

where $s=\frac{\gamma}{P_D\zeta_D^{\mathrm{L}}(l)}$ *when* $0<l\leq d_D$ *and* $s=\frac{\gamma}{P_D\zeta_D^{\mathrm{NL}}(l)}$ *when* $l>d_D$.

Proof. The typical D2D receiver has a distance of l to an active D2D transmitter. The coverage probability can be written as

$$
\begin{aligned}
T_D^{\mathrm{L}} &= \Pr\left[SINR^{L} > \gamma \,|\mathrm{LOS}\right] \\
&= \Pr\left[\frac{P_D \zeta_D^{\mathrm{L}}(l)\, h}{I_{cellular} + I_{d2d} + N_0} > \gamma \,|\mathrm{LOS}\right] \\
&= \mathbb{E}_{[I_{agg}]}\left[\Pr\left[h > \frac{\gamma\left(I_{cellular} + I_{d2d} + N_0\right)}{P_D \zeta_D^{\mathrm{L}}(l)} \,|\mathrm{LOS}, I_{agg}\right]\right] \\
&= \mathbb{E}_{[I_{agg}]}\left\{\exp\left[-\frac{\gamma\left(I_{cellular} + I_{d2d} + N_0\right)}{P_D \zeta_D^{\mathrm{L}}(l)}\right]\right\} \\
&= \exp\left(-2\pi\tilde{\lambda}\int_0^{d_D} \frac{\mathrm{Pr_D}^{\mathrm{L}}(u)\, u}{1 + \left(sP_D\zeta_D^{\mathrm{L}}(u)\right)^{-1}} du\right) \\
&\times \exp\left(-2\pi\tilde{\lambda}\int_{d_D}^{+\infty} \frac{\left[1 - \mathrm{Pr_D}^{\mathrm{L}}(u)\right] u}{1 + \left(sP_D\zeta_D^{\mathrm{NL}}(u)\right)^{-1}} du\right) \\
&\times \exp\left(-2\pi\lambda_d\int_0^{d_D} \frac{\mathrm{Pr_D}^{\mathrm{L}}(u)\, u}{1 + \left(sP_D\zeta_D^{\mathrm{L}}(u)\right)^{-1}} du\right) \\
&\times \exp\left(-2\pi\lambda_d\int_{d_D}^{+\infty} \frac{\left[1 - \mathrm{Pr_D}^{\mathrm{L}}(u)\right] u}{1 + \left(sP_D\zeta_D^{\mathrm{NL}}(u)\right)^{-1}} du\right) \\
&\times \exp\left(-\frac{\gamma N_0}{P_D \zeta_D^{\mathrm{L}}(l)}\right)
\end{aligned} \tag{4.44}
$$

where $s = \frac{\gamma}{P_D \zeta_D^{\mathrm{L}}(l)}$. The logic of the calculation of T_D^{NL} is similar to that of T_D^{L}. Which concludes our proof. □

4.4 Simulation and Discussion

According to the 3GPP Long Term Evolution (LTE) specifications [128], we set the system bandwidth to 10MHz, carrier frequency f_c to 2GHz. The transmit power of each BS and each D2D transmitter are set to $P_B = 24\,\mathrm{dBm}$ and $P_D = 24\,\mathrm{dBm}$, respectively. Moreover, the threshold for selecting cellular mode communication is $\beta = -80 \sim -30\mathrm{dBm}$. The noise powers are set to $-95\,\mathrm{dBm}$ (including a noise figure of 9 dB at the receivers). Besides, the CU density λ_u is set to $300\,\mathrm{UEs/km}^2$, which leads to $q = 4.05$ in (4.7) and (4.8) [135]. The simulation parameters are summarized in Table 4.1.

Validation of Theorem 6 and 4 In this subsection, we present Monte Carlo sim-

Table 4.1 : Simulation Parameters

Parameters	Values	Parameters	Values
BW	10MHz	f_c	2GHz
λ_u	300 UEs/km^2	N_0	-95 dBm
α_{BL}	2.09	A_{BL}	$10^{-4.11}$
α_{BN}	3.75	A_{BN}	$10^{-3.29}$
α_{DL}	2	A_{DL}	$10^{-3.845}$
α_{DN}	4	A_{DN}	$10^{-5.578}$
P_b	24 dBm	P_d	24 dBm

ulation results to investigate the coverage probability and validate the analytical results in Theorem 6.

In Fig. 4.2, we plot the results of the coverage probability of cellular tier, we can draw the following observations:

- The analytical results of the coverage probability from Eq.(4.26) match well with the simulation results, which validates our analysis and shows that the adopted model accurately captures the features of the cellular tier in D2D-enhanced cellular networks.

- The coverage probability decreases with the increase of SINR threshold because a higher SINR requirement makes it more difficult to satisfy the coverage criterion in Eq.(4.20).

- For cellular tier, the coverage probability decreases as the interference management threshold beta increases because the larger beta, the more TU will operate in D2D mode and generate more interference to the cellular tier.

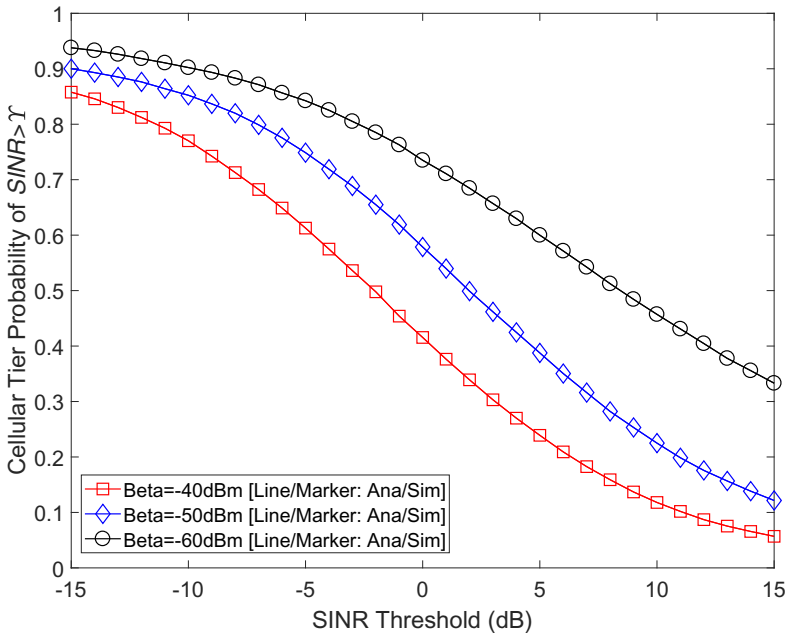

Figure 4.2 : The Coverage Probability $p_c^{\text{cov}}(\lambda, \gamma)$ vs. SINR threshold ($\lambda_b = 100\,\text{BSs/km}^2$, $\lambda_u = 300\,\text{UEs/km}^2$, $\lambda_{TU} = 150\,\text{UEs/km}^2$).

Validation of on the Coverage Probability for D2D tier

In this subsection, we present Monte Carlo simulation results to investigate the coverage probability and validate the analytical results in Theorem 4, we set the distance l is 30m.

In Fig. 4.3, we plot the results of the coverage probability of the D2D tier, we can draw the following observations:

- The analytical results of the coverage probability from Eq.(4.42) match well with the simulation results, which validates our analysis and shows that the adopted model accurately captures the features of the D2D tier in D2D-enhanced cellular networks.

- For D2D tier, the coverage probability decreases as the interference management threshold beta increases because the larger beta, the more TU will op-

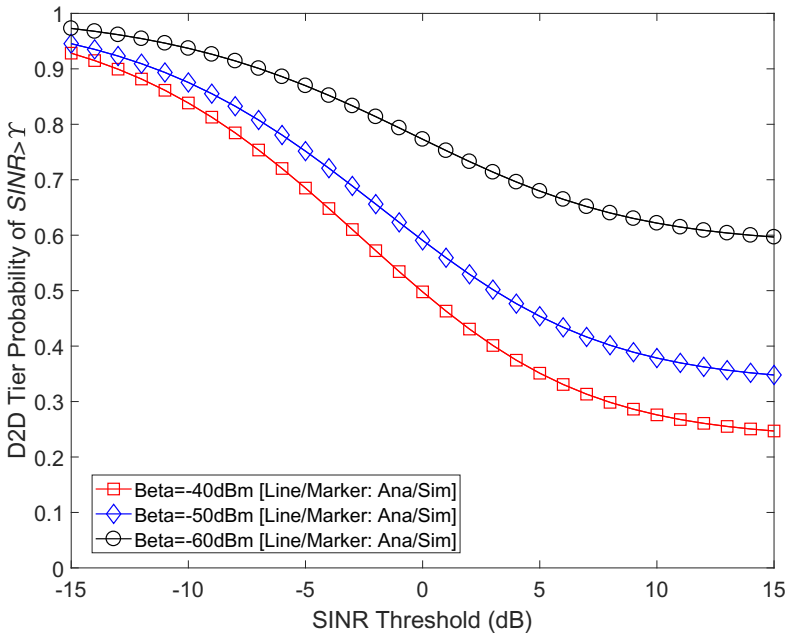

Figure 4.3 : The Coverage Probability of D2D tier vs. SINR threshold (λ_b = 100 BSs/km^2, λ_u = 300 UEs/km^2, λ_{TU} = 150 UEs/km^2).

erate in D2D mode and generate more interference to the D2D tier as well.

The Performance Impact of Proportional Fair Scheduler on the Coverage Probability

In this subsection, we consider the proportional fair scheduler to investigate the performance impact of the proportional fair scheduler on the coverage probability.

To fully study the coverage probability with respect to the BS density with or without the PF scheduler, the results of coverage probability with various BS density and γ_0=0 dB are plotted in Fig 4.4. From this figure, we can draw the following observations:

- As predicted in Theorem 6, although the PF scheduler shows a better performance than the RR one for all BS densities, such performance gain diminishes as the network evolves into an UDN due to the loss of multi-user diversity. As

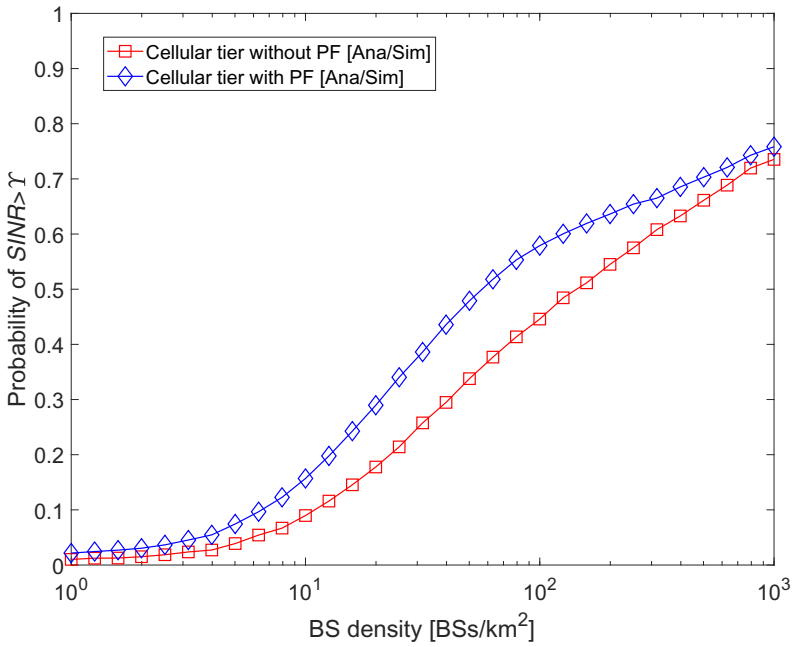

Figure 4.4 : The Coverage Probability $p^{\text{cov}}(\lambda, \gamma)$ vs. BS density ($\gamma_0 = 0\,\text{dB}$, $\lambda_u = 300\,\text{UEs/km}^2$, $\lambda_{TU} = 150\,\text{UEs/km}^2$, β=50dBm).

can be seen from Fig. 4.4, the performance gain of the PF scheduler continuously decreases from around 100 % (ratio=2) when $\lambda = 1\,\text{BSs/km}^2$ toward zero (ratio=1) in UDNs, e.g., $\lambda = 10^3\,\text{BSs/km}^2$.

- The detailed explanation of the performance behavior in Fig. 4.4 is provided as follows:
  - When $\lambda \in [10^0, 10^1]$ BSs/km^2, the network is noise-limited, and thus the coverage probabilities of both RR and PF increase with the BS density λ as the network is lightened up with more BSs.
  - When $\lambda \in [10^1, 10^2]$ BSs/km^2, the increase rate of $p^{\text{cov}}(\lambda, \gamma)$ of the PF scheduler decrease. This is because *(i)* the signal power is enhanced by LoS transmissions, as shown by the $p^{\text{cov}}(\lambda, \gamma)$ of the RR scheduler in that BS density region; while *(ii)* the multi-user diversity decreases in

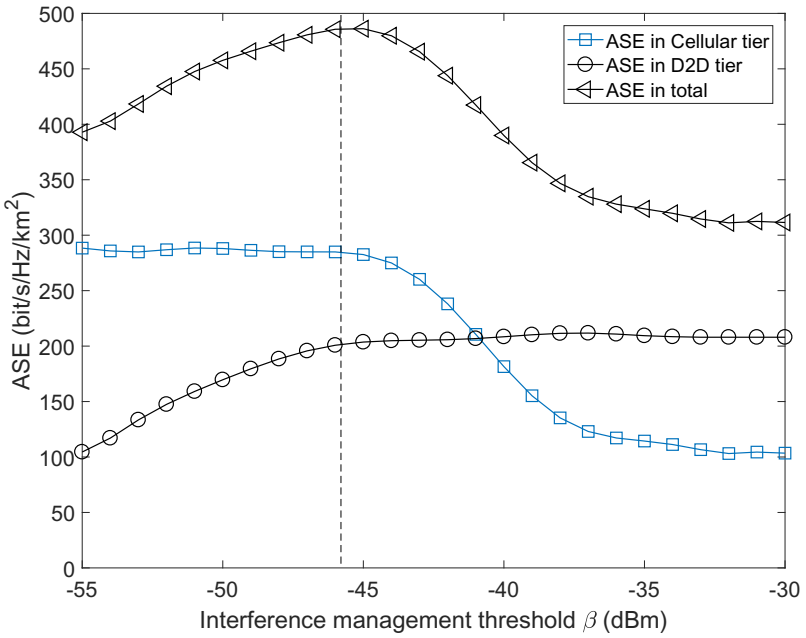

Figure 4.5 : The ASE $A^{\mathrm{ASE}}(\lambda, \gamma_0)$ vs. β ($\lambda_b = 100\,\mathrm{BSs/km}^2$,$\gamma_0 = 0\,\mathrm{dB}$, $\lambda_u = 300\,\mathrm{UEs/km}^2$, $\lambda_{Tu} = 150\,\mathrm{UEs/km}^2$).

that BS density region as exhibited in Fig. 4.4; and *(iii)* the above two factors roughly cancel each other out.

– When $\lambda > 10^2\,\mathrm{BSs/km}^2$, the coverage probabilities of both RR and PF continuously increase. Such performance behavior can be attributed to the BS idle mode operations, i.e., *(i)* the signal power continues increasing with the network densification, and *(ii)* the interference power is controlled because not all BSs are turned on and emit interference.

The Performance Impact of Mode Selection Threshold on the ASE

In this subsection, we investigate the performance impact of mode selection threshold on the ASE and we find there exists an optimal beta that can achieve the maximum ASE of the D2D-enabled cellular network.

The analytical results of ASE with γ_0=0 dB vs various β values are shown in

Eq.(5.10). Fig.4.5 illustrates the ASEs of Cellular links, D2D links and of the whole network with respect to different mode selection thresholds β . From this figure we can draw the following observations:

- When $\beta \in [-55dBm, -46dBm]$, the total ASE increases as the D2D links increases, because the D2D links do not generate a lot of interference to the cellular tier.

- An optimal β around -46 dBm which can achieve the maximum ASE there is a tradeoff between ASE increase for D2D links and ASE reduction for cellular links.

- When $\beta \in [-46dBm, -36dBm]$, the total ASE decreases because the D2D links generate more interference which makes the coverage probability of cellular UEs suffer. The ASE and the coverage probability of cellular links also decrease because the aggregate interference is now mostly LoS interference.

- When $\beta \in [-36dBm, -30dBm]$, the total ASE stay stable as well as the D2D ASE because the percentage of D2D UE is approaching 100%, which has been analyzed in Eq.(4.17).

From Fig.4.1, we can see that the additional D2D links make a significant contribution to the ASE performance and the D2D links will increase as β increase for all different densities of BS. At first, D2D links will enhance the ASE performance but they do not generate a lot of interference to the cellular tier. Then the increase of D2D transmitter will generate more interference which makes the coverage probability of cellular UEs suffer. The optimal β can be found in this stage for different densities of BS. At last stay stable as well as the D2D ASE because the percentage of D2D UE is approaching 100%. Above all, there exists an optimal β that can achieve the maximum ASE of the D2D-enabled cellular network while the

coverage probability in the cellular tier is guaranteed. The mode selection threshold can control the interference from both cellular tier and D2D tier. In addition, the D2D tier can nearly double the ASE for the network when appropriately choosing the threshold for mode selection.

4.5 Summary

In this chapter, we extended the system we designed in Chapter 3 with considering the PF scheduler in the cellular tier. With considering the PF scheduler, our results showed that the interference management method mitigates large interference from D2D transmitter to cellular network and the PF scheduler can improve the network performance significantly when the BS density is smaller than 10^{-3}BSs/km^2. Moreover, we concluded that D2D tier can improve the network performance when the threshold parameter is appropriately chosen and there exists an optimal β to achieve the maximum ASE while guaranteeing the coverage probability performance of cellular network.

Chapter 5

Optimal Antenna Downtilt in UDN

5.1 Introduction

In this chapter, we investigate the impact of the antenna pattern and downtilt on the performance of the downlink (DL) cellular networks, in terms of the coverage probability and the area spectral efficiency. We also derive the analytical expressions for the optimal antenna downtilt that can achieve the best coverage probability of the network given a certain BS density.

The rest of this chapter is structured as follows: Section 5.2 describes the system model. Section 5.3 presents our theoretical results on the coverage probability, the optimal antenna downtilt and the simplified results for 3GPP special cases.Numerical results are discussed in Section 5.4, with remarks shedding new light on the relevance of our results in guiding the network deployment. Finally, conclusions are drawn in Section 5.5.

5.2 System Model

In this section, we will first explain the scenario of the 3D random cellular network. Then, we will present the path loss model and the antenna patterns considered in this chapter.

5.2.1 Scenario Description

We consider a 3D random cellular network with downlink (DL) transmissions, where BSs are deployed on a plane according to an HPPP Φ_b of intensity λ_B

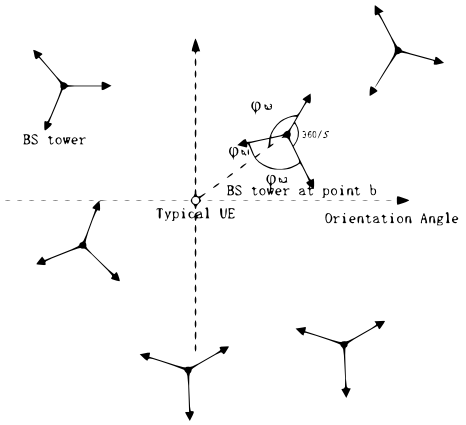

Figure 5.1 : An illustration of the 3D horizontal angle. The solid black dots indicate BSs, black arrows indicate the direction of the main beam for each sector.

BSs/km^2. UEs are also Poissonly distributed in the considered area with an intensity of λ_{UE} UEs/km^2. In this model, BSs transmit at a power P_B, a UE can reliably communicate with a BS only when its downlink signal-to-interference-plus-noise ratio (SINR) is greater than γ. For each base station, we consider there are S sectors. We only consider one antenna in each sector and only the main lobe beamforming gain is considered, the beamforming includes the the horizontal and vertical antenna beamforming gain. In the same BS tower, the horizontal angle between the main beams of two adjacent sectors is set to $\frac{360}{S}$ degrees. The orientations of the sectors are randomly and uniformly distributed in $[0, 2\pi)$. For example, for LTE macrocell BSs, $S = 3$ and the horizontal angle between two adjacent sectors in the same BS tower is 120 degrees. Each sector has the vertical antenna pattern, we denote the horizontal direction as 0 degree. Hence, the vertical antenna downtilt angle and the angle from the BS antenna to the UE antenna by θ_{tilt} and θ, respectively, as shown in Fig.5.2.

Without loss of generality, we conduct analysis and simulation on a typical mobile user located at the origin, similar to [21, 141, 142]. Note that λ_{UE} is assumed to be sufficiently larger than λ_B so that each BS has at least one associated UE in its

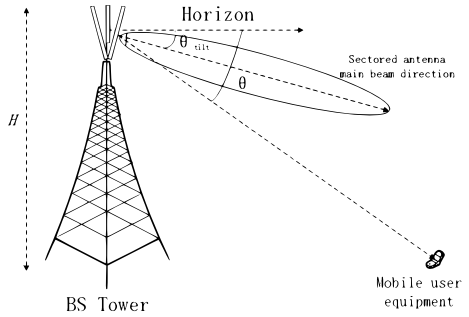

Figure 5.2 : An illustration of the 3D vertical angle.

coverage [30, 127, 133]. The two-dimensional (2D) distance between an arbitrary BS and an arbitrary UE is denoted by r. Moreover, the absolute antenna height difference between a BS and a UE is denoted by L. Note that the value of L is in the order of several meters. Hence, the 3D distance w between a BS and a UE can be expressed as

$$w = \sqrt{r^2 + L^2}, \tag{5.1}$$

where $L = H - h$ and H is the antenna height of BS and h is the antenna height of UE. Intuitively, the antenna height of BS should decrease as the network becomes dense, however, there is no consensus on how H should decrease with an increase in λ_B. In this work, we assume that H, and thus L, are constants. For the current 4G networks, parameter L is around 8.5m because the picocell BS antenna height and the UE antenna height are assumed to be 10m and 1.5m, respectively [26].

5.2.2 Path Loss Model

The path loss function $\zeta(w)$ is segmented into N pieces with each piece denoted by $\zeta_n(w)$ [128]. Besides, $\zeta_n^{\mathrm{L}}(w)$, $\zeta_n^{\mathrm{NL}}(w)$ and $\mathrm{Pr}_n^{\mathrm{L}}(w)$ are the n-th piece of the path loss function for the LoS transmission, the n-th piece of the path loss function for the NLoS transmission, and the n-th piece of the LoS probability function, respectively.

It can be written as

$$\zeta(w)=\begin{cases}\zeta_1(w)=\begin{cases}\zeta_1^{\mathrm{L}}(w), & \text{with probability } \Pr_1^{\mathrm{L}}(w)\\ \zeta_1^{\mathrm{NL}}(w), & \text{with probability } \left(1-\Pr_1^{\mathrm{L}}(w)\right)\end{cases}\\ \zeta_2(w)=\begin{cases}\zeta_2^{\mathrm{L}}(w), & \text{with probability } \Pr_2^{\mathrm{L}}(w)\\ \zeta_2^{\mathrm{NL}}(w), & \text{with probability } \left(1-\Pr_2^{\mathrm{L}}(w)\right)\end{cases}\\ \vdots\\ \zeta_n(w)=\begin{cases}\zeta_n^{\mathrm{L}}(w), & \text{with probability } \Pr_n^{\mathrm{L}}(w)\\ \zeta_n^{\mathrm{NL}}(w), & \text{with probability } \left(1-\Pr_n^{\mathrm{L}}(w)\right)\end{cases}\end{cases}. \tag{5.2}$$

Each piece $\zeta_n(w), n\in\{1,2,\ldots,N\}$ is modeled as

$$\zeta_n(w)=\begin{cases}\zeta_n^{\mathrm{L}}(w)=A^{\mathrm{L}}w^{-\alpha_n^{\mathrm{L}}}, & \text{LoS Probability: } \Pr_n^{\mathrm{L}}(w)\\ \zeta_n^{\mathrm{NL}}(w)=A^{\mathrm{NL}}w^{-\alpha_n^{\mathrm{NL}}}, & \text{NLoS Probability: } 1-\Pr_n^{\mathrm{L}}(w)\end{cases}, \tag{5.3}$$

where A^{L} and A^{NL} are the path losses at a reference distance $w=1$ for the LoS and the NLoS cases, respectively. α_n^{L} and α_n^{NL} are the path loss exponents for the LoS and the NLoS cases, respectively. In practice, A^{L}, A^{NL}, α_n^{L} and α_n^{NL} are constants obtainable from field tests and continuity constraints [125]. The LoS probability can be computed by the following piecewise function modeled as [16],

$$\Pr^{\mathrm{L}}(w)=\begin{cases}\Pr_1^{\mathrm{L}}(w), & L<w\le d_1\\ \Pr_2^{\mathrm{L}}(w), & d_1<w<d_2\\ \vdots & \vdots\\ \Pr_n^{\mathrm{L}}(w), & w>d_{n-1}\end{cases}, \tag{5.4}$$

which means the link from the typical UE to the typical BS has a LoS path or a NLoS path with probability $\Pr^{\mathrm{L}}(w)$ and $1-\Pr^{\mathrm{L}}(w)$, respectively, $n\in\{1,2,\cdots,N\}$.

5.2.3 3D Antenna Pattern

3D antenna patterns are introduced in this subsection. According to [19] and the 3GPP [26], UE antenna pattern is assumed to be isotropic and the 3D antenna gain of each sector antenna in the BS can be approximated in dBi as

$$G(\varphi_{b,i}, \theta_b, \theta_{tilt})^{\mathtt{dBi}} = G_h(\varphi_{b,i}) + G_v(\theta_b, \theta_{tilt}) + G_m, \tag{5.5}$$

where $G_h(\varphi_{b,i})$ and $G_v(\theta_b, \theta_{tilt})$ are the normalized horizontal and vertical antenna gain from the i-th sector of the BS at point b to the typical UE in dBi, respectively. G_m is the maximum antenna gain. The 3D pattern is assumed to be fixed, i.e., no adaptive beamforming is employed. The parameter $\varphi_{b,i}$ is the horizontal angle relative the main lobe beam pointing direction from the i-th ($i \in 1, 2, 3, ..., S$) sector of the BS at point b to the typical UE, i.e., horizontal departure angles for one BS-to-UE link. For the BS to UE link, there are S horizontal departure angles for the S sectors' antennas, we sort such angles in an ascending order and denote them as $\varphi_{b,1} \leq ... \leq \varphi_{b,S}$, where b is point in the map which represent the BS location. An example is shown in Fig.5.1. As we denote the horizontal direction as 0 degree, θ_{tilt} is the downtilt angle of the BS antennas, and $0 \leq \theta_{tilt} \leq 90$ degrees is the negative elevation angle relative the horizontal plane (i.e., $\theta_{tilt} = 0$ is along the horizontal plane, and $\theta_{tilt} \geq 0$ is downwards). $\theta_b = \arctan\left(\frac{L}{r_b}\right)$ is the angle between the horizontal direction and the direction from the BS at point b to the typical UE. Parameter r_b is the distance from the BS at point b to the typical UE.

5.2.4 User Association and Performance Metrics

In this chapter, we assume a practical user association strategy (UAS) that each UE connects to the sector of the BS with the strongest average received power strength P^* [16, 21] which can be written as

$$P^* = \max_{\Phi_b} \{P_B G(\varphi_{b,i}, \theta_b, \theta_{tilt}) \zeta_b (d_b)\} \tag{5.6}$$

where $G(\varphi_{b,i}, \theta_b, \theta_{tilt}) = 10^{\frac{1}{10}G(\varphi_{b,i},\theta_b,\theta_{tilt})^{\mathtt{dBi}}}$, d_b is the distance from the BS at point b to the typical UE. P_B and $\zeta_b(d_b)$ are the transmission power of BS and the path loss from the BS at the point b to the typical UE, respectively.

Based on the above definitions, when the user associates with the sector of the macrocell BS at point $\bar{X}$, we define the coverage probability as a probability that a receiver's signal-to-interference-plus-noise ratio (SINR) is above a pre-designated threshold γ:

$$p^{\text{cov}}(\lambda_B, \gamma) = \Pr[\text{SINR} > \gamma], \tag{5.7}$$

where the SINR is calculated as

$$\text{SINR} = \frac{P_B G(\varphi_{\bar{b},1}, \theta_b, \theta_{tilt}) \zeta_{\bar{b}}(r)\, g}{I_{\text{agg}} + N_0}, \tag{5.8}$$

where g is the channel gain of Rayleigh fading, which is modeled as an exponential random variable (RV) with a mean of one. Parameter r is the distance from the associated BS at point $\bar{b}$ to the typical UE. Parameter N_0 is the additive white Gaussian noise (AWGN) power at each UE. Parameter I_{agg} is the cumulative interference given by

$$\begin{aligned} I_{\text{agg}} = &\sum_{i=2}^{S} P_B G(\varphi_{\bar{b},i}, \theta_{\bar{b}}, \theta_{tilt}) \zeta_{\bar{b}}(r)\, g_{\bar{b}} \\ &+ \sum_{b \in \Phi_b/\bar{b}} \sum_{i=1}^{S} P_B G(\varphi_{b,i}, \theta_b, \theta_{tilt}) \zeta_b(d_b)\, g_b. \end{aligned} \tag{5.9}$$

where d_b is the distance from the BS at point b to the typical UE. The symbol $\zeta_b(d_b)$ is the path loss function from the BS at point b to the typical UE. The first term of Eq.(5.9) represents the intra-cell inter-sector interference while the second represents the inter-cell interference.

Similar to [16,133], the area spectral efficiency in bps/Hz/km^2 can be formulated

as

$$A^{\mathrm{ASE}}\left(\lambda_B, \gamma_0\right) = \lambda_B \int_{\gamma_0}^{\infty} \log_2\left(1+x\right) f_X\left(\lambda_B, \gamma_0\right) dx, \tag{5.10}$$

where γ_0 is the minimum working SINR for the considered network, and $f_X\left(\lambda_B, \gamma_0\right)$ is the probability density function (PDF) of the SINR observed at the typical receiver for a particular value of λ_B.

5.3 Performance of the UDN Applying Antenna Downtilt

Using the 3D model and the stochastic geometry theory, we study the performance of cellular network and derive the optimal antenna downtilt for each certain base station density in this section. Without any loss of generality, we assume that the mobile user under consideration is located at the origin.

5.3.1 Coverage Probablity

Based on the path loss model in Eq.(5.2) and the adopted UAS, our results of $p^{\mathrm{cov}}\left(\lambda_B, \gamma\right)$ can be summarized in Theorem 6.

Theorem 6. *Considering the path loss model in Eq.(5.2) and the presented UAS, the probability of coverage* $p^{\mathrm{cov}}\left(\lambda_B, \gamma\right)$ *can be derived as*

$$p^{cov}\left(\lambda_B, \gamma\right) = \sum_{n=1}^{N} \left(T_n^L + T_n^{NL}\right) \tag{5.11}$$

where

$$\begin{aligned} T_n^L = & \int_0^{\frac{\pi}{S}} \int_{\sqrt{d_{n-1}^2 - L^2}}^{\sqrt{d_n^2 - L^2}} \\ & \times \Pr\left[\frac{P_B G(\varphi_{\bar{b},1}, \theta_{\bar{b}}, \theta_{tilt}) \zeta_{\bar{b}}^L\left(w\right) g_{\bar{b}}}{I_{\mathrm{agg}} + N_0} > \gamma \middle| w, \varphi_{\bar{b},1}\right] \\ & \times f_{R,n}^{\mathrm{L}}\left(r\right) f\left(\varphi\right) dr d\varphi \end{aligned} \tag{5.12}$$

which represent the signal is in the n-th piece of path loss function for the LoS transmission,

$$T_n^{NL} = \int_0^{\frac{\pi}{S}} \int_{\sqrt{d_{n-1}^2 - L^2}}^{\sqrt{d_n^2 - L^2}} \times \Pr\left[\frac{P_B G(\varphi_{\bar{b},1}, \theta_{\bar{b},}, \theta_{tilt}) \zeta_{\bar{b}}^{NL}(w)\, g_{\bar{b}}}{I_{\text{agg}} + N_0} > \gamma \middle| w, \varphi_{\bar{b},1} \right] \times f_{R,n}^{\text{NL}}(r)\, f(\varphi)\, dr d\varphi \tag{5.13}$$

which represent the signal is in the n-th piece of path loss function for the NLoS transmission. I_{agg} *is the aggregation interference from the LoS path and NLoS path.* $f(\varphi)$ *is the distribution of the smallest horizontal angle from the signal BS to the typical UE. Based on the assumptions in the system model, the angle* φ *is uniformly distributed in* $\left[0, \frac{\pi}{S}\right]$*, so* $f(\varphi) = \frac{S}{\pi}$ *when* $0 < \varphi < \frac{\pi}{S}$*. Where* $f_{R,n}^{\text{L}}(r)$ *and* $f_{R,n}^{\text{NL}}(r)$ *are the distance distribution of the n-piece signal link when the link is LoS and NLoS, which can be written as*

$$\begin{aligned} f_{R,n}^{\text{L}}(r) = {} & \exp\left(\int_0^{r_2} Pr_n^L(u) 2\pi u \lambda_B du \right) \\ & \times \exp\left(\int_0^{r_1} \left(1 - Pr_n^L(u)\right) 2\pi u \lambda_B du \right) \\ & \times \exp\left(\int_0^{r} Pr_n^L(u) 2\pi u \lambda_B du \right) \\ & \times Pr_n^L(u) 2\pi u \lambda_B, \end{aligned} \tag{5.14}$$

$$\begin{aligned} f_{R,n}^{\text{NL}}(r) = {} & \exp\left(\int_0^{r_4} Pr_n^L(u) 2\pi u \lambda_B du \right) \\ & \times \exp\left(\int_0^{r_3} \left(1 - Pr_n^L(u)\right) 2\pi u \lambda_B du \right) \\ & \times \exp\left(\int_0^{r} \left(1 - Pr_n^L(u)\right) 2\pi u \lambda_B du \right) \\ & \times \left(1 - Pr_n^L(u)\right) 2\pi u \lambda_B \end{aligned} \tag{5.15}$$

where $r_{\{1,2,3,4\}}$ *are given implicitly by the following equations as*

$$r_1^2 = \left(\frac{G(\varphi_{\bar{b},1}, \theta_{\bar{b}}, \theta_{tilt}) A_L}{G(\varphi_{b_1,1}, \theta_{b_1}, \theta_{tilt}) A_{NL}} \right)^{-\frac{2}{\alpha_{NL}}} \left(r^2 + L^2\right)^{\frac{\alpha_L}{\alpha_{NL}}} \tag{5.16}$$

and

$$r_2^2 = \left(\frac{G(\varphi_{\bar{b},1}, \theta_{\bar{b}}, \theta_{tilt})}{G(\varphi_{b_2,1}, \theta_{b_2}, \theta_{tilt})} \right)^{-\frac{2}{\alpha_L}} \left(r^2 + L^2 \right) \tag{5.17}$$

and

$$r_3^2 = \left(\frac{G(\varphi_{\bar{b},1}, \theta_{\bar{b}}, \theta_{tilt})}{G(\varphi_{b_3,1}, \theta_{b_3}, \theta_{tilt})} \right)^{-\frac{2}{\alpha_{NL}}} \left(r^2 + L^2 \right) \tag{5.18}$$

and

$$r_4^2 = \left(\frac{G(\varphi_{\bar{b},1}, \theta_{\bar{b}}, \theta_{tilt}) A_{NL}}{G(\varphi_{b_4,1}, \theta_{b_4}, \theta_{tilt}) A_L} \right)^{-\frac{2}{\alpha_L}} \left(r^2 + L^2 \right)^{\frac{\alpha_{NL}}{\alpha_L}}, \tag{5.19}$$

$\Pr\left[\frac{P_B G(\varphi_{\bar{b},1}, \theta_{\bar{b}}, \theta_{tilt}) \zeta_{\bar{b}}^{L}(w) g_{\bar{b}}}{I_r + N_0} > \gamma \middle| w, \varphi_{\bar{b},1} \right]$ *and* $\Pr\left[\frac{P_B G(\varphi_{\bar{b},1}, \theta_{\bar{b}}, \theta_{tilt}) \zeta_{\bar{b}}^{NL}(w) g_{\bar{b}}}{I_r + N_0} > \gamma \middle| w, \varphi_{\bar{b},1} \right]$ *can be respectively computed by*

$$\begin{aligned} &\Pr\left[\frac{P_B G(\varphi_{\bar{b},1}, \theta_{\bar{b}}, \theta_{tilt}) \zeta_{\bar{b}}^{L}(w) g_{\bar{b}}}{I_r + N_0} > \gamma \middle| w, \varphi_{\bar{b},1} \right] \\ &= \exp\left(- \frac{\gamma \mathrm{N}_0}{\mathrm{P_B G}(\varphi_{\bar{\mathrm{b}},1}, \theta_{\bar{\mathrm{b}}}, \theta_{\mathrm{tilt}}) \mathrm{A^L} \left(\mathrm{r}^2 + \mathrm{L}^2 \right)^{-\frac{\alpha^{\mathrm{L}}}{2}}} \right) \\ &\times L_{I_{\mathrm{agg}}} \left(\frac{\gamma}{\mathrm{P_B G}(\varphi_{\bar{\mathrm{b}},1}, \theta_{\bar{\mathrm{b}}}, \theta_{\mathrm{tilt}}) \mathrm{A^L} \left(\mathrm{r}^2 + \mathrm{L}^2 \right)^{-\frac{\alpha^{\mathrm{L}}}{2}}} \right). \end{aligned} \tag{5.20}$$

and

$$\begin{aligned} &\Pr\left[\frac{P_B G(\varphi_{\bar{b},1}, \theta_{\bar{b}}, \theta_{tilt}) \zeta_{\bar{b}}^{NL}(w) g_{\bar{b}}}{I_r + N_0} > \gamma \middle| w, \varphi_{\bar{b},1} \right] \\ &= \exp\left(- \frac{\gamma \mathrm{N}_0}{\mathrm{P_B G}(\varphi_{\bar{\mathrm{b}},1}, \theta_{\bar{\mathrm{b}}}, \theta_{\mathrm{tilt}}) \mathrm{A^{NL}} \left(\mathrm{r}^2 + \mathrm{L}^2 \right)^{-\frac{\alpha^{\mathrm{NL}}}{2}}} \right) \\ &\times L_{I_{\mathrm{agg}}} \left(\frac{\gamma}{\mathrm{P_B G}(\varphi_{\bar{\mathrm{b}},1}, \theta_{\bar{\mathrm{b}}}, \theta_{\mathrm{tilt}}) \mathrm{A^{NL}} \left(\mathrm{r}^2 + \mathrm{L}^2 \right)^{-\frac{\alpha^{\mathrm{NL}}}{2}}} \right). \end{aligned} \tag{5.21}$$

where $L_{I_{\mathrm{agg}}} \left(\frac{\gamma}{\mathrm{P_B G}(\varphi_{\bar{\mathrm{b}},1}, \theta_{\bar{\mathrm{b}}}, \theta_{\mathrm{tilt}}) \mathrm{A^L w}^{-\alpha^{\mathrm{L}}}} \right)$ *and* $L_{I_{\mathrm{agg}}} \left(\frac{\gamma}{\mathrm{P_B G}(\varphi_{\bar{\mathrm{b}},1}, \theta_{\bar{\mathrm{b}}}, \theta_{\mathrm{tilt}}) \mathrm{A^{NL} w}^{-\alpha^{\mathrm{NL}}}} \right)$ *are the Laplace transform of* I_{agg} *evaluated at* s *and* I_{agg} *is the aggregation interference at the typical UE.*

Proof. For clarity, we first summarize our ideas to prove Theorem 6. In order to evaluate $p^{\mathrm{cov}}(\lambda_B, \gamma)$, the first key step is to calculate the distance PDFs for the

events that the typical UE is associated with the strongest BS with a LoS path or that with a NLoS path, so that the integral of Pr[SINR $> \gamma$] can be performed over the distance w. The second key step is to calculate Pr[SINR $> \gamma$] for the LoS and the NLoS cases conditioned on w and $\varphi_{\bar{b},1}$. Since the two events that the typical UE is connected to a BS with a LoS path and that with a NLoS path are disjoint events, we have the probability of coverage $p^{\text{cov}}(\lambda_B, \gamma)$ can be derived as

$$
\begin{aligned}
& p^{\text{cov}}(\lambda_B, \gamma) \\
&= \int_0^{\frac{\pi}{S}} \int_0^{\infty} \Pr\left[\frac{P_B G(\varphi_{\bar{b},1}, \theta_b, \theta_{tilt}) \zeta(r)\, g}{I_{\text{agg}} + N_0} > \gamma \middle| r \right] \\
&\times f_R(r)\, f(\varphi)\, dr d\varphi \\
&= \int_0^{\frac{\pi}{S}} \int_0^{\sqrt{d_1^2 - L^2}} \Pr\left[\frac{P_B G(\varphi_{\bar{b},1}, \theta_b, \theta_{tilt}) \zeta_1^L(r)\, g}{I_{\text{agg}} + N_0} > \gamma \middle| r \right] \\
&\times f_{R,1}^{\text{L}}(r)\, f(\varphi)\, dr d\varphi \\
&+ \int_0^{\frac{\pi}{S}} \int_0^{\sqrt{d_1^2 - L^2}} \Pr\left[\frac{P_B G(\varphi_{\bar{b},1}, \theta_b, \theta_{tilt}) \zeta_1^{NL}(r)\, g}{I_{\text{agg}} + N_0} > \gamma \middle| r \right] \\
&\times f_{R,1}^{\text{NL}}(r)\, f(\varphi)\, dr d\varphi \\
&\vdots \\
&+ \int_0^{\frac{\pi}{S}} \int_{\sqrt{d_{n-1}^2 - L^2}}^{\infty} \Pr\left[\frac{P_B G(\varphi_{\bar{b},1}, \theta_b, \theta_{tilt}) \zeta_n^L(r)\, g}{I_{\text{agg}} + N_0} > \gamma \middle| r \right] \\
&\times f_{R,n}^{\text{L}}(r)\, f(\varphi)\, dr d\varphi \\
&+ \int_0^{\frac{\pi}{S}} \int_{\sqrt{d_{n-1}^2 - L^2}}^{\infty} \Pr\left[\frac{P_B G(\varphi_{\bar{b},1}, \theta_b, \theta_{tilt}) \zeta_n^{NL}(r)\, g}{I_{\text{agg}} + N_0} > \gamma \middle| r \right] \\
&\times f_{R,n}^{\text{NL}}(r)\, f(\varphi)\, dr d\varphi \\
&= \sum_{n=1}^{N} \left(T_n^L + T_n^{NL} \right)
\end{aligned}
\tag{5.22}
$$

where $f_R(r)$ is the distance distributions of the signal link which can be divided to $f_{R,n}^{\text{L}}(r)$ and $f_{R,n}^{\text{NL}}(r)$, $f_{R,n}^{\text{L}}(r)$ and $f_{R,n}^{\text{NL}}(r)$ are the distance distribution of the n-piece signal link when the link is LoS and NLoS, I_{agg} is the aggregation interference from the LoS path and NLoS path. N_0 is the additive white Gaussian noise (AWGN)

power at each UE. In the following, we show how to compute $f_{R,n}^{\mathrm{L}}(r)$ in Eq.(5.22) first. To that end, we define three events as follows:

Event B^L: The nearest BS with a LoS path and the horizontal arrive angle of the antenna $\varphi_{\bar{b},1}$ to the typical UE, is located at distance R^L. According to [30], the CCDF of R^L is written as $\overline{F}_r^L(r) = \exp\left(-\int_0^r \Pr_n^L(u) 2\pi u \lambda_B du\right)$. Taking the derivative of $(1 - \overline{F}_r^L(r))$ with regard to w, we can get the PDF of R^L as

$$f_r^L(r) = \exp\left(\int_0^r \Pr^{\mathrm{L}}(u) 2\pi u \lambda_B du\right) \Pr_n^{\mathrm{L}}(u) 2\pi u \lambda_B. \tag{5.23}$$

Event C^{NL} conditioned on the value of R^L: Given that $R^L = r$, the typical UE is then associated with such BS at distance $R^L = r$. To make the typical UE associated with the LoS BS at distance $R^L = r$, such BS should give the strongest average received power strength from such BS to the typical UE, i.e., there should be no BS with a NLoS path and the horizontal arrive angle of the antenna $\varphi_{b_1,1}$ inside the disk centered on the UE with a radius of $r_1 < r$ to outperform such LoS BS at distance $R^L = r$, where $G(\varphi_{b_1,1}, \theta_{b_1}, \theta_{tilt}) \zeta^{NL}(w_1) = G(\varphi_{\bar{b},1}, \theta_{\bar{b}}, \theta_{tilt}) \zeta^L(w)$ and $w_1 = \sqrt{r_1^2 + L^2}$. BS at point b_1 is located at the distance r_1 to the typical UE. Such conditional probability of C^{NL} on the condition of $R^L = r$ can be computed by

$$\begin{aligned} &\Pr\left[C^{NL} \middle| R^L = r\right] \\ =&\exp\left(\int_0^{r_1} \left(1 - \Pr^{\mathrm{L}}(u)\right) 2\pi u \lambda_B du\right). \end{aligned} \tag{5.24}$$

Event D^L conditioned on the value of R^L: Given that $R^{NL} = r$, the typical UE is then associated with such BS at distance $R^{NL} = r$. To make the typical UE associated with the LoS BS at distance $R^L = r$, there also should be no BS with a LoS path and the horizontal arrive angle of the antenna $\varphi_{b_2,1}$ inside the disk centered on the UE with a radius of $r_2 < r$ to outperform such LoS BS at distance $R^L = r$, where $G(\varphi_{b_2,1}, \theta_{b_2}, \theta_{tilt}) \zeta^L(w_2) = G(\varphi_{\bar{b},1}, \theta_{\bar{b}}, \theta_{tilt}) \zeta^L(w)$ and

$w_2 = \sqrt{r_2^2 + L^2}$. BS at point b_2 is located at the distance r_2 to the typical UE. Such conditional probability of D^L on the condition of $R^{NL} = r$ can be computed by

$$\Pr\left[D^L \middle| R^L = r\right] = \exp\left(\int_0^{r_2} \Pr^{\mathrm{L}}(u) 2\pi u \lambda_B du\right). \tag{5.25}$$

we can get the PDF of r^L as

$$f_R^{\mathrm{L}}(r) = \Pr\left[C^{NL} \middle| R^L = r\right] \Pr\left[D^L \middle| R^L = r\right] f_R^L(r). \tag{5.26}$$

Considering the distance range of $d_{n-1} < \sqrt{r^2 + L^2} < d_n$, we can extract the segment of $f_{R,n}^{\mathrm{L}}(r)$ from $f_R^{\mathrm{L}}(r)$as

$$\begin{aligned} f_{R,n}^{\mathrm{L}}(r) = & \exp\left(\int_0^{r_2} \Pr_n^{\mathrm{L}}(u) 2\pi u \lambda_B du\right) \\ & \times \exp\left(\int_0^{r_1} \left(1 - \Pr_n^{\mathrm{L}}(u)\right) 2\pi u \lambda_B du\right) \\ & \times \exp\left(\int_0^{r} \Pr_n^{\mathrm{L}}(u) 2\pi u \lambda_B du\right) \Pr_n^{\mathrm{L}}(u) 2\pi u \lambda_B. \end{aligned} \tag{5.27}$$

where

$$r_1^2 = \left(\frac{G(\varphi_{\bar{b},1}, \theta_{\bar{b}}, \theta_{tilt}) A_L}{G(\varphi_{b_1,1}, \theta_{b_1}, \theta_{tilt}) A_{NL}}\right)^{-\frac{2}{\alpha_{NL}}} \left(r^2 + L^2\right)^{\frac{\alpha_L}{\alpha_{NL}}}, \tag{5.28}$$

and

$$r_2^2 = \left(\frac{G(\varphi_{\bar{b},1}, \theta_{\bar{b}}, \theta_{tilt})}{G(\varphi_{b_2,1}, \theta_{b_2}, \theta_{tilt})}\right)^{-\frac{2}{\alpha_L}} \left(r^2 + L^2\right). \tag{5.29}$$

Having obtained $f_{R,n}^{\mathrm{L}}(r)$, we move on to evaluate $\Pr\left[SINR > \gamma \middle| w, \varphi_{\bar{b},1}, \mathrm{LoS}\right]$ in Eq.(5.22) as

$$\begin{aligned} & \Pr\left[\frac{P_B G(\varphi_{\bar{b},1}, \theta_r, \theta_{tilt}) \zeta_{\bar{b}}^L(w)\, g_{\bar{b}}}{I_{\mathrm{agg}} + N_0} > \gamma \middle| w, \varphi_{\bar{b},1}\right] \\ = & \Pr\left[g_{\bar{b}} > \frac{\gamma\left(I_{\mathrm{agg}} + N_0\right)}{P_B G(\varphi_{\bar{b},1}, \theta_r, \theta_{tilt}) A^L \left(r^2 + L^2\right)^{-\frac{\alpha^L}{2}}} \middle| w, \varphi_{\bar{b},1}\right] \\ = & \exp\left(-\frac{\gamma \mathrm{N}_0}{\mathrm{P_B G}(\varphi_{\bar{\mathrm{b}},1}, \theta_{\mathrm{r}}, \theta_{\mathrm{tilt}}) \mathrm{A}^{\mathrm{L}} \left(\mathrm{r}^2 + \mathrm{L}^2\right)^{-\frac{\alpha^{\mathrm{L}}}{2}}}\right) L_{I_{\mathrm{agg}}}^L(s), \end{aligned} \tag{5.30}$$

where I_{agg} is the aggregation interference from the LoS path and NLoS path. $s = \frac{\gamma}{\mathrm{P_B G(\varphi_{\bar{b},1}, \theta_r, \theta_{tilt}) A^L w^{-\alpha^L}}}$,

$$
\begin{aligned}
L_{I_{\text{agg}}}^{L}(s) &= \mathbb{E}_{[I_{agg}]}\left\{\exp\left(-sI_{\text{agg}}\right)\right\} \\
&= \mathbb{E}_{[\phi,\{g\}]}\left\{\exp\left[-s\left(\sum_{i\in\phi_b/b}\sum_{n=1}^{S} P_B g_i \zeta_i G(\varphi_{i,n},\theta_u,\theta_{tilt})\right.\right.\right. \\
&\quad \left.\left.\left. + \sum_{n=2}^{S} P_B A^L \left(r^2+L^2\right)^{-\frac{\alpha^L}{2}} G(\varphi_{b,n},\theta_r,\theta_{tilt}) g\right)\right]\right\} \\
&= \exp\left(-2\pi\lambda_B \int_0^{\frac{\pi}{s}} \int_r^{\infty} (1- \right. \\
&\quad \left. - \mathbb{E}_{\{g\}}\left\{\exp\left(-s\sum_{n=1}^{s} P_B \zeta(u)\, G(\varphi_{b,n},\theta_u,\theta_{tilt})\right)\right\}\right) \\
&\quad \times u f(\varphi_{b,1})\, du d\varphi_{b,1}) \\
&\quad \times \prod_{n=2}^{S} \mathbb{E}_{\{g\}}\left\{\exp\left[P_B A^L \left(r^2+L^2\right)^{-\frac{\alpha^L}{2}} G(\varphi_{b,n},\theta_r,\theta_{tilt})\right]\right\} \\
&= \exp\left(-2\pi\lambda_B \int_0^{\frac{\pi}{s}} \int_r^{\infty}\right. \\
&\quad \left. \times \left(\frac{u}{1+\left(s\sum_{n=1}^{s} P_B \zeta(u)\, G(\varphi_{b,n},\theta_u,\theta_{tilt})\right)^{-1}} du\right)\right. \\
&\quad \times f(\varphi_{b,1})\, d\varphi_{b,1}) \\
&\quad \times \prod_{n=2}^{S}\left(\frac{1}{P_B A^L \left(r^2+L^2\right)^{-\frac{\alpha^L}{2}} G(\varphi_{b,n},\theta_r,\theta_{tilt}) - 1}\right)
\end{aligned}
\tag{5.31}
$$

where $\theta_u = \arctan\left(\frac{L}{u}\right)$ is a function of u, when the antenna heigth difference is a constant and $G(\varphi_{b,n},\theta_u,\theta_{tilt})$ is a determined variable conditioned on $\varphi_{b,1}$ and u. Similar to the process of LoS, we have omitted the proof steps of the computation of $f_{R,n}^{\text{NL}}(r)$ in Eq.(5.22) and $\Pr\left[\, SINR > \gamma \middle| \, w, \varphi_{\bar{b},1}\right] \text{NLoS}\right]$ in Eq.(5.22) for brevity. Our proof is thus completed. □

5.3.2 Optimal Antenna Downtilt

In order to get the optimal antenna downtilt to maximize the coverage probability, we take the derivative of the coverage probability and find the optimal point for each BS density. In this subsection, we first present Lemma 3 to show that there always exists a unique solution of the optimal antenna downtilt, and then we present the solution of the optimal antenna downtilt for a given BS density.

Lemma 3. *For a typical UE, the coverage probability is a function of the antenna downtilt and there is a unique solution of the antenna downtilt to achieve the maximum coverage probability for a certain BS density.*

Proof. The coverage probability can be written as follows,

$$\begin{aligned} p^{\mathrm{cov}}\left(\lambda_B,\gamma\right) &= \int_0^{\frac{\pi}{S}}\int_0^{\infty} \Pr\left[\frac{P_B\, G(\varphi_{\bar{b},1},\theta_b,\theta_{tilt})\zeta\left(r\right) g}{I_{\mathrm{agg}}+N_0} > \gamma \middle| r\right] \\ &\quad \times f_R\left(r\right) f\left(\varphi\right) dr d\varphi \\ &= \int_0^{\frac{\pi}{S}}\int_0^{\infty} \Pr\left[g > \frac{\gamma\left(I_{\mathrm{agg}}+N_0\right)}{P_B G(\varphi_{\bar{b},1},\theta_b,\theta_{tilt})\zeta\left(r\right)} \middle| r\right] \\ &\quad \times f_R\left(r\right) f\left(\varphi\right) dr d\varphi \\ &= \int_0^{\infty} \mathbb{E}_{\mathrm{signal,I}}\left[\exp\left(-\frac{\gamma\left(\mathrm{I_{agg}}+\mathrm{N_0}\right)}{\mathrm{P_B G}(\varphi_{\bar{\mathrm{b}},1},\theta_{\mathrm{r}},\theta_{\mathrm{tilt}})\zeta\left(\mathrm{r}\right)}\right) \middle| r\right] \\ &\quad \times f_R\left(r\right) dr \end{aligned} \tag{5.32}$$

where 'signal' means the average signal power for a typical UE, $\zeta\left(r\right)$ is the path loss function.

From this equation, we can see that as long as the average SINR has one and only one maximum value, then the coverage probability also has one and only one maximum value. For a typical UE, the signal and cumulative interference expressions have been shown in Eq.(5.6) and Eq.(5.9), both the signal and interference power change with $G(\varphi_{b,i},\theta_b,\theta_{tilt})$. In particular, $G(\varphi_{b,i},\theta_b,\theta_{tilt})$ changes with the antenna downtilt and it achieves the maximum value when $\theta_{tilt}=\theta_b=\arctan\left(\frac{L}{d}\right)$, where

L is the height difference and d is the distance from transmitter to the receiver. Based on the antenna pattern model, both the signal power and the aggregate interference power are increasing as the antenna downtilt grows from 0 degree and then decreasing as the antenna gradually looks downward. As the antenna downtilt increases, the aggregate interference will hit the maximum level earlier than the signal power because the average distance from the interfering BSs to the typical UE is larger than the distance from the associated BS to the typical UE. Then, the average signal continually increases and the interference decreases. So, the SINR expression will increase at this stage. When $\theta_{tilt} > \arctan\left(\frac{L}{r}\right)$, where r is the distance from the typical BS to the typical UE, both the signal power and the aggregate interference power are decreasing. During this stage, the decreasing rate of the signal power is larger than the decreasing rate of the interference power with respect to the antenna downtilt as the average distance from the associated BS to the typical UE is smaller than the distance from the interfering BSs to the typical UE, and hence the change of the antenna downtilt angle has a larger impact on the former case then that on the latter one. There are two possible cases for the SINR expression: 1) It increases first and then decreases; 2) It monotonically decreases. In both cases, there exists a solution of antenna downtilt to achieve the maximum coverage probability for a certain BS density during this stage. In addition, both the interference and the signal power expressions are all concave functions with respect to the antenna downtilt when $\theta_{tilt} > \arctan\left(\frac{L}{r}\right)$so that the average SINR function is a concave function. Hence there only exists one optimal point, which concludes our proof. □

It is difficult to have a more concrete proof, so we using the toy example to explain this question based on the SINR statistics on average.

Lemma 4. *As a toy example, the signal power and the aggregate interference power*

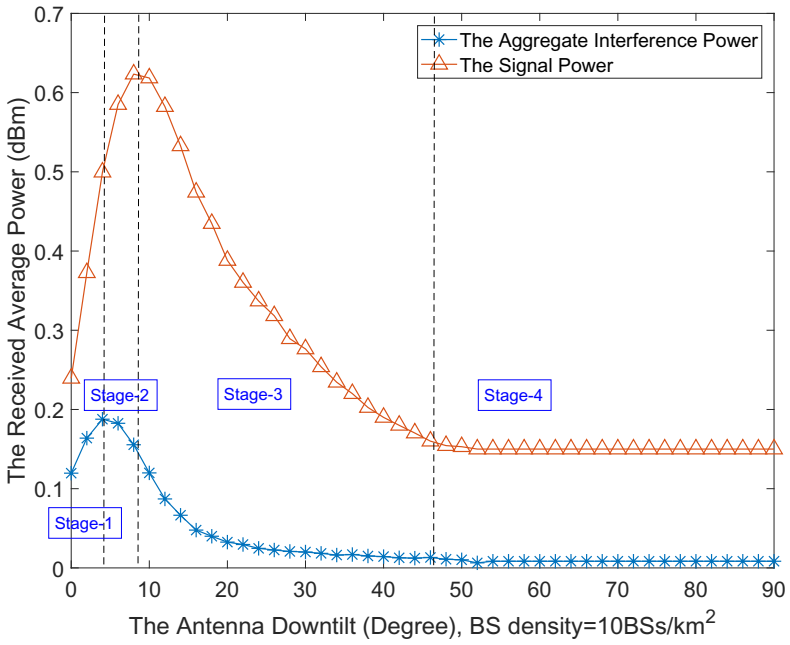

Figure 5.3 : The average signal and cumulative interference power with antenna downtilt and a BS density of 10BSs/km^2.

have been plotted in Fig. 2 assuming the LTE macrocell BS model with a BS density of 10 BSs/km^2.

As the aggregate interference hits its maximum earlier than the signal power, there are four stages of the functions of the signal power and the aggregate interference power as the antenna downtilt increases from 0 to 90 degrees. In stage 1, both the signal power and the aggregate interference power will initially increase as the antenna downtilt grows from zero. The increasing rate of the signal power is larger than the increasing rate of the aggregate interference power with respect to the antenna downtilt. Hence, the average SINR function will increase during stage 1.In stage 2, the aggregate interference power becomes a monotonically decreasing function and the signal power will continue increasing with respect to the antenna downtilt. Hence, the average SINR function will continue increasing in stage 2.In stage 3, both the signal power and the aggregate interference power are decreasing.

During this stage, the decreasing rate of the signal power is larger than the decreasing rate of the interference power with respect to the antenna downtilt. There are two possible cases for the SINR function: 1) It increases first and then decreases; 2) It monotonically decreases. In both cases, there exists a solution of antenna downtilt in stage 2 or 3 to achieve the maximum coverage probability for a certain BS density. In stage 4, both the interference and the signal power are constants. Hence, the average SINR function becomes a constant independent of the antenna downtilt. To sum up, there exists a unique solution of antenna downtilt in stage 2 or 3 to achieve the maximum coverage probability for a certain BS density.

Proof. A large antenna downtilt reduces inter-cell interference power, while at the same time decreases signal powers for cell edge UEs. On the other hand, a small antenna downtilt leads to the opposite case. Therefore, different antenna downtilts achieve different tradeoffs between the signal power and the interference power, and hence there exists an optimal antenna downtilt to achieve the maximum coverage probability for each BS density. □

In the following, we will present such a unique and optimal antenna downtilt with respect to the BS density, which is summarized as Theorem 7.

Theorem 7. *For a certain BS density λ_B, the optimal antenna downtilt can be found by the following equation:*

$$\theta_{tilt} = \arg_{\theta_{tilt}} \left\{ dP_c^L(\theta_{tilt}) + dP_c^{NL}(\theta_{tilt}) + dP_c^{Noise}(\theta_{tilt}) = 0 \right\} \tag{5.33}$$

where

$$dP_c^L(\theta_{tilt}) = -2\pi\lambda_B \sum_{n=1}^{N} \int_{\sqrt{d_{n-1}^2 - L^2}}^{\sqrt{d_n^2 - L^2}} \int_r^{\infty} \left(\mathrm{Pr}_n^{\mathrm{L}}(u) \right) \gamma$$

$$\times \left(\frac{u^2+L^2}{r^2+L^2}\right)^{\frac{\alpha^L}{2}} \left[\frac{u\sum_{n=1}^{S} \frac{\partial G(\varphi_{b,n},\theta_u,\theta_{tilt})}{\partial \theta_{tilt}} G(\varphi_{\bar{b},1},\theta_r,\theta_{tilt})}{\left(\gamma a + G(\varphi_{\bar{b},1},\theta_r,\theta_{tilt})\left(\frac{u^2+L^2}{r^2+L^2}\right)^{\frac{\alpha^L}{2}}\right)^2} \right.$$

$$\left. - \frac{\frac{\partial G(\varphi_{\bar{b},1},\theta_r,\theta_{tilt})}{\partial \theta_{tilt}} \sum_{n=1}^{S} G(\varphi_{b,n},\theta_u,\theta_{tilt})}{\left(\gamma a + G(\varphi_{\bar{b},1},\theta_r,\theta_{tilt})\left(\frac{u^2+L^2}{r^2+L^2}\right)^{\frac{\alpha^L}{2}}\right)^2} \right] \times f_{R,n}^{\mathrm{L}}(r)\, dudr$$

$$-2\pi\lambda_B \sum_{n=1}^{N} \int_{\sqrt{d_{n-1}^2-L^2}}^{\sqrt{d_n^2-L^2}} \int_r^{\infty} \left(Pr_{\mathrm{n}}^{L}(\mathrm{u})\right) A^L A^{NL} \gamma$$

$$\times \frac{(u^2+L^2)^{\frac{\alpha^L}{2}}}{(r^2+L^2)^{\frac{\alpha^{NL}}{2}}} \left[\frac{u\sum_{n=1}^{S} \frac{\partial G(\varphi_{b,n},\theta_u,\theta_{tilt})}{\partial \theta_{tilt}} G(\varphi_{\bar{b},1},\theta_r,\theta_{tilt})}{\left(\gamma A^L a + \frac{G(\varphi_{\bar{b},1},\theta_r,\theta_{tilt}) A^{NL}(u^2+L^2)^{\frac{\alpha^L}{2}}}{(r^2+L^2)^{\frac{\alpha^{NL}}{2}}}\right)^2} \right.$$

$$\left. - \frac{\frac{\partial G(\varphi_{\bar{b},1},\theta_r,\theta_{tilt})}{\partial \theta_{tilt}} \sum_{n=1}^{S} G(\varphi_{b,n},\theta_u,\theta_{tilt})}{\left(\gamma A^L a + \frac{G(\varphi_{\bar{b},1},\theta_r,\theta_{tilt}) A^{NL}(u^2+L^2)^{\frac{\alpha^L}{2}}}{(r^2+L^2)^{\frac{\alpha^{NL}}{2}}}\right)^2} \right] \times f_{R,n}^{\mathrm{NL}}(r)\, dudr, \tag{5.34}$$

$$dP_c^{NL}(\theta_{tilt}) = -2\pi\lambda_B \sum_{n=1}^{N} \int_{\sqrt{d_{n-1}^2-L^2}}^{\sqrt{d_n^2-L^2}} \left(1 - \mathrm{Pr}_n^{\mathrm{L}}(u)\right)$$

$$\times A^L A^{NL} \gamma \frac{(u^2+L^2)^{\frac{\alpha^{NL}}{2}}}{(r^2+L^2)^{\frac{\alpha^L}{2}}}$$

$$\times \left[\frac{u\sum_{n=1}^{S} \frac{\partial G(\varphi_{b,n},\theta_u,\theta_{tilt})}{\partial \theta_{tilt}} G(\varphi_{\bar{b},1},\theta_r,\theta_{tilt})}{\left(\gamma A^{NL} a + \frac{G(\varphi_{\bar{b},1},\theta_r,\theta_{tilt}) A^{L}(u^2+L^2)^{\frac{\alpha^{NL}}{2}}}{(r^2+L^2)^{\frac{\alpha^{L}}{2}}}\right)^2} \right.$$

$$\left. - \frac{\frac{\partial G(\varphi_{\bar{b},1},\theta_r,\theta_{tilt})}{\partial \theta_{tilt}} \sum_{n=1}^{S} G(\varphi_{b,n},\theta_u,\theta_{tilt})}{\left(\gamma A^{NL} a + \frac{G(\varphi_{\bar{b},1},\theta_r,\theta_{tilt}) A^{L}(u^2+L^2)^{\frac{\alpha^{NL}}{2}}}{(r^2+L^2)^{\frac{\alpha^{L}}{2}}}\right)^2} \right]$$

$$
\begin{aligned}
&\times f_{R,n}^{\mathrm{L}}(r)\,dudr \\
&-2\pi\lambda_B\sum_{n=1}^{N}\int_{\sqrt{d_{n-1}^2-L^2}}^{\sqrt{d_n^2-L^2}}\left(1-\mathrm{Pr}_n^{\mathrm{L}}(u)\right)\gamma\left(\frac{u^2+L^2}{r^2+L^2}\right)^{\frac{\alpha^{NL}}{2}} \\
&\times\left[\frac{u\sum_{n=1}^{S}\frac{\partial G(\varphi_{b,n},\theta_u,\theta_{tilt})}{\partial\theta_{tilt}}G(\varphi_{\bar{b},1},\theta_r,\theta_{tilt})}{\left(\gamma a+G(\varphi_{\bar{b},1},\theta_r,\theta_{tilt})\left(\frac{u^2+L^2}{r^2+L^2}\right)^{\frac{\alpha^{NL}}{2}}\right)^2}\right. \\
&\left.-\frac{\frac{\partial G(\varphi_{\bar{b},1},\theta_r,\theta_{tilt})}{\partial\theta_{tilt}}\sum_{n=1}^{S}G(\varphi_{b,n},\theta_u,\theta_{tilt})}{\left(\gamma a+G(\varphi_{\bar{b},1},\theta_r,\theta_{tilt})\left(\frac{u^2+L^2}{r^2+L^2}\right)^{\frac{\alpha^{NL}}{2}}\right)^2}\right] \\
&\times f_{R,n}^{\mathrm{NL}}(r)\,dudr,
\end{aligned}
\tag{5.35}
$$

$$
\begin{aligned}
dP_c^{Noise}(\theta_{tilt}) = &\sum_{n=1}^{N}\int_{\sqrt{d_{n-1}^2-L^2}}^{\sqrt{d_n^2-L^2}}\left(r^2+L^2\right)^{\frac{\alpha^L}{2}} \\
&\times\frac{\gamma\mathrm{N}_0\frac{\partial\mathrm{G}(\varphi_{\bar{\mathrm{b}},1},\theta_{\mathrm{r}},\theta_{\mathrm{tilt}})}{\partial\theta_{\mathrm{tilt}}}}{\mathrm{P_B}\mathrm{G}^2(\varphi_{\bar{\mathrm{b}},1},\theta_{\mathrm{r}},\theta_{\mathrm{tilt}})\mathrm{A}^{\mathrm{L}}}f_{R,n}^{\mathrm{L}}(r)\,dr \\
&+\sum_{n=1}^{N}\int_{\sqrt{d_{n-1}^2-L^2}}^{\sqrt{d_n^2-L^2}}\left(r^2+L^2\right)^{\frac{\alpha^{NL}}{2}} \\
&\times\frac{\gamma\mathrm{N}_0\frac{\partial\mathrm{G}(\varphi_{\bar{\mathrm{b}},1},\theta_{\mathrm{r}},\theta_{\mathrm{tilt}})}{\partial\theta_{\mathrm{tilt}}}}{\mathrm{P_B}\mathrm{G}^2(\varphi_{\bar{\mathrm{b}},1},\theta_{\mathrm{r}},\theta_{\mathrm{tilt}})\mathrm{A}^{\mathrm{NL}}}f_{R,n}^{\mathrm{NL}}(r)\,dr
\end{aligned}
\tag{5.36}
$$

where $a=\sum_{n=1}^{S}G(\varphi_{b,n},\theta_u,\theta_{tilt})$, $f_{R,n}^{\mathrm{L}}(r)$ *and* $f_{R,n}^{\mathrm{NL}}(r)$ *can be found in Theorem 6,* $\frac{\partial G(\varphi_{\bar{b},1},\theta_r,\theta_{tilt})}{\partial\theta_{tilt}}$, $\frac{\partial G(\varphi_{b,n},\theta_u,\theta_{tilt})}{\partial\theta_{tilt}}$ are the derivatives for θ_{tilt}.

Proof. In Theorem 6, the coverage probability can be written as Eq.(5.22). As λ_B,γ are constants, to get the derivative of $p^{\mathrm{cov}}(\lambda_B,\gamma)$ respect to θ_{tilt}, we treat the antenna pattern gain in the horizontal direction as another independent variable. Except for the signal, the other factors which lead to the optimal antenna downtilt can be divided into the noise part Ω_{noise}, the LoS interference part $\Omega_{I_{LoS}}$ and the NLoS interference part $\Omega_{I_{NLoS}}$. Then we let the derivative of Eq.(5.22) be zero, thus

all parts in Eq.(5.22) should be zero. Take the first part of Eq.(5.22) as an example,

$$p_1^{\text{cov}}(\lambda_B,\gamma)=\int_0^{\frac{\pi}{6}}\int_0^{\sqrt{d_1^2-L^2}}\exp\left\{\Omega_{noise}+\Omega_{I_{LoS}}+\Omega_{I_{NLoS}}\right\}$$
$$\times f_{R,1}^{\text{L}}(r)\,f(\varphi)\,drd\varphi \tag{5.37}$$

and

$$\int_0^{\sqrt{d_1^2-L^2}}\left\{\Omega_{noise}+\Omega_{I_{LoS}}+\Omega_{I_{NLoS}}\right\}'_{\theta_{tilt}} f_{R,1}^{\text{L}}(r)\,dr=0 \tag{5.38}$$

where

$$\begin{aligned}
&\Omega_{I_{LoS}}+\Omega_{I_{NLoS}}+\Omega_{noise}\\
=&-2\pi\lambda_B\left(\int_r^{d_1}\frac{\text{Pr}_1^{\text{L}}(u)u}{1+\frac{G(\varphi_{\bar{b},1},\theta_r,\theta_{tilt})}{\gamma\sum_{n=1}^{S}G(\varphi_{b,n},\theta_u,\theta_{tilt})}\left(\frac{u^2+L^2}{r^2+L^2}\right)^{\frac{\alpha^L}{2}}}du\right.\\
&\left.+\int_{\sqrt{d_{n-1}^2-L^2}}^{\infty}\frac{\text{Pr}_n^{\text{L}}(u)u}{1+\frac{G(\varphi_{\bar{b},1},\theta_r,\theta_{tilt})}{\gamma\sum_{n=1}^{S}G(\varphi_{b,n},\theta_u,\theta_{tilt})}\left(\frac{u^2+L^2}{r^2+L^2}\right)^{\frac{\alpha^L}{2}}}du\right)\\
&\vdots\\
&-2\pi\lambda_B\left(\int_r^{d_1}\frac{(1-\text{Pr}_1^{\text{L}}(u))u}{1+\frac{G(\varphi_{\bar{b},1},\theta_r,\theta_{tilt})A^L}{\gamma\sum_{n=1}^{S}A^{NL}G(\varphi_{b,n},\theta_u,\theta_{tilt})}\frac{(u^2+L^2)^{\frac{\alpha^{NL}}{2}}}{(r^2+L^2)^{\frac{\alpha^L}{2}}}}du\right.\\
&\left.+\int_{\sqrt{d_{n-1}^2-L^2}}^{\infty}\frac{\left(1-\text{Pr}_n^{\text{L}}(u)\right)u}{1+\frac{G(\varphi_{\bar{b},1},\theta_r,\theta_{tilt})A^L}{\gamma\sum_{n=1}^{S}A^{NL}G(\varphi_{b,n},\theta_u,\theta_{tilt})}\frac{(u^2+L^2)^{\frac{\alpha^{NL}}{2}}}{(r^2+L^2)^{\frac{\alpha^L}{2}}}}du\right)\\
&-\frac{\gamma\text{N}_0}{\text{P}_\text{B}\text{G}(\varphi_{\bar{\text{b}},1},\theta_\text{r},\theta_\text{tilt})\text{A}^\text{L}\left(\text{r}^2+\text{L}^2\right)^{-\frac{\alpha^\text{L}}{2}}}
\end{aligned} \tag{5.39}$$

which concludes our proof. □

From Theorem 7, we can draw the following insights:

- There are three components in Eq.(5.33) which contribute to the optimal antenna downtilt, include the LoS links and the NLoS links shown in Eq.(5.34) and Eq.(5.35) and the noise shown in Eq.(5.36), respectively.

- When the networks are sparse, the signal is mostly NLoS and the noise is the dominant factor. Therefore, the NLoS links and noise are the major ones that determine the optimal downtilt. As the BS density increases, most signals and some interference links transit from NLoS to LoS, and hence, all components in Eq.(5.33) should be taken into account. When the BS density is sufficiently large, almost all signals and the major interference links are LoS, and the noise is negligible compared to the signal or interference. Therefore, the LoS links become the major component that determines the optimal downtilt.

As the main purpose of this work is to investigate the relationship between network performance and the antenna downtilt, we consider a simplified version of the aforementioned path loss model, that is a two-piece path loss model, and a linear LoS probability function defined by the 3GPP [124] as a special case in the numerical part. The path loss model can be written as

$$\zeta\left(w\right)=\begin{cases} A^{\mathrm{L}}w^{-\alpha^{\mathrm{L}}}, & \text{LoS Probability: } \Pr^{\mathrm{L}}\left(w\right) \\ A^{\mathrm{NL}}w^{-\alpha^{\mathrm{NL}}}, & \text{NLoS Probability: } 1-\Pr^{\mathrm{L}}\left(w\right) \end{cases}, \tag{5.40}$$

regarding realistic path loss models,

$$\Pr^{\mathrm{L}}\left(r\right)=\begin{cases} 1-\frac{w}{d_1} & 0<w\leq d_1 \\ 0 & w>d_1 \end{cases}, \tag{5.41}$$

where d_1 is the 3D cut-off distance of the LoS link for BS-to-UE links. The adopted linear LoS probability function is very useful because it can include other LoS probability functions as its special cases [16]. For the 3GPP special case, according to Theorem 6, $p^{\mathrm{cov}}\left(\lambda_B,\gamma\right)$ can then be computed by

$$p^{\mathrm{cov}}\left(\lambda_B,\gamma\right)=T_1^L+T_1^{NL}+T_2^{NL}. \tag{5.42}$$

The results of the 3GPP special case can be obtained by plugging (5.40), (5.41)

and $n = 2$ into Theorem 1 and Theorem 3. We can obtain the coverage probability and the optimal antenna downtilt which is numerically solvable for the 3GPP case.

Here, we will discuss the antenna pattern for both the LTE macrocell BS model and the LTE picocell BS model.

For the LTE macrocell BS model, we use 3 sectors BS tower and a 3D antenna pattern defined in [26] for each sector, where

$$G_h(\varphi_{b,i}) = -\min\left[12\left(\frac{\varphi_{b,i}}{B_h}\right)^2, SLL_{az}\right], \tag{5.43}$$

and

$$G_v(\theta_b, \theta_{tilt}) = -\min\left[12\left(\frac{\theta_b - \theta_{tilt}}{B_{v1}}\right)^2, SLL_{el}\right], \tag{5.44}$$

where $B_h = 65$ degrees and $B_{v1} = 10$ degrees are the horizontal and vertical half power beamwidth, $SLL_{az} = 20$dB and $SLL_{el} = 20$dB [94] are the side lobe levels (SLL) in the azimuth and elevation planes. The maximum antenna gain $G_m = 14$dBi from [124].

Using the Eq.(5.5), Eq.(5.43) and Eq.(5.44), we have

$$\frac{\partial G(\varphi_{\bar{b},1}, \theta_r, \theta_{tilt})}{\partial \theta_{tilt}} = \frac{2a_r}{b}(\theta_r - \theta_{tilt}) \exp\left[-\frac{(\theta_r - \theta_{tilt})^2}{b}\right] \tag{5.45}$$

and

$$\frac{\partial G(\varphi_{b,n}, \theta_u, \theta_{tilt})}{\partial \theta_{tilt}} = \frac{2a_{u,i}}{b}(\theta_u - \theta_{tilt}) \exp\left[-\frac{(\theta_u - \theta_{tilt})^2}{b}\right] \tag{5.46}$$

where $\theta_r = \arctan\left(\frac{L}{r}\right)$, $\theta_u = \arctan\left(\frac{L}{u}\right)$, $a_r = 10^{\left[-1.2\left(\frac{\varphi_{\bar{b},1}}{B_h}\right)^2 + G_m\right]}$, $a_{u_i} = 10^{\left[-1.2\left(\frac{\varphi_{u,i}}{B_h}\right)^2 + G_m\right]}$ are independent of θ_{tilt}. Plugging Eq.(5.45) and Eq.(5.46) into Theorem 7, and considering the two-piece path loss model, we can obtain the optimal downtilt expressions for macrocell BSs.

Very similar to macrocell BSs, for the LTE picocell BS model, we consider a dipole antenna pattern to investigate the impact of the vertical downtilt. Note that

such antenna pattern is more practical for the study of SCNs. The dipole antenna is omni-directional in horizontal direction, i.e., $G_h(\varphi_{b,i}) = 0$dB [19, 143] and only one sector in one BS tower, i.e., $S = 1$. With electrical downtilt [143, 144], the vertical pattern of the dipole antenna main lobe can be approximated as

$$G_v(\theta_b, \theta_{tilt}) = 10 \log_{10} \left|\cos^n \left(\theta_b - \theta_{tilt}\right)\right|, \tag{5.47}$$

where $n = 47.64$ for a 4-element half-wave dipole antenna .

5.4 Simulation and Discussion

In this section, we investigate the network performance and use numerical results to establish the accuracy of our analysis. The 3GPP special cases studied in Section 3.4 have been considered in this section. The analytical results are compared with Monte Carlo simulation results in terms of the coverage probability and the optimal antenna downtilt. According to the 3GPP standard [26], we adopt the following parameters: $d_1 = 300$m, $\alpha^L = 2$, $\alpha^{NL} = 3.75$, $A^L = 10^{-10.38}$, $A^{NL} = 10^{-14.54}$, $P_B = 46$dBm for the LTE macrocell BSs while $P_B = 24$dBm for the LTE picocell BSs, $P_N = -95$dBm (including a noise figure of 9 dB at the receivers). In this part, we present Monte Carlo simulation results to investigate the coverage probability and validate the analytical results in Theorem 6. In Fig.5.4, we plot the coverage probability for (i) the LTE macrocell BS model with two different BS densities and a BS height of 20m, and (ii) the LTE picocell BS model with two different BS heights and a BS density of 100 BSs/km^2. The SINR threshold and the UE antenna height are set to $\gamma = 0$dB and 1.5m, respectively [26]. As can be seen from Fig.5.4, our analytical results, which are given by Theorem 6, match the simulation results very well, and we can draw the following observations:

- For a certain BS density, there exists an optimal antenna downtilt which can achieve the maximum coverage probability. Antenna downtilt has a significant

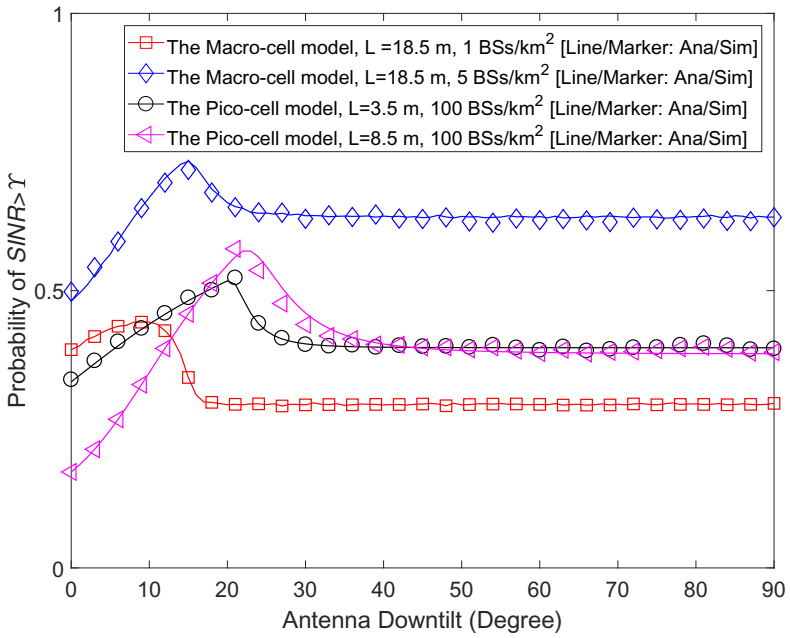

Figure 5.4 : Coverage probability vs. antenna downtilt of the LTE macrocell BS with $\gamma = 0$ dB.

impact on the coverage probability both in the LTE macrocell BS model and the LTE picocell BS model.

- In essence, a large antenna downtilt reduces inter-cell interference power, while at the same time decreases signal powers for cell edge UEs. On the other hand, a small antenna downtilt leads to the opposite case. Therefore, an appropriate antenna downtilt can achieve the balance between boosting the signal power and mitigating the interference power.

- The optimal antenna downtilt increases as the BS density increases because the denser the BS network, the more near-sighted the BS will look downward since the distance from the typical UE to its associated BS is generally shorter as the network becomes denser.

In the following, we validate the analytical results in Theorem 7 by providing

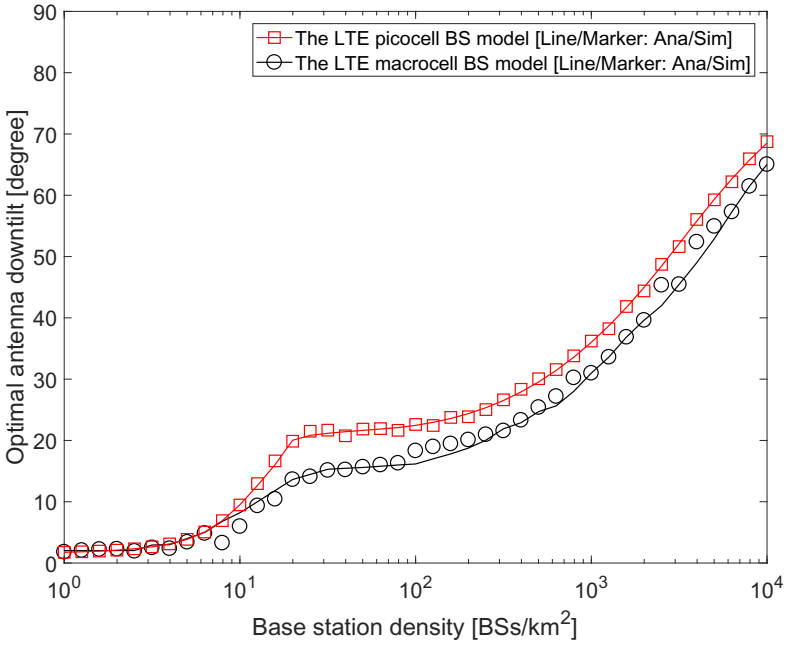

Figure 5.5 : Optimal antenna downtilt vs. base station density with $\gamma = 0$ dB.

Monte Carlo simulation results.

In Fig.5.5, we show the optimal downtilt of the LTE picocell model and the LTE macrocell model as the BS density increases with $\gamma = 0$dB. The antenna height difference L is set to 8.5m. As can be seen from Fig.5.5, our analytical results, given by Theorem 7, match the simulation results very well, which validates the accuracy of our analysis. Moreover, we can draw the following observations:

- Under the two different models, an optimal antenna downtilt can be found for any given base station density to obtain the highest coverage probability. The optimal antenna downtilt increases as the BS density increases.

- The optimal antenna downtilt shows a significant change of trend when the BS density is around $10^{1.1}$ BSs/km^2. This is because most signals and interference are NLoS when the networks are sparse (the BS density ¡ 10 BSs/km^2) and these signals and the dominant interference begin to transit from NLoS to LoS

when the BS density increases beyond $10^{1.1}$ BSs/km^2. Hence the increasing speed of the optimal antenna downtilt is slowing down since a strong LoS signal power supports a relatively small antenna downtilt.

- When considering the LTE macrocell BS model, the optimal antenna downtilt is smaller than the LTE picocell BS model because the antenna can look a bit farther to boost the signal power at the cell-edge area since the interference is less severe with the 3-sector directional antenna pattern.

As showed above, we have verified the accuracy of our theoretical analysis. We can see that our theoretical analysis matches well with the numerical results. But in the 5G cellular network, it makes more sense to deploy the picocell BSs to serve the UEs which is an even denser network, i.e., the BS density is larger than 20 BSs/km^2. Hence, we will focus on the LTE picocell model with the omni-directional antenna pattern to investigate the impact of the optimal antenna pattern on the network performance of dense networks in the following. Fig.5.6 shows the performance impact of BS deployment on the coverage probability. Here, we use the LTE macrocell BS model. From Fig.5.6, we can see that:

- For hexagonal deployment, although the coverage probability is larger than the PPP model, there still exists one optimal antenna downtilt which can achieve the maximum coverage probability for each certain BS density as well.

- The coverage probablity is larger when deployed as hexagons.

In the following, we will show the optimal antenna downtilt with simple path loss model.

In the above figures, we show the optimal downtilt of the LTE picocell model with the BS density increase with $\gamma = 0dB$ and the optimal antenna downtilt with

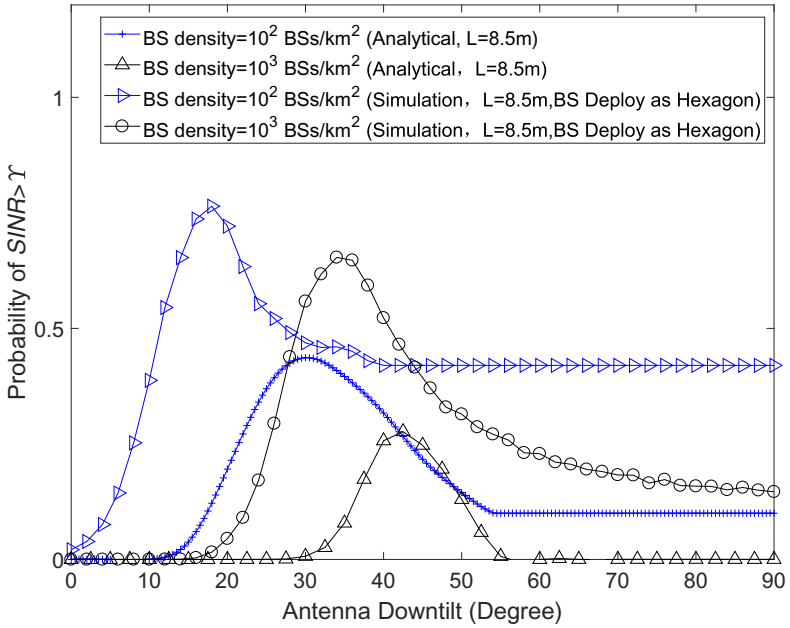

Figure 5.6 : The Performance Impact of BS deployment on the Coverage Probability with $\gamma = 0dB$.

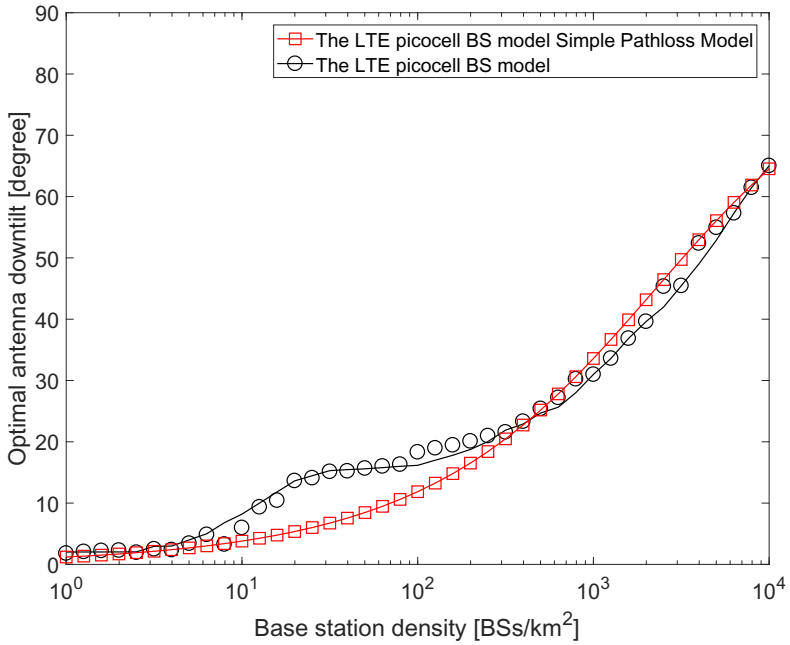

Figure 5.7 : Optimal Antenna downtilt vs. BS density of the LTE picocell model with adopted path loss model and the simple path loss model.

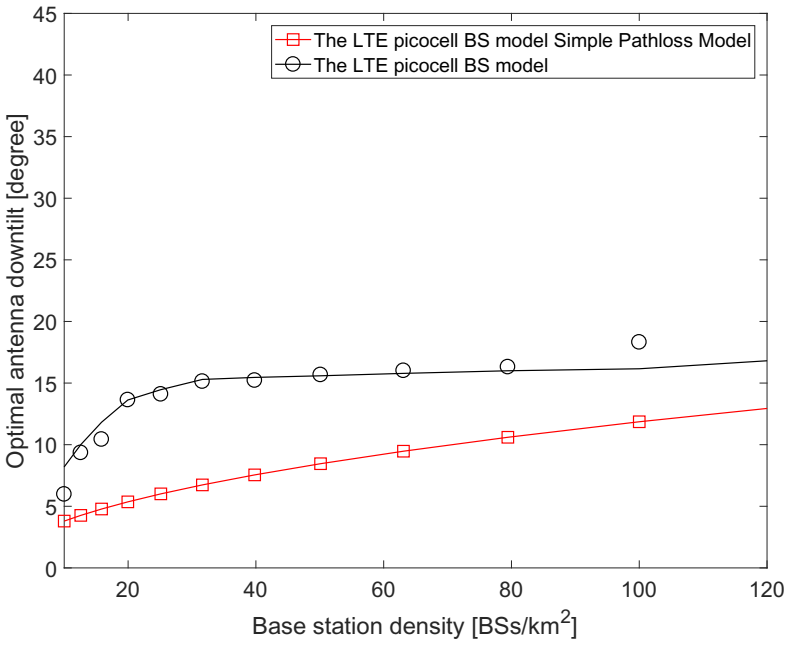

Figure 5.8 : Optimal Antenna downtilt vs. BS density 10 and 100 BSs/km^2 of the LTE picocell model with adopted path loss model and the simple path loss model

simple path loss model which is a single slope path loss model with $\alpha = 3.75$. As we can observe in Fig.5.7 and Fig.5.8, we can draw the following observations:

- Between the BS density from 10 BSs/km^2 to 200 BSs/km^2, the results with the LoS/NLoS first grow faster, then grow slower than that with a simple path loss model.
- From 35 BSs/km^2 and 100 BSs/km^2, the optimal antenna downtilt remains almost the stable because some interference turn from the NLoS to LoS path, the optimal antenna downtilt need to reduce the sudden increase of the interference.

In this following, we consider the omni-directional antenna pattern with $\lambda_B = 10^3$ BSs/km^2 to investigate the performance impact of BS antenna height on the coverage probability. From Fig.5.9, we can see that:

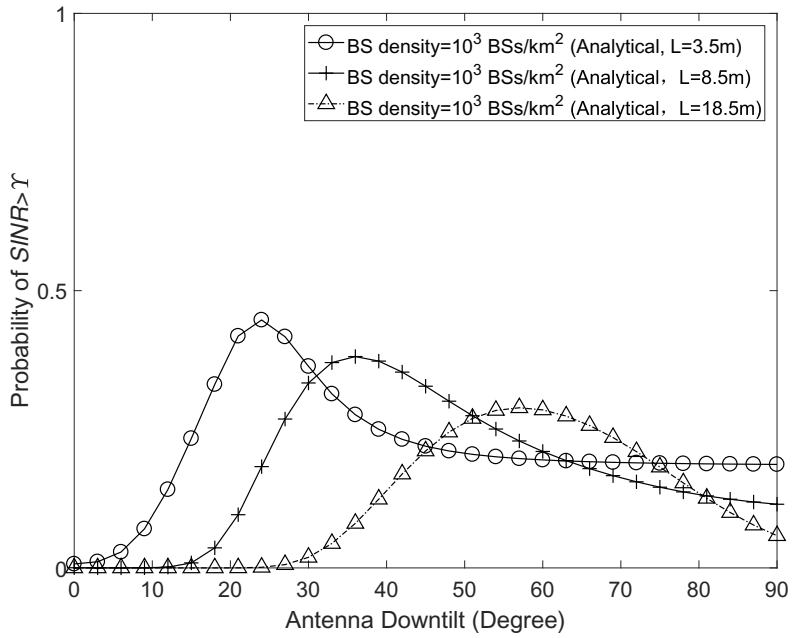

Figure 5.9 : The performance impact of BS antenna height on the coverage probability with $\gamma = 0$ dB.

- For each antenna height, there exists an optimal antenna downtilt which can achieve the maximum coverage probability.

- The higher the BS antenna, the lower the coverage probability. This is because a larger L implies a tighter cap on the signal power and the interference power. In addition, a larger antenna height difference leads to a larger optimal antenna downtilt because $\theta_b = \arctan\left(\frac{L}{r_b}\right)$ (r_b is the distance from the BS at point b to the typical UE).

In this following, we investigate the coverage probability and the ASE with the optimal antenna downtilt compared with the results in [19]. Here, the optimal network-wide antenna downtilt means adopting the optimal antenna downtilt for every BS in the network.

Fig.5.10 shows the coverage probability with the optimal antenna downtilt and

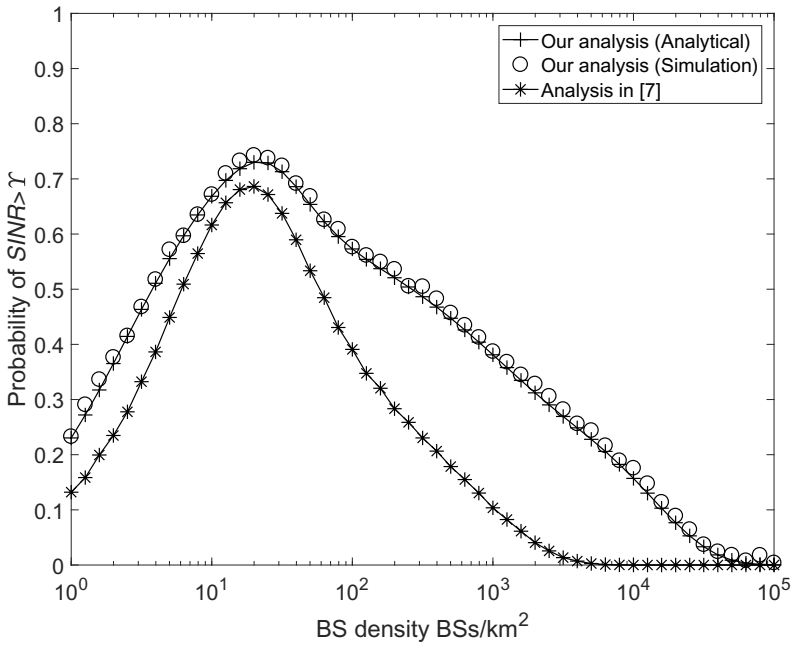

Figure 5.10 : Coverage probability vs. base station density with the optimal antenna downtilt and $\gamma = 0$ dB.

without any downtilt. As we can observe from Fig.5.10:

- The antenna downtilt does not change the trend of the coverage probability, i.e., it first increases and then decreases to zero as BS density increases.
- The coverage probability performance with the optimal antenna downtilt is always better than that without antenna downtilt. The coverage probability reaches zero when the BS density is 3×10^4 BSs/km^2, while it is around 3×10^3 BSs/km^2 in the previous work [16].

In the following, we present the ASE performance with the optimal antenna downtilt.

Fig.5.11 shows the ASE with and without optimal antenna downtilt. From Fig.5.11, we can draw the following observations:

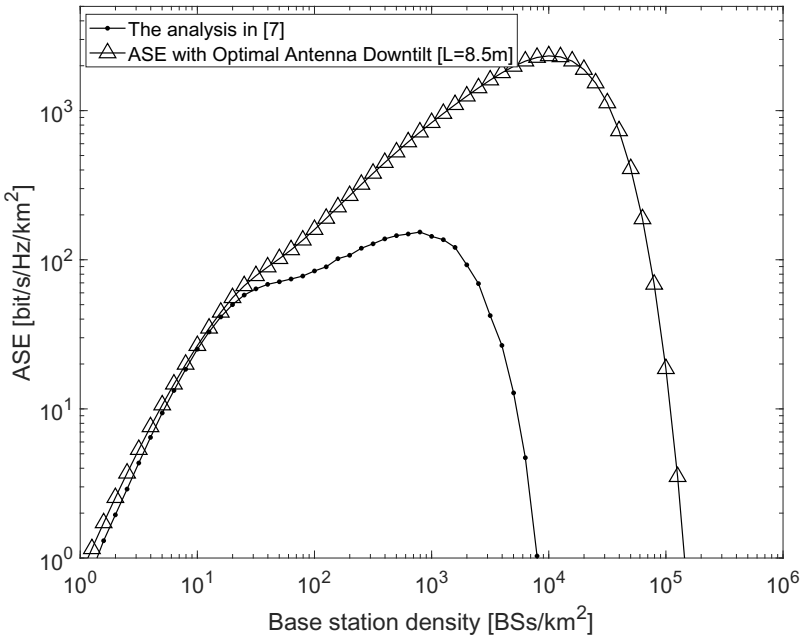

Figure 5.11 : $A^{ASE}(\lambda, \gamma_0)$ vs. base station density with the optimal antenna downtilt and without antenna downtilt.

- After using the optimal antenna downtilt, the ASE increases as BS density increases until 2×10^4 BSs/km^2, then it decreases to zero when BS density is around 2×10^5 BSs/km^2.
- The optimal antenna downtilt improves the ASE significantly and delay the ASE crash by nearly one order of magnitude in terms of the base station density.

In Fig.5.12, we investigate the performance of coverage probability under the assumptions of Rayleigh fading for NLoS transmissions and Rician fading ($K = 10$) for LoS transmissions. From Fig.5.12, we can see that Rician fading makes no difference when the BS density is smaller than 8×10^3 BSs/km^2, and then the ASE crash happens earlier than the case with Rayleigh fading. The intuition is that Rayleigh fading exhibits more channel fluctuation than Rician fading, and hence it

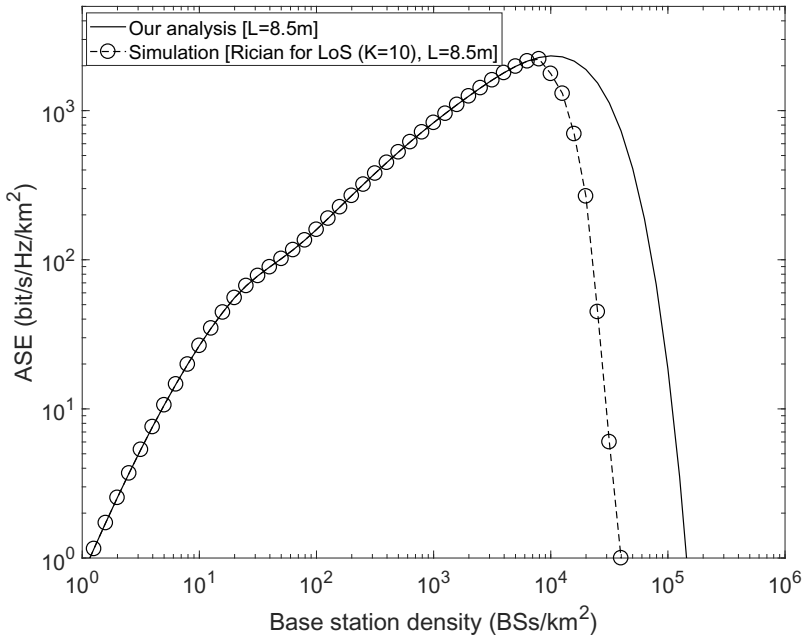

Figure 5.12 : $A^{ASE}(\lambda, \gamma_0)$ vs base station density (Rayleigh fading for NLoS transmissions and Rician fading ($K = 10$) for LoS transmissions with $\gamma = 0$dB).

can mildly combat the ASE Crash by providing an opportunistic channel gain to the signal power. However, such beneficial channel fluctuation is insignificant compared to the ASE Crash, which is caused by the physical limitation on capping the signal power.

5.5 Summary

In this chapter, we invesigated the technology of the antenna pattern to boost the network performance. We show that there exists an optimal antenna downtilt to achieve the maximum coverage probability for each BS density. Our results show that using the optimal antenna downtilt can improve the ASE performance significantly. Specifically, it can delay the ASE crash by nearly one order of magnitude in terms of the BS density. As our future work, we will consider the optimal antenna height with a multi-antenna setup in cellular networks.

Chapter 6

Conclusion

This thesis has presented works on the performance analysis of the ultra dense network using the tool of stochastic geometry to improve the capacity of cellular networks. In chapter 3 and 4, a new D2D system model considering the LoS/NLoS path loss has been designed. In chapter 5, the optimal antenna downtilt has been achieved, applying the optimal antenna downtilt can boost the network performance significantly. In the following, the key results and findings of this thesis are summarised.

In Chapter 3, we designed a D2D enhanced cellular network to boost the network capacity. We proposed a mode selection method which can eliminate the potential overlarge interferene in a D2D-enhanced uplink cellular network, where the locations of all mobile UEs are modeled as a PPP distribution. In particular, each UE selects its operation mode based on its downlink received power and a threshold β. The practical path loss model and slow shadow fading are considered in modeling the power attenuation. This interference management scheme mitigates the potential overlarge interferene from D2D transmitter to cellular network. Moreover, we analytically evaluated the coverage probability and the ASE for various values of the mode selection threshold β. Our results showed that the D2D links could provide high ASE when the threshold parameter is appropriately chosen. More importantly, we concluded that there exists an optimal β to achieve the maximum ASE while guaranteeing the coverage probability performance of cellular network.

In Chapter 4, we extended the system we designed in Chapter 3 with considering

the PF scheduler in the cellular tier. With consideration of the PF scheduler, our results showed that the interference management method mitigates large interference from D2D transmitter to cellular network and the PF scheduler can improve the network performance significantly when the BS density is smaller than 10^{-3}BSs/km^2. Moreover, we concluded that the D2D tier can improve the network performance when the threshold parameter is appropriately chosen and there exists an optimal β to achieve the maximum ASE while guaranteeing the coverage probability performance of cellular network.

In Chapter 5, we investigated the impact of the 3D practical antenna pattern and downtilt on the performance of DL cellular networks. We show that there exists an optimal antenna downtilt to achieve the maximum coverage probability for each BS density. Analytical results were obtained for the optimal antenna downtilt and the coverage probability. Our results showed that there are three components determining the optimal antenna downtilt, and the optimal antenna downtilt increases as the BS density grows. Compared with previous works in [16], we found that using the optimal antenna downtilt can improve the ASE performance significantly. Specifically, it can delay the ASE crash by nearly one order of magnitude in terms of the BS density.

In addition to the key results and findings summarised above, there are still some research problems to be investigated in the future. This includes considering other factors of realistic networks in the theoretical analysis for SCNs, practical directional antennas [19] and non-PPP deployments of BSs [145] and considering the optimal antenna height with a multi-antenna setup in cellular networks. We will also consider3D antenna patterns in the scenarios of future UAV and LEO satellite networking beyond 5G.

Bibliography

[1] C. V. N. Index, "Global mobile data traffic forecast update, 2015–2020 white paper," *link: http://goo. gl/ylTuVx*, 2016.

[2] X. Ge, S. Tu, G. Mao, C. X. Wang, and T. Han, "5G ultra-dense cellular networks," *IEEE Wireless Communications*, vol. 23, pp. 72–79, February 2016.

[3] J. Guo, J. Yuan, and J. Zhang, "An achievable throughput scaling law of wireless device-to-device caching networks with distributed mimo and hierarchical cooperations," *IEEE Transactions on Wireless Communications*, vol. 17, no. 1, pp. 492–505, 2017.

[4] J. Guo, W. Yu, and J. Yuan, "Enhancing cellular performance through device-to-device distributed mimo," *IEEE Transactions on Communications*, vol. 66, no. 12, pp. 6096–6109, 2018.

[5] X. Lin, J. G. Andrews, and A. Ghosh, "Spectrum sharing for device-to-device communication in cellular networks," *IEEE Transactions on Wireless Communications*, vol. 13, pp. 6727–6740, Dec 2014.

[6] H. ElSawy, E. Hossain, and M. S. Alouini, "Analytical modeling of mode selection and power control for underlay D2D communication in cellular networks," *IEEE Transactions on Communications*, vol. 62, pp. 4147–4161, Nov 2014.

[7] A. Ramezani-Kebrya, M. Dong, B. Liang, G. Boudreau, and S. H. Seyedmehdi, "Joint power optimization for device-to-device communication in cellular

networks with interference control," *IEEE Transactions on Wireless Communications*, vol. 16, pp. 5131–5146, Aug 2017.

[8] N. Lee, X. Lin, J. G. Andrews, and R. W. Heath, "Power control for D2D underlaid cellular networks: Modeling, algorithms, and analysis," *IEEE Journal on Selected Areas in Communications*, vol. 33, no. 1, pp. 1–13, 2015.

[9] J. Liu, H. Nishiyama, N. Kato, and J. Guo, "On the outage probability of device-to-device-communication-enabled multichannel cellular networks: An rss-threshold-based perspective," *IEEE Journal on Selected Areas in Communications*, vol. 34, pp. 163–175, Jan 2016.

[10] D. Marshall, S. Durrani, J. Guo, and N. Yang, "Performance comparison of device-to-device mode selection schemes," in *2015 IEEE 26th Annual International Symposium on Personal, Indoor, and Mobile Radio Communications (PIMRC)*, pp. 1536–1541, Aug 2015.

[11] A. Abdallah, M. M. Mansour, and A. Chehab, "A distance-based power control scheme for d2d communications using stochastic geometry," in *2017 IEEE 86th Vehicular Technology Conference (VTC-Fall)*, pp. 1–6, Sept 2017.

[12] H. Min, J. Lee, S. Park, and D. Hong, "Capacity enhancement using an interference limited area for device-to-device uplink underlaying cellular networks," *IEEE Transactions on Wireless Communications*, vol. 10, pp. 3995–4000, December 2011.

[13] G. George, R. K. Mungara, and A. Lozano, "An analytical framework for device-to-device communication in cellular networks," *IEEE Transactions on Wireless Communications*, vol. 14, pp. 6297–6310, Nov 2015.

[14] S. Lv, C. Xing, Z. Zhang, and K. Long, "Guard zone based interference management for D2D-Aided underlaying cellular networks," *IEEE Transactions*

on Vehicular Technology, vol. 66, pp. 5466–5471, June 2017.

[15] P. Mach, Z. Becvar, and T. Vanek, "In-band device-to-device communication in ofdma cellular networks: A survey and challenges," *IEEE Communications Surveys Tutorials*, vol. 17, pp. 1885–1922, Fourthquarter 2015.

[16] M. Ding, P. Wang, D. Lpez-Prez, G. Mao, and Z. Lin, "Performance impact of LoS and NLoS transmissions in dense cellular networks," *IEEE Transactions on Wireless Communications*, vol. 15, pp. 2365–2380, Mar. 2016.

[17] Y. J. Chun, S. L. Cotton, H. S. Dhillon, A. Ghrayeb, and M. O. Hasna, "A stochastic geometric analysis of device-to-device communications operating over generalized fading channels," *IEEE Transactions on Wireless Communications*, vol. 16, pp. 4151–4165, July 2017.

[18] ArrayComm & William Webb. Ofcom, 2007.

[19] D. López-Pérez, M. Ding, H. Claussen, and A. H. Jafari, "Towards 1 Gbps/UE in cellular systems: Understanding ultra-dense small cell deployments," *IEEE Communications Surveys & Tutorials*, vol. 17, no. 4, pp. 2078–2101, 2015.

[20] X. Zhang and J. G. Andrews, "Downlink cellular network analysis with multi-slope path loss models," *IEEE Transactions on Communications*, vol. 63, pp. 1881–1894, May 2015.

[21] T. Bai and R. W. Heath, "Coverage and rate analysis for millimeter-wave cellular networks," *IEEE Transactions on Wireless Communications*, vol. 14, pp. 1100–1114, Feb 2015.

[22] M. Ding and D. López-Pérez, "Performance impact of base station antenna heights in dense cellular networks," *IEEE Transactions on Wireless Communications*, vol. 16, pp. 8147–8161, Dec 2017.

[23] I. Atzeni, J. Arnau, and M. Kountouris, "Performance analysis of ultra-dense networks with elevated base stations," in *2017 15th International Symposium on Modeling and Optimization in Mobile, Ad Hoc, and Wireless Networks (WiOpt)*, pp. 1–6, May 2017.

[24] A. D. Gandhi, "Significant gains in coverage and downlink capacity from optimal antenna downtilt for closely-spaced cells in wireless networks," in *2014 23rd Wireless and Optical Communication Conference (WOCC)*, pp. 1–6, May 2014.

[25] S. M. Razavizadeh, M. Ahn, and I. Lee, "Three-dimensional beamforming: A new enabling technology for 5G wireless networks," *IEEE Signal Processing Magazine*, vol. 31, pp. 94–101, Nov 2014.

[26] 3GPP, "TR 36.814: Further advancements for E-UTRA physical layer aspects (Release 9)," Mar. 2010.

[27] H. C. Nguyen, I. Rodriguez, T. B. Sorensen, J. Elling, M. B. Gentsch, M. Sorensen, and P. Mogensen, "Validation of tilt gain under realistic path loss model and network scenario," in *2013 IEEE 78th Vehicular Technology Conference (VTC Fall)*, pp. 1–5, Sept 2013.

[28] J. Fan, G. Y. Li, and X. Zhu, "Vertical beamforming with downtilt optimization in downlink cellular networks," in *2015 IEEE Global Communications Conference (GLOBECOM)*, pp. 1–5, Dec 2015.

[29] M. Haenggi, *Stochastic Geometry for Wireless Networks*. Cambridge University Press, 2012.

[30] J. G. Andrews, F. Baccelli, and R. K. Ganti, "A tractable approach to coverage and rate in cellular networks," *IEEE Transactions on Communications*, vol. 59, pp. 3122–3134, November 2011.

[31] T. D. Novlan, H. S. Dhillon, and J. G. Andrews, "Analytical modeling of uplink cellular networks," *IEEE Transactions on Wireless Communications*, vol. 12, pp. 2669–2679, June 2013.

[32] M. Ding and D. López-Pérez, "Please lower small cell antenna heights in 5G," in *2016 IEEE Global Communications Conference (GLOBECOM)*, pp. 1–6, Dec 2016.

[33] M. Ding, D. López-Pérez, G. Mao, Z. Lin, and S. K. Das, "DNA-GA: A tractable approach for performance analysis of uplink cellular networks," *IEEE Transactions on Communications*, vol. 66, pp. 355–369, Jan 2018.

[34] X. Ge, X. Tian, Y. Qiu, G. Mao, and T. Han, "Small-cell networks with fractal coverage characteristics," *IEEE Transactions on Communications*, vol. 66, pp. 5457–5469, Nov 2018.

[35] T. Samarasinghe, H. Inaltekin, and J. S. Evans, "On optimal downlink coverage in poisson cellular networks with power density constraints," *IEEE Transactions on Communications*, vol. 62, pp. 1382–1392, April 2014.

[36] M. Haenggi, "The meta distribution of the sir in poisson bipolar and cellular networks," *IEEE Transactions on Wireless Communications*, vol. 15, pp. 2577–2589, April 2016.

[37] N. Deng and M. Haenggi, "The meta distribution of the sinr in mm-wave d2d networks," in *GLOBECOM 2017 - 2017 IEEE Global Communications Conference*, pp. 1–6, Dec 2017.

[38] N. Deng and M. Haenggi, "A fine-grained analysis of millimeter-wave device-to-device networks," *IEEE Transactions on Communications*, vol. 65, pp. 4940–4954, Nov 2017.

[39] Q. Cui, X. Yu, Y. Wang, and M. Haenggi, "The sir meta distribution in poisson cellular networks with base station cooperation," *IEEE Transactions on Communications*, vol. 66, pp. 1234–1249, March 2018.

[40] Y. Wang, Q. Cui, M. Haenggi, and Z. Tan, "On the sir meta distribution for poisson networks with interference cancellation," *IEEE Wireless Communications Letters*, vol. 7, pp. 26–29, Feb 2018.

[41] X. Zhou, J. Guo, S. Durrani, and M. D. Renzo, "Power beacon-assisted millimeter wave ad hoc networks," *IEEE Transactions on Communications*, vol. 66, pp. 830–844, Feb 2018.

[42] A. Thornburg and R. W. Heath, "Ergodic rate of millimeter wave ad hoc networks," *IEEE Transactions on Wireless Communications*, vol. 17, pp. 914–926, Feb 2018.

[43] J. Park, J. G. Andrews, and R. W. Heath, "Inter-operator base station coordination in spectrum-shared millimeter wave cellular networks," *IEEE Transactions on Cognitive Communications and Networking*, vol. PP, no. 99, pp. 1–1, 2018.

[44] D. Malak, M. Al-Shalash, and J. G. Andrews, "Spatially correlated content caching for device-to-device communications," *IEEE Transactions on Wireless Communications*, vol. 17, pp. 56–70, Jan 2018.

[45] N. Kouzayha, Z. Dawy, J. G. Andrews, and H. ElSawy, "Joint downlink/uplink rf wake-up solution for iot over cellular networks," *IEEE Transactions on Wireless Communications*, vol. 17, pp. 1574–1588, March 2018.

[46] S. S. Kalamkar and M. Haenggi, "The spatial outage capacity of wireless networks," *IEEE Transactions on Wireless Communications*, vol. PP, no. 99, pp. 1–1, 2018.

[47] R. Jurdi, A. K. Gupta, J. G. Andrews, and R. W. Heath, "Modeling infrastructure sharing in mmwave networks with shared spectrum licenses," *IEEE Transactions on Cognitive Communications and Networking*, vol. PP, no. 99, pp. 1–1, 2018.

[48] A. K. Gupta, J. G. Andrews, and R. W. Heath, "Macrodiversity in cellular networks with random blockages," *IEEE Transactions on Wireless Communications*, vol. 17, pp. 996–1010, Feb 2018.

[49] C. S. Choi, J. O. Woo, and J. G. Andrews, "An analytical framework for modeling a spatially repulsive cellular network," *IEEE Transactions on Communications*, vol. 66, pp. 862–874, Feb 2018.

[50] A. AlAmmouri, J. G. Andrews, and F. Baccelli, "Sinr and throughput of dense cellular networks with stretched exponential path loss," *IEEE Transactions on Wireless Communications*, vol. 17, pp. 1147–1160, Feb 2018.

[51] M. Afshang and H. S. Dhillon, "Poisson cluster process based analysis of hetnets with correlated user and base station locations," *IEEE Transactions on Wireless Communications*, vol. PP, no. 99, pp. 1–1, 2018.

[52] Y. Zhu, L. Wang, K. K. Wong, and R. W. Heath, "Secure communications in millimeter wave ad hoc networks," *IEEE Transactions on Wireless Communications*, vol. 16, pp. 3205–3217, May 2017.

[53] X. Yu, J. Zhang, M. Haenggi, and K. B. Letaief, "Coverage analysis for millimeter wave networks: The impact of directional antenna arrays," *IEEE Journal on Selected Areas in Communications*, vol. 35, pp. 1498–1512, July 2017.

[54] A. H. Jafari, D. Lpez-Prez, M. Ding, and J. Zhang, "Performance analysis of dense small cell networks with practical antenna heights under rician fading," *IEEE Access*, vol. 6, pp. 9960–9974, 2018.

[55] M. N. Kulkarni, A. Ghosh, and J. G. Andrews, "A comparison of mimo techniques in downlink millimeter wave cellular networks with hybrid beamforming," *IEEE Transactions on Communications*, vol. 64, pp. 1952–1967, May 2016.

[56] M. Salehi, A. Mohammadi, and M. Haenggi, "Analysis of d2d underlaid cellular networks: Sir meta distribution and mean local delay," *IEEE Transactions on Communications*, vol. 65, pp. 2904–2916, July 2017.

[57] V. V. Chetlur and H. S. Dhillon, "Downlink coverage analysis for a finite 3-d wireless network of unmanned aerial vehicles," *IEEE Transactions on Communications*, vol. 65, pp. 4543–4558, Oct 2017.

[58] M. N. Kulkarni, J. G. Andrews, and A. Ghosh, "Performance of dynamic and static tdd in self-backhauled millimeter wave cellular networks," *IEEE Transactions on Wireless Communications*, vol. 16, pp. 6460–6478, Oct 2017.

[59] L. Wu, Y. Zhong, W. Zhang, and M. Haenggi, "Scalable transmission over heterogeneous networks: A stochastic geometry analysis," *IEEE Transactions on Vehicular Technology*, vol. 66, pp. 1845–1859, Feb 2017.

[60] Y. Wang, M. Haenggi, and Z. Tan, "The meta distribution of the sir for cellular networks with power control," *IEEE Transactions on Communications*, vol. PP, no. 99, pp. 1–1, 2017.

[61] L. Wang, K. K. Wong, R. W. Heath, and J. Yuan, "Wireless powered dense cellular networks: How many small cells do we need?," *IEEE Journal on Selected Areas in Communications*, vol. 35, pp. 2010–2024, Sept 2017.

[62] H. Sun, M. Sheng, M. Wildemeersch, T. Q. S. Quek, and J. Li, "Traffic adaptation and energy efficiency for small cell networks with dynamic tdd," *IEEE*

Journal on Selected Areas in Communications, vol. 34, pp. 3234–3251, Dec 2016.

[63] G. George, R. K. Mungara, A. Lozano, and M. Haenggi, "Ergodic spectral efficiency in mimo cellular networks," *IEEE Transactions on Wireless Communications*, vol. 16, pp. 2835–2849, May 2017.

[64] I. Flint, H. B. Kong, N. Privault, P. Wang, and D. Niyato, "Analysis of heterogeneous wireless networks using poisson hard-core hole process," *IEEE Transactions on Wireless Communications*, vol. 16, pp. 7152–7167, Nov 2017.

[65] Y. Li, J. G. Andrews, F. Baccelli, T. D. Novlan, and C. J. Zhang, "Design and analysis of initial access in millimeter wave cellular networks," *IEEE Transactions on Wireless Communications*, vol. 16, pp. 6409–6425, Oct 2017.

[66] N. Deng, W. Zhou, and M. Haenggi, "Heterogeneous cellular network models with dependence," *IEEE Journal on Selected Areas in Communications*, vol. 33, pp. 2167–2181, Oct 2015.

[67] N. Deng, W. Zhou, and M. Haenggi, "The ginibre point process as a model for wireless networks with repulsion," *IEEE Transactions on Wireless Communications*, vol. 14, pp. 107–121, Jan 2015.

[68] H. H. Yang, G. Geraci, T. Q. S. Quek, and J. G. Andrews, "Cell-edge-aware precoding for downlink massive mimo cellular networks," *IEEE Transactions on Signal Processing*, vol. 65, pp. 3344–3358, July 2017.

[69] J. G. Andrews, T. Bai, M. N. Kulkarni, A. Alkhateeb, A. K. Gupta, and R. W. Heath, "Modeling and analyzing millimeter wave cellular systems," *IEEE Transactions on Communications*, vol. 65, pp. 403–430, Jan 2017.

[70] A. K. Gupta, A. Alkhateeb, J. G. Andrews, and R. W. Heath, "Gains of restricted secondary licensing in millimeter wave cellular systems," *IEEE Journal on Selected Areas in Communications*, vol. 34, pp. 2935–2950, Nov 2016.

[71] D. Malak, M. Al-Shalash, and J. G. Andrews, "Optimizing content caching to maximize the density of successful receptions in device-to-device networking," *IEEE Transactions on Communications*, vol. 64, pp. 4365–4380, Oct 2016.

[72] A. K. Gupta, J. G. Andrews, and R. W. Heath, "On the feasibility of sharing spectrum licenses in mmwave cellular systems," *IEEE Transactions on Communications*, vol. 64, pp. 3981–3995, Sept 2016.

[73] Y. Li, F. Baccelli, J. G. Andrews, T. D. Novlan, and J. C. Zhang, "Modeling and analyzing the coexistence of wi-fi and lte in unlicensed spectrum," *IEEE Transactions on Wireless Communications*, vol. 15, pp. 6310–6326, Sept 2016.

[74] H. Elshaer, M. N. Kulkarni, F. Boccardi, J. G. Andrews, and M. Dohler, "Downlink and uplink cell association with traditional macrocells and millimeter wave small cells," *IEEE Transactions on Wireless Communications*, vol. 15, pp. 6244–6258, Sept 2016.

[75] J. Park, N. Lee, J. G. Andrews, and R. W. Heath, "On the optimal feedback rate in interference-limited multi-antenna cellular systems," *IEEE Transactions on Wireless Communications*, vol. 15, pp. 5748–5762, Aug 2016.

[76] C. Li, J. Zhang, J. G. Andrews, and K. B. Letaief, "Success probability and area spectral efficiency in multiuser mimo hetnets," *IEEE Transactions on Communications*, vol. 64, pp. 1544–1556, April 2016.

[77] X. Lin, R. W. Heath, and J. G. Andrews, "The interplay between massive mimo and underlaid d2d networking," *IEEE Transactions on Wireless Communications*, vol. 14, pp. 3337–3351, June 2015.

[78] N. Deng, M. Haenggi, and Y. Sun, "Millimeter-wave device-to-device networks with heterogeneous antenna arrays," *IEEE Transactions on Communications*, pp. 1–1, 2018.

[79] A. Rajanna and M. Haenggi, "Enhanced cellular coverage and throughput using rateless codes," *IEEE Transactions on Communications*, vol. 65, pp. 1899–1912, May 2017.

[80] D. Malak, H. S. Dhillon, and J. G. Andrews, "Optimizing data aggregation for uplink machine-to-machine communication networks," *IEEE Transactions on Communications*, vol. 64, pp. 1274–1290, March 2016.

[81] Y. Li, F. Baccelli, H. S. Dhillon, and J. G. Andrews, "Statistical modeling and probabilistic analysis of cellular networks with determinantal point processes," *IEEE Transactions on Communications*, vol. 63, pp. 3405–3422, Sept 2015.

[82] X. Lin, L. Jiang, and J. G. Andrews, "Performance analysis of asynchronous multicarrier wireless networks," *IEEE Transactions on Communications*, vol. 63, pp. 3377–3390, Sept 2015.

[83] S. Singh, X. Zhang, and J. G. Andrews, "Joint rate and sinr coverage analysis for decoupled uplink-downlink biased cell associations in hetnets," *IEEE Transactions on Wireless Communications*, vol. 14, pp. 5360–5373, Oct 2015.

[84] S. Singh, M. N. Kulkarni, A. Ghosh, and J. G. Andrews, "Tractable model for rate in self-backhauled millimeter wave cellular networks," *IEEE Journal on Selected Areas in Communications*, vol. 33, pp. 2196–2211, Oct 2015.

[85] Q. Ye, M. Al-Shalash, C. Caramanis, and J. G. Andrews, "Distributed resource allocation in device-to-device enhanced cellular networks," *IEEE Transactions on Communications*, vol. 63, pp. 441–454, Feb 2015.

[86] A. K. Gupta, H. S. Dhillon, S. Vishwanath, and J. G. Andrews, "Downlink multi-antenna heterogeneous cellular network with load balancing," *IEEE Transactions on Communications*, vol. 62, pp. 4052–4067, Nov 2014.

[87] R. Tanbourgi, S. Singh, J. G. Andrews, and F. K. Jondral, "A tractable model for noncoherent joint-transmission base station cooperation," *IEEE Transactions on Wireless Communications*, vol. 13, pp. 4959–4973, Sept 2014.

[88] Y. Zhong, M. Haenggi, T. Q. S. Quek, and W. Zhang, "On the stability of static poisson networks under random access," *IEEE Transactions on Communications*, vol. 64, pp. 2985–2998, July 2016.

[89] A. Guo, Y. Zhong, W. Zhang, and M. Haenggi, "The gauss-poisson process for wireless networks and the benefits of cooperation," *IEEE Transactions on Communications*, vol. 64, pp. 1916–1929, May 2016.

[90] R. K. Ganti and M. Haenggi, "Asymptotics and approximation of the sir distribution in general cellular networks," *IEEE Transactions on Wireless Communications*, vol. 15, pp. 2130–2143, March 2016.

[91] U. Schilcher, S. Toumpis, M. Haenggi, A. Crismani, G. Brandner, and C. Bettstetter, "Interference functionals in poisson networks," *IEEE Transactions on Information Theory*, vol. 62, pp. 370–383, Jan 2016.

[92] Z. Tong and M. Haenggi, "Throughput analysis for full-duplex wireless networks with imperfect self-interference cancellation," *IEEE Transactions on Communications*, vol. 63, pp. 4490–4500, Nov 2015.

[93] S. Khavari Moghaddam and S. M. Razavizadeh, "Joint tilt angle adaptation and beamforming in multicell multiuser cellular networks," *Comput. Electr. Eng.*, vol. 61, pp. 195–207, July 2017.

[94] N. Seifi, R. W. Heath, M. Coldrey, and T. Svensson, "Adaptive multicell 3-D beamforming in multiantenna cellular networks," *IEEE Transactions on Vehicular Technology*, vol. 65, pp. 6217–6231, Aug 2016.

[95] N. Seifi, J. Zhang, R. W. Heath, T. Svensson, and M. Coldrey, "Coordinated 3d beamforming for interference management in cellular networks," *IEEE Transactions on Wireless Communications*, vol. 13, pp. 5396–5410, Oct 2014.

[96] G. Nigam, P. Minero, and M. Haenggi, "Spatiotemporal cooperation in heterogeneous cellular networks," *IEEE Journal on Selected Areas in Communications*, vol. 33, pp. 1253–1265, June 2015.

[97] C. Li, J. Zhang, M. Haenggi, and K. B. Letaief, "User-centric intercell interference nulling for downlink small cell networks," *IEEE Transactions on Communications*, vol. 63, pp. 1419–1431, April 2015.

[98] X. Zhang and J. G. Andrews, "Downlink cellular network analysis with multi-slope path loss models," *IEEE Transactions on Communications*, vol. 63, pp. 1881–1894, May 2015.

[99] T. D. Novlan, H. S. Dhillon, and J. G. Andrews, "Analytical modeling of uplink cellular networks," *IEEE Transactions on Wireless Communications*, vol. 12, pp. 2669–2679, June 2013.

[100] Y. J. Chun, S. L. Cotton, H. S. Dhillon, A. Ghrayeb, and M. O. Hasna, "A stochastic geometric analysis of device-to-device communications operating over generalized fading channels," *IEEE Transactions on Wireless Communications*, vol. 16, pp. 4151–4165, July 2017.

[101] N. Lee, X. Lin, J. G. Andrews, and R. W. Heath, "Power control for d2d underlaid cellular networks: Modeling, algorithms, and analysis," *IEEE Journal on Selected Areas in Communications*, vol. 33, pp. 1–13, Jan 2015.

[102] H. Wei, N. Deng, W. Zhou, and M. Haenggi, "Approximate sir analysis in general heterogeneous cellular networks," *IEEE Transactions on Communications*, vol. 64, pp. 1259–1273, March 2016.

[103] M. Mozaffari, W. Saad, M. Bennis, and M. Debbah, "Unmanned aerial vehicle with underlaid device-to-device communications: Performance and tradeoffs," *IEEE Transactions on Wireless Communications*, vol. 15, pp. 3949–3963, June 2016.

[104] N. Seifi, R. W. Heath, M. Coldrey, and T. Svensson, "Adaptive multicell 3-d beamforming in multiantenna cellular networks," *IEEE Transactions on Vehicular Technology*, vol. 65, pp. 6217–6231, Aug 2016.

[105] A. Asadi, Q. Wang, and V. Mancuso, "A survey on device-to-device communication in cellular networks," *IEEE Communications Surveys Tutorials*, vol. 16, no. 4, pp. 1801–1819, 2014.

[106] H. Ding, X. Wang, D. B. da Costa, and J. Ge, "Interference modeling in clustered device-to-device networks with uniform transmitter selection," *IEEE Transactions on Wireless Communications*, vol. 16, pp. 7906–7918, Dec 2017.

[107] J. Liu, M. Sheng, L. Liu, Y. Shi, and J. Li, "Modeling and analysis of SCMA enhanced D2D and cellular hybrid network," *IEEE Transactions on Communications*, vol. 65, pp. 173–185, Jan 2017.

[108] M. Gharbieh, A. Bader, H. E. Sawy, H. Yang, M. Alouini, and A. Adinoyi, "Self-organized scheduling request for uplink 5g networks: A d2d clustering approach," *IEEE Transactions on Communications*, pp. 1–1, 2018.

[109] J. Liu, H. Nishiyama, N. Kato, and J. Guo, "On the outage probability of device-to-device-communication-enabled multichannel cellular networks: An

RSS-Threshold-Based perspective," *IEEE Journal on Selected Areas in Communications*, vol. 34, pp. 163–175, Jan 2016.

[110] M. Peng, Y. Li, T. Q. S. Quek, and C. Wang, "Device-to-device underlaid cellular networks under rician fading channels," *Wireless Communications, IEEE Transactions on*, vol. 13, no. 8, pp. 4247–4259, 2014.

[111] R. Margolies, A. Sridharan, V. Aggarwal, R. Jana, N. K. Shankaranarayanan, V. A. Vaishampayan, and G. Zussman, "Exploiting mobility in proportional fair cellular scheduling: Measurements and algorithms," *IEEE/ACM Transactions on Networking*, vol. 24, pp. 355–367, Feb 2016.

[112] Y. Cheng, P. Fu, Y. Ding, B. Li, and X. Yuan, "Proportional fairness in cognitive wireless powered communication networks," *IEEE Communications Letters*, vol. 21, pp. 1397–1400, June 2017.

[113] M. Hojeij, C. A. Nour, J. Farah, and C. Douillard, "Waterfilling-based proportional fairness scheduler for downlink non-orthogonal multiple access," *IEEE Wireless Communications Letters*, vol. 6, pp. 230–233, April 2017.

[114] J. Choi and S. Bahk, "Cell-throughput analysis of the proportional fair scheduler in the single-cell environment," *IEEE Transactions on Vehicular Technology*, vol. 56, pp. 766–778, March 2007.

[115] J. Wu, N. B. Mehta, A. F. Molisch, and J. Zhang, "Unified spectral efficiency analysis of cellular systems with channel-aware schedulers," *IEEE Transactions on Communications*, vol. 59, pp. 3463–3474, December 2011.

[116] A. H. Jafari, D. Lopez-Perez, M. Ding, and J. Zhang, "Study on scheduling techniques for ultra dense small cell networks," in *2015 IEEE 82nd Vehicular Technology Conference (VTC2015-Fall)*, pp. 1–6, Sept 2015.

[117] A. M. Hunter, J. G. Andrews, and S. Weber, "Transmission capacity of ad hoc networks with spatial diversity," *IEEE Transactions on Wireless Communications*, vol. 7, pp. 5058–5071, December 2008.

[118] M. Danneberg, J. Holfeld, M. Grieger, M. Amro, and G. Fettweis, "Field trial evaluation of UE specific antenna downtilt in an LTE downlink," in *2012 International ITG Workshop on Smart Antennas (WSA)*, pp. 274–280, March 2012.

[119] N. Seifi, M. Coldrey, M. Matthaiou, and M. Viberg, "Impact of base station antenna tilt on the performance of network MIMO systems," in *2012 IEEE 75th Vehicular Technology Conference (VTC Spring)*, pp. 1–5, May 2012.

[120] M. Baianifar, S. Khavari, S. M. Razavizadeh, and T. Svensson, "Impact of user height on the coverage of 3D beamforming-enabled massive MIMO systems," in *2017 IEEE 28th Annual International Symposium on Personal, Indoor, and Mobile Radio Communications (PIMRC)*, pp. 1–5, Oct 2017.

[121] S. K. Moghaddam and S. M. Razavizadeh, "Joint tilt angle adaptation and beamforming in multicell multiuser cellular networks," *Computers & Electrical Engineering*, vol. 61, pp. 195–207, 2017.

[122] A. Fotouhi, M. Ding, and M. Hassan, "Flying drone base stations for macro hotspots," *IEEE Access*, vol. 6, pp. 19530–19539, 2018.

[123] T. Ding, M. Ding, G. Mao, Z. Lin, A. Y. Zomaya, and D. Lpez-Prez, "Performance analysis of dense small cell networks with dynamic tdd," *IEEE Transactions on Vehicular Technology*, vol. 67, pp. 9816–9830, Oct 2018.

[124] 3GPP, "TR 36.828: Further enhancements to LTE Time Division Duplex (TDD) for Downlink-Uplink (DL-UL) interference management and traffic adaptation," Jun. 2012.

[125] Spatial Channel Model AHG, "Subsection 3.5.3, Spatial Channel Model Text Description V6.0," Apr. 2003.

[126] 3GPP, "TR 36.877 (RAN4) LTE Device-to-Device (D2D) Proximity Services (ProSe) UE radio transmission and reception," Mar 2015.

[127] M. Ding and M. D. Lopez-Perez, "A new capacity scaling law in ultra-dense networks," *arXiv:1704.00399 [cs.NI]*, Apr. 2017.

[128] 3GPP, "TR 36.872: Small cell enhancements for E-UTRA and E-UTRAN - Physical layer aspects," Dec. 2013.

[129] M. D. Renzo, W. Lu, and P. Guan, "The intensity matching approach: A tractable stochastic geometry approximation to system-level analysis of cellular networks," *IEEE Transactions on Wireless Communications*, vol. 15, pp. 5963–5983, Sept 2016.

[130] M. Haenggi, "On distances in uniformly random networks," *IEEE Transactions on Information Theory*, vol. 51, pp. 3584–3586, Oct 2005.

[131] J.S.Roessler, "LTE-Advanced (3GPP Rel.12) technology introduction white paper," 2015.

[132] P. Mach, Z. Becvar, and T. Vanek, "In-band device-to-device communication in ofdma cellular networks: A survey and challenges," *IEEE Communications Surveys & Tutorials*, vol. 17, no. 4, pp. 1885–1922, 2015.

[133] M. Ding, D. Lpez-Prez, G. Mao, P. Wang, and Z. Lin, "Will the area spectral efficiency monotonically grow as small cells go dense?," *IEEE GLOBECOM 2015*, pp. 1–7, Dec. 2015.

[134] S. Lee and K. Huang, "Coverage and economy of cellular networks with many base stations," *IEEE Communications Letters*, vol. 16, pp. 1038–1040, Jul.

2012.

[135] M. Ding, D. L. Perez, G. Mao, and Z. Lin, "Study on the idle mode capability with los and nlos transmissions," in *2016 IEEE Global Communications Conference (GLOBECOM)*, pp. 1–6, Dec 2016.

[136] I. Gradshteyn and I. Ryzhik, *Table of Integrals, Series, and Products (7th Ed.)*. Academic Press, 2007.

[137] F. Liu, J. Riihijärvi, and M. Petrova, "Robust data rate estimation with stochastic sinr modeling in multi-interference ofdma networks," in *Sensing, Communication, and Networking (SECON), 2015 12th Annual IEEE International Conference on*, pp. 211–219, IEEE, 2015.

[138] E. Liu and K. K. Leung, "Expected throughput of the proportional fair scheduling over rayleigh fading channels," *IEEE Communications Letters*, vol. 14, no. 6, 2010.

[139] J. Wu, N. B. Mehta, A. F. Molisch, and J. Zhang, "Unified spectral efficiency analysis of cellular systems with channel-aware schedulers," *IEEE Transactions on Communications*, vol. 59, no. 12, pp. 3463–3474, 2011.

[140] M. Ding, D. L. Pérez, A. H. Jafari, G. Mao, and Z. Lin, "Ultra-dense networks: A new look at the proportional fair scheduler," in *GLOBECOM 2017-2017 IEEE Global Communications Conference*, pp. 1–7, IEEE, 2017.

[141] X. Ge, B. Yang, J. Ye, G. Mao, C. X. Wang, and T. Han, "Spatial spectrum and energy efficiency of random cellular networks," *IEEE Transactions on Communications*, vol. 63, pp. 1019–1030, March 2015.

[142] R. Zi, X. Ge, J. Thompson, C. X. Wang, H. Wang, and T. Han, "Energy efficiency optimization of 5g radio frequency chain systems," *IEEE Journal on Selected Areas in Communications*, vol. 34, pp. 758–771, April 2016.

[143] X. Li, T. Bai, and R. W. Heath, "Impact of 3d base station antenna in random heterogeneous cellular networks," in *2014 IEEE Wireless Communications and Networking Conference (WCNC)*, pp. 2254–2259, April 2014.

[144] F. Gunnarsson, M. N. Johansson, A. Furuskar, M. Lundevall, A. Simonsson, C. Tidestav, and M. Blomgren, "Downtilted base station antennas-a simulation model proposal and impact on HSPA and LTE performance," in *Vehicular Technology Conference, 2008. VTC 2008-Fall. IEEE 68th*, pp. 1–5, IEEE, 2008.

[145] M. Ding and D. Lopez-Perez, "On the performance of practical ultra-dense networks: The major and minor factors," in *2017 15th International Symposium on Modeling and Optimization in Mobile, Ad Hoc, and Wireless Networks (WiOpt)*, pp. 1–8, May 2017.